2020

A Finite Volume Model for Predicting Water Vapour Transport in Conjugate Fluid/Porous/Solid Domains

Christian Fischer
Western University

A Finite Volume Model for Predicting Water Vapour Transport in Conjugate Fluid/Porous/Solid Domains

(Spine Title: Water Vapour Transport in Conjugate Domains)

(Thesis Format: Monograph)

by

Christian Fischer

Graduate Program in Engineering
Department of Mechanical & Material Engineering

Submitted in Partial fulfillment
Of the requirements for the degree of
Master of Engineering Science

The School of Graduate and Postdoctoral Studies
The University of Western Ontario
London, Ontario, Canada
Nov, 2011

THE UNIVERSITY OF WESTERN ONTARIO

SCHOOL OF GRADUATE AND POSTDOCTORAL STUDIES

CERTIFICATE OF EXAMINATION

Supervisor	Examiners
Dr. Anthony Straatman	Dr. A. Ray
	Dr. K. Siddiqui
	Dr. J. Yang

The thesis by

Christian Fischer

entitled:

A Finite Volume Model for Predicting Water Vapour Transport in Conjugate Fluid/Porous/Solid Domains

is accepted in partial fulfillment of the

requirements for the degree of

Master of Engineering Science

Date

Chair of the Thesis Examination Board

Abstract

The principle aim of the presented work is to extend the capability of conjugate heat/flow models to include moisture exchange such that applications in food storage/ripening and heating, ventilation, and air conditioning (HVAC) can be simulated. To accomplish this, several modifications were made to an existing finite-volume model developed in-house. The most significant change was the implementation of a mass fraction transport equation to track the evolution of the water vapour field in all regions of the conjugate domain. This approach also required re-formulation of the energy transport model to account for a dry air/water vapour binary mixture. Developments in the porous regions are implemented using the technique of volume averaging, wherein the governing equations are considered macroscopically. A non-equilibrium approach in volume averaging the species and energy transport equations is implemented to allow more versatility for future work. This non-equilibrium versatility is beneficial over traditional equilibrium approaches, as often in agricultural or processing applications, internal moisture and temperature conditions dictate the transfer between constituents. Additionally, these conjugate domains consist of fluid-porous, fluid-solid, and porous-solid interfaces, and interface conditions between governing equations must be developed. Applications in the HVAC industry are chosen for validation, as the model is utilized to predict operating temperatures in evaporative cooling cycles, and study energy and humidity transport throughout these domains.

Keywords: *porous media, conjugate vapour transfer, conjugate heat transfer, finite-volume discretzation, Interface conditions*

Acknowledgments

I would like to thank Dr. Tony Straatman for his guidance and suggestions, and for his continuous support throughout this project. Furthermore, I would also like to thank all of my friends and colleagues in the lab for their help, advice, and their ability to maintain a good lab atmosphere throughout the project. This includes; L. Betchen, C. DeGroot, M. Farroknejad, C. Johnson, and J. Cepek.

Often, the only way to move forward when a hurdle is encountered in research is to take your mind off of things, and have a home cooked meal. With this being said, finally I would like to thank my parents, brother, and grandmas for all their support throughout the last two years.

Contents

List of Tables

List of Figures

S	Source
Sc	Shmidt Number
Sh_{sur}	Interfacial Sherwood number
t	Time
t	Tangent unit vector
T	Temperature
u	Diffusive velocity
U	Magnitude of inlet velocity (x-direction)
v	Velocity vector
V	Volume
x	Position vector
y	Position vector
Y	Mass Fraction

Greek Letters

α	Upwinding direction
β	Blending factor
Γ	Diffusion coefficient
δ_{ij}	Kronecker Delta
ε	Porosity
ζ	Mixture property
κ	Reaction rate coefficient
μ	Dynamic Viscosity
μ_B	Brinkman Viscosity
σ_{ij}	Stress Tensor
ρ	Density
Φ	Limiter function for TVD advection scheme
ψ	Transported variable
ω_{rel}	Relative humidity
ω_{spec}	Specific humidity

Subscripts/Superscripts

A	Component A of binary mixture
B	Component B of binary mixture

Chapter 1 - Introduction and Literature Review

1.1 Motivation

Processes that undergo moisture transfer are common in many applications of engineering. In particular, chemical engineering relies heavily on moisture exchange in food processing, where the manipulation of moisture can be used for sanitation, quality enhancement, ease of handling in production facilities, and product shelf life extension. In mechanical and civil engineering, wicking processes are important for moisture removal, and often water vapour is manipulated to create energy potential for applications such as the conditioning of air in buildings. These processes introduce engineering challenges in design and modeling and it is desirable to have insight to control them. Often, the materials and domains under consideration have a structure that enables permeation by gas or fluid. If this is the case, it is possible to use modelling techniques developed for porous media to simulate flows and exchanges in these applications.

A porous media can be generally defined as a heterogeneous system consisting of a solid matrix with fluid voids. This definition allows for a wide range of scales. The pore or void size may be of the order of the molecular size $3 < d < 7$Å (d is the average pore or void diameter), or as large as centimetres as in food stuffs (figure 1.1). The scale of the problem must be carefully considered when a solution approach is formulated for the domain, as mathematical treatments of this medium require scale

constraints. Also, porous structures often vary in geometry, some being oriented similarly to packed beds of particles where others take on the form of interconnected ligaments or spherical shaped voids. The type of structure affects the transport of fluid, energy, and species through the domain; and in addition, the amount of available surface area for exchange between constituents. This increased surface area is one of the main reasons for using porous materials because exchange of energy and mass can be enhanced over simple manufactured geometries.

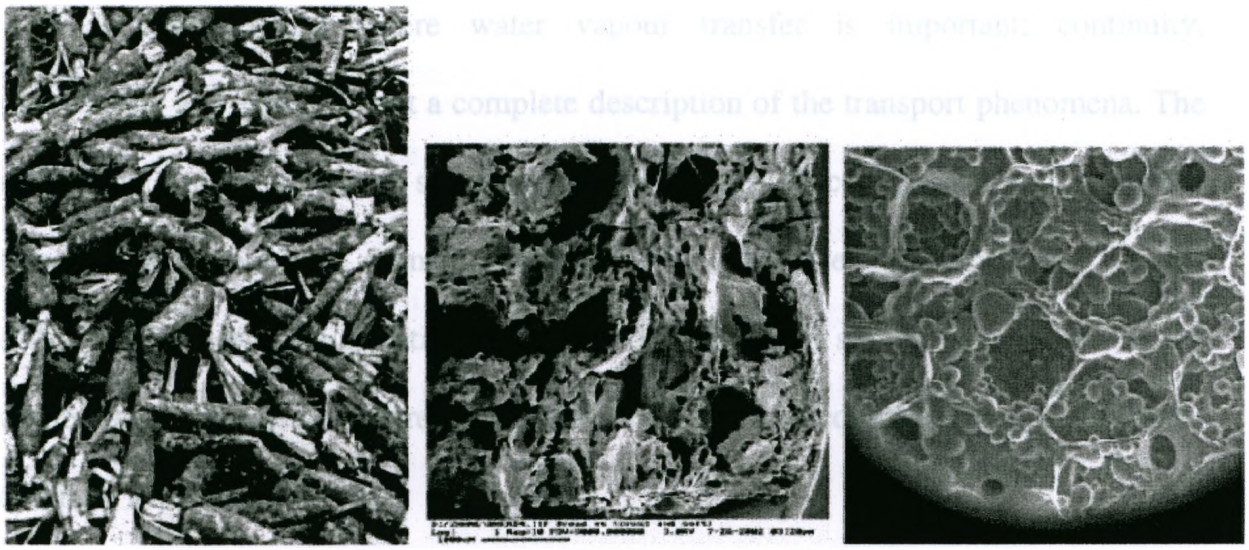

Figure 1-1 Food systems: left – bulk chicory roots, middle – SEM image of bread, right – SEM image of uncooked potato [1]

CFD techniques in modelling porous domains, until recently, have focussed solely on fluid flow and heat transfer. The benefit of modelling these transported variables using a porous media approach is that the concept of volume averaging [2, 3] may be applied to eliminate computing pore level flow, thereby simplifying the entire media to a continuum. The solid and fluid constituents of the porous domain may be treated as a single continuum when volume averaging is applied to the mass, momentum, and energy equations. There is also versatility in the volume averaging

approach, as derivation of the governing equations may be performed treating the fluid and solid components as separate constituents. This is often done to the conservation of energy equation under the assumption of local thermal non-equilibrium (LTNE), whereby the temperature of the fluid and solid are computed separately [4]. The LTNE approach is necessary for cases where the conductivity ratio of the solid to fluid is too large, but it is also useful for cases where an accurate value of temperature in the solid is needed to properly estimate coefficients in an energy or moisture exchange law.

In applications where water vapour transfer is important; continuity, momentum, and energy is not a complete description of the transport phenomena. The addition of a mass fraction or species conservation must be considered to fully describe transport throughout the domain. Theoretical models have been developed for this additional conservation equation. These models follow a similar progression as the conservation of energy, where representing the porous medium as a single or multi-continua is proposed [2, 4].

The differential forms of the equations described, which govern transport through the porous media, serve as the basis for computational models through a single medium type. However, when developing a computational model for applications that transmit moisture; such as air conditioning and food processing/storage, it is also imperative that the model is constructed with the ability to simulate transport through multiple domain types such as pure fluid, porous, and solid. This is due to the geometric configurations encountered in such processes. Furthermore, a model must also be able to include interfaces between medium types. There have been few models presented that accomplish this task.

complex physics. The model will also adopt a local thermal non-equilibrium model for the energy equation to enable accurate exchange models to be used. The model will be used in this thesis to carry out simulations of direct, indirect, and Maisotsenko evaporative cooling.

The following literature review is separated into three main sections: Porous media modelling where porous modelling techniques will be explained with a focus on multi-component flow, applications and modelling of porous domains in the food industry, including current modelling techniques in this sector; and application and modelling of evaporative cooling in the HVAC industry.

1.2 Literature Review

1.2.1 Porous Media Modeling

Prediction of flow characteristics in porous media has been studied for over a century. Notable milestones which are relevant to this work are the findings of Darcy, who was able to relate pressure drop to bulk velocity using an empirical constant [7]. Darcy's law is given as

$$-\nabla p = \frac{\mu}{K}\langle u \rangle , \tag{1.1}$$

where p is the pressure, K is the permeability of the porous media, μ is the dynamic viscosity and ⟨u⟩ the vector of average velocity. The Darcy equation shows a linear relation between pressure and bulk velocity. An unfamiliar term in this expression is the permeability, and as given in equation 1.1, this parameter is a measure of the ability of the porous material to allow fluid to flow through it. Although this expression is

useful, it is only valid in viscous dominated flows, where the Reynolds number is low. This is not always practical and for flows that are not limited by this criterion, a more advanced representation is needed.

Once the Reynolds number exceeds one, the Darcy equation alone is no longer valid and an alternate correlation is needed to accurately model the effect of the porous structure on the flow. Ergun developed an expression by considering granular solids, which is capable of resolving higher Reynolds numbers by taking into account density, viscosity, porosity, and geometric parameters of the solid particles. Ergun's equation contains a linear term similar to the Darcy equation, and a quadratic term accounting for the effects of inertia but is limited to porous media of specific internal structure. Ward [11] was able to take this correlation and make it applicable to other internal structures using dimensional analysis to show that the quadratic term in Ergun's equation could be represented in terms of the dynamic pressure, the square-root of permeability and a drag coefficient. This new expression contains a term similar to the original works of Darcy, and a general term to account for inertial effects given as

$$-\nabla p = \frac{\mu}{K}\langle u\rangle + \frac{\rho C_E}{\mu}|\langle u\rangle|\langle u\rangle\,. \tag{1.2}$$

The C_E term is called the Ergun coefficient, and accounts for the form drag in the medium. Although Ergun originally stated that this coefficient could be reduced to a single value for all forms of porous media, this has been shown to be incorrect. This model breaks down where macroscopic gradients exist in the flow, such as next to a wall in the boundary layer region, and hence more sophisticated techniques must be applied to capture the flow in these regions. The use of volume averaging of the

general transport equations over the porous domain is a technique that enables a broad extension to the simple porous media modelling afforded through the use of equations 1.1 and 1.2.

The volume averaging method, developed independently by Whitaker and Slattery [2, 3], is a method for modelling flow and energy transport in porous media. The transport equations are applicable in the difficult regions mentioned above (gradients near walls), as they are developed from the transport equations in a single constituent continuum and therefore contain all relevant terms that resolve gradients. The idea of this method is to not resolve the flow within the domain on the pore scale; rather the transport equations are integrated over a representative volume (discussed further in chapter 2), resolving only the bulk flow. This method is also extended to mass fraction and thermal fields, where Whitaker used volume averaging to look at energy and mass fraction transport for drying processes [7]. It is noted that volume averaging alone does not present a closed form of the above equations rather it leaves integral terms that are functions of pore level flow. In order to solve for the bulk flow, closure methods must be used to manipulate these terms. These closure techniques are not the purpose of this work however, it is stated that closure can be achieved by two methods; the first is the use of constitutive equations where examination of flow at the pore scale is needed, and the second, a semi-heuristic method that replaces the integral terms with terms that relate to the volume averaged parameters often coming from empirical relations such as the Darcy or Ergun equations. This work uses the semi-heuristic form of closure to represent the final form of the volume averaged equations.

Vafai and Tien [12] introduced a method of semi-heuristically closing the volume averaged momentum equations combining all unknown parameters and replacing them with a body force term of the form of the Ergun extended Darcy law. Thus, the closed form of the transport equations require a permeability, and an Ergun coefficient. Vafai and Tien also used this method to close the energy equations, where the additional integral terms arising from volume averaging were once again combined. This combined term was classified as an effective heat flux vector multiplied by an effective thermal conductivity. In flows with a high Peclet number (Pe = RePr), thermal dispersion must also be considered. Thermal dispersion is a transport process that occurs as a result of departures of the local velocity from the volume-averaged velocity. These local "fluctuations" promote local mixing and result in enhanced transport that must be accounted for in high Pe flows. Quintard et al [13], Sahouri and Kaviany [14] have conducted experiments to characterize the thermal dispersion in the volume averaged equations in terms of the local Peclet number. Kaviany [4] furthered this study looking at the closure terms in the mass fraction equations analogously to the energy equations and developed closed forms of these transport equations.

Betchen et al [6] studied the effects of local thermal non-equilibrium in graphite foams. This work developed a finite volume model for fluid flow and heat transfer in conjugate fluid, porous, solid domains. The novelty of this work lies in the thermal non-equilibrium development, as well as the model's ability to solve though conjugate domain interfaces without oscillation. This work used the concept of effective thermo-physical properties to represent exchange coefficients in the porous

media. As graphite foams do not have well established models for representing these effective properties, calibration of the model was required to correctly predict the flow in the graphite.

The effect of local non-equilibrium between constituents in the mass fraction and energy equations was also studied in the works of Quintard et al and Kaviany [13], where unlike the studies mentioned, transport of energy and mass through the medium was divided into transport through the solid and fluid separately. Volume averaging in a non-equilibrium representation of the domain is similar to the equilibrium case, however additional terms are present representing the interfacial exchange between constituents. The model is similar to that which was developed years earlier by Whitaker for drying, with the differences lying in the closure of the equations. Semi-heuristic closure is once again developed for these equations where it is important to consider the effects of excess surface accumulation, convection, diffusion, adsorption, and non-equilibrium sources when closing the equations [4].

1.2.2 Applications and modelling of porous domains in the food industry

The ability to control moisture is crucial in the food sector for many reasons. One example is in processing facilities, where a dried product is easier to mix, mill and segregate. Moisture and heat diffusion are also manipulated for sanitation, as insects and other microorganisms are destroyed at low relative humidity with accompanying temperatures at or above 60 degrees Celsius [8]. Furthermore, quality may be altered by moisture control, as certain products are dried to enhance quality, improve palatability, and increase metabolic conversions as well as digestibility. Finally,

moisture and heat manipulation have a large impact on storage life, where often a target equilibrium relative humidity (ERH) of less than 70% is desired to minimize spoilage due to insects and micro-organisms; and to reduce unfavourable oxidative and enzymatic reactions [8].

There have been many models that have been formulated to predict heat and mass transfer within stored bulk food. Initially, one dimensional models of pure heat and mass diffusion were extensively studied in the late 1960's [10]. This approach was extended to very basic modeling of air flow in sealed bins, where the domain was mapped using two dimensional finite element techniques [15]. More recent studies used finite element methods to predict streamlines of air through a three dimensional bulk media, in conjunction with a one dimensional finite difference model for determining temperature, as well as moisture changes in the air. The main issue with this modelling approach is that the prediction of streamlines is accomplished by interpolation and also, the method implies a fictitious movement of the solid as during multiple iterations of the drying period, the streamlines are adjusted[16,17]. Another method of evaluating the partial differential equations encountered in resolving transport in food stuffs is seen in the Wang et al. model extended by Tassou and Xiang [18], where a finite volume technique is presented that also includes transpiration, as well as the effect of respiration in a vegetable storage facility. Respiration effects were added utilizing a model developed by Becker et al [19], where the heat generated by the product is correlated to the rate of carbon dioxide or water production. The fluid flow in the food store, modeled similarly to a packed bed, was accounted for in the

momentum equations by using a Darcy term momentum sink to model the effects of the additional drag, which limits the model to low Reynolds numbers.

Most methods above were utilized to model small particle food bulks where large moisture and temperature gradients between the produce and fluid are not expected. With increased particle size, such as apples, or potatoes, larger gradients may exist. Yongfu Xu [10], proposed a model to simulate such particles in bulk storage of food stuffs. This implemented four transport equations to simulate three dimensional mass, momentum, energy, and mass fraction of water exchange in the macro-domain of food particle storage units. The model idealized individual bulk items (potatoes) as spherical particles to estimate moisture content, temperature difference, conductivity and moisture diffusivity, allowing local heat and mass transfer properties within the particle to be evaluated. Locally, a single particle is considered as a sphere consisting of concentric shells with negligible variation of fluid conditions around the individual particle over a time interval. Finally, the surface conditions between the macro domain and individual particle are governed by the water activity of the product, obtained experimentally. Although the governing equations were listed for flow in the overall food store, little information was given about the techniques used to resolve these equations across the domain. Also, although the model maps an individual particle to determine surface conditions for moisture exchange, the energy, and species transport across the macro-domain is not fully considered to be in local equilibrium. Finally, though the model explains multiple medium configurations (fluid, porous, solid), a conjugate framework is never analyzed.

Although all models mentioned above considered the domain to consist of spherical type products, simulations have also been conducted that consider non-spherical packing arrangements. Hoang et al [21] simulated a domain of bulk chicory roots where 3 dimensional transport of momentum, mass and energy was considered. The bulk store of chicory roots is considered to be a porous media, and the volume averaging technique was used to simulate storage conditions. A non-equilibrium approach for energy and vapour content in this model allowed the moisture content to be monitored in the solid constituent, however little detail about volume averaging of the transport equations is given. Also, although the model does show results for a conjugate domain, no mention of any special treatment at fluid porous interfaces is made for any of the equations. This model does compare simulation to experimental data, where a maximum error of 10% in measured weight loss is obtained after the initial cooling period.

The main benefits of the porous models are that all relevant variables (mass, momentum, energy, and mass fraction) are solved for, rather than models developed in the past which either study a single particle within a truncated domain, or make many simplifications of the domain. This is the advantage of volume averaging the domain, as detailed geometric dimensions of individual items are not needed; rather the domain is viewed as homogeneous with parameters accounting for the effects of the porous type structure.

1.2.3 Evaporative Cooling

Heating, Ventilation, and Air conditioning (HVAC) is a large field of Engineering with many applications. Particular interests in this field include

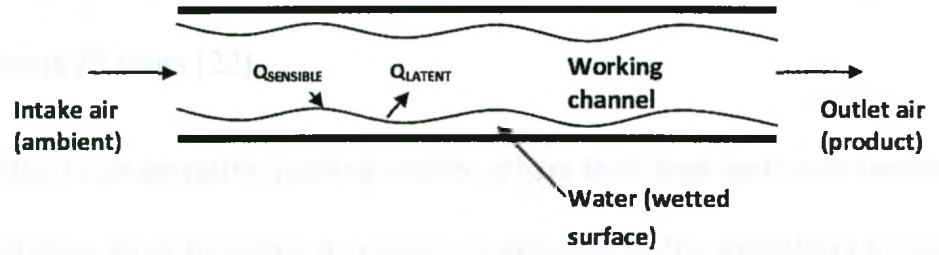

Figure 1-2 Direct evaporative cooler

Indirect evaporative cooling operates similarly to direct evaporative systems; however the working and conditioned air channels are separated. If each channel is analyzed, it is seen that the working or wet air channel functions as a direct evaporative cooler, where as the dry air channel is cooled by using a counter-flow or cross flow heat exchanger, utilizing the sensible exchange of energy through the wall that separates the two channels (Fig 1.3). This limits the amount of water vapour in the outlet air channel; unlike the direct evaporative design, to the initial specific humidity of the inlet air.

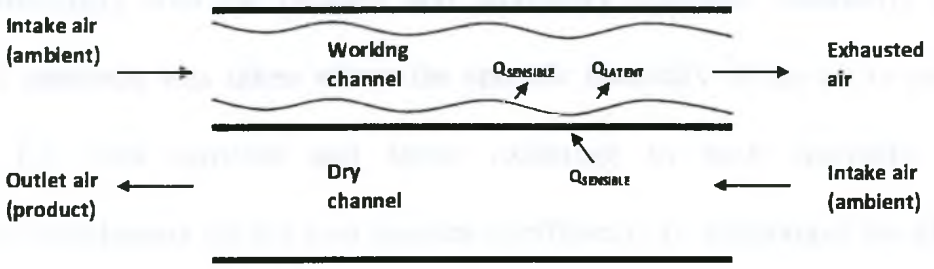

Figure 1-3 Indirect evaporative cooler

Finally, dual evaporative cooling incorporates aspects from both the direct and indirect configurations. The benefit of this approach is the ability to control the output air temperature; as well as, the amount of moisture contained in the air. With the

constant refining in manufacturing techniques, these systems have become more popular in the past 25 years [22].

Modelling of evaporative cooling cycles, where both heat and mass transfer are present in fluid flow have followed a similar progression to the modelling techniques developed for the food industry. Initial models were developed for spray evaporative cooling, where airflow would be cooled in channels, through a series of plates as it was misted with water. The modelling consisted of two approaches, the first being to evaluate the channel as a series of small sections. Each section consisted of a volume containing a plate, covered by water exposed to flowing air. Mass and energy balances were considered over each element given a known inlet condition, and summed over the domain to calculate the outlet conditions [23]. The second approach was to construct overall balances of the system, ignoring intricate transfer inside the device with the goal solely to predict the exit conditions [23]. Further development in modelling lead itself into indirect evaporative cooling, where cross flow designs were studied, considering both the primary and secondary channels. Similarly, a single dimensional approach was taken where the specific humidity of the air is neglected, accounting for both sensible and latent exchange in both channels through experimental correlations for the heat transfer coefficient. To understand the effects of latent heat transfer, additional models solved heat and mass transfer in the secondary channel developing both sensible and latent Nusselt number correlations [24]. Again, the primary focus of these models is to predict the output temperature of the system.

It is advantageous to use porous material in all types of evaporative cooling designs, as in direct applications, the increased surface area allows more contact time

between the flowing air and water enhancing mass transfer. In indirect applications, the porous materials offer the same benefits as in the direct applications, with the additional benefit of the ability to choose a material that can increase heat exchange between the primary and secondary channels. The benefits of using porous material make them desirable in evaporative cooling however makes the modeling associated with their study, more complex.

1.2.4 Summary

Porous media models have been under development for over a century. There have been many methods established to characterize the flow in this material. Early studies accounted for the effects of the media by equating the pressure drop across it to linear and quadratic bulk velocity terms. More recently, the method of volume averaging has been used as it is able to include the effects of macro gradients due to wall effects. The method of volume averaging is not restricted to mass and momentum, and can also be used to account for energy and mass fraction transport within the porous domain. This method of treating the domain allows us to simulate processes that would normally require high computational cost. For example, using porous media models in the food industry will produce methods of ensuring more accurate estimates for quality control and processing conditions. Furthermore, using porous representations of bulk food allow the overall domain to be modelled, as more direct modelling techniques aimed at simulating individual product and fluid product interaction would once again be too computationally intensive. This modelling strategy is not solely focussed on one industry, as it may be extended to evaporative cooling processes. Evaporative cooling; gaining more research interest as an environmentally

friendly method of conditioning air benefits from the use of porous materials, as with a greater surface area to volume ratios these material lead to higher mass and energy transfer rates, which allows more efficient cooling than conventional spray coolers. With these materials used in evaporative cooler configurations, the domain of interest is best modelled using a porous media modelling approach. This allows the study of direct, indirect, and more recent dual-stage configurations to be made, with goals of predicting performance and air conditions.

1.3 Objectives

As stated earlier, the aim of the present work is to extend the capability of an in-house conjugate heat/flow model to include moisture exchange such that applications in food storage/ripening and heating, ventilation, and air conditioning (HVAC) may be considered. Development of this model will follow the works of Whitaker [2, 7], where the transport equations will be volume averaged throughout the porous part of the conjugate domain. This derivation will follow a non-equilibrium approach for species and heat transfer [4, 6, 13] as this allows more versatility in the model. This non-equilibrium versatility is beneficial over traditional equilibrium approaches, as in food applications; often the product's internal moisture and temperature conditions dictate the transfer between constituents. Although this is a more versatile approach, extra transfer terms do exist between the constituents and the derivation must ensure proper representation flux between constituents.

As mentioned, the potential for the domain to consist of more than one medium type (a conjugate domain) does exist, and therefore the model must be developed such that it can resolve any interface discrepancies in the transport equations. The works of

Kaviany [4] and Betchen et al. [6] at the interface governing the discrete form of the continuity, momentum, and energy equations is to be extended to also apply to the mass fraction equations. This development will ensure that physically reasonable estimates in the computational domain over interfaces are made for pressure, velocity, temperature, and species as well as associated flux terms.

Though the model makes distinction between constituents in the fluid and porous domain, the assumption of equilibrium between species is made in this model. Therefore the water vapour and air in the fluid regions, both in and out of the porous media are assumed to be a constant temperature mixture. Additionally, the solid constituent in the porous structure is considered to be in equilibrium with any water it may contain.

In full form, the general model will predict fluid flow, temperature distributions in fluid, solid and porous domains, relative and specific humidity's, and any exchange between constituents. It is also developed as an un-steady model where the ability of studying moisture evolution within the porous media over time is possible. This work will look at the field of evaporative cooling, where configurations of cooling cycles; both direct, and indirect as well as a novel dual stage cycle will be modelled. The efficiencies of these devices will be evaluated at steady conditions and a comparison of all three styles of cooling made.

1.4 Outline of Thesis

The subsequent chapters of this thesis are organized to address the above objectives. A brief outline of the chapters are:

- *Chapter 2*: The governing equations for mass, momentum, energy, and species are introduced for a single constituent medium. The process of volume averaging is discussed where this methodology is used to investigate transport through porous media. Finally, the governing equations for transport in the porous part of the domain are presented in closed volume averaged form.
- *Chapter 3*: The finite volume method for a general conservation equation is discussed aimed at development of a computational model. The equations presented in chapter two will be discretized for each media, where any challenges in the model will be discussed and clarified.
- *Chapter 4*: As the computational model is developed for a conjugate domain, interfaces between mediums do exist. This chapter will explain the methodology of dealing with interface discrepancies in all of the transport equations.
- *Chapter 5*: This chapter will validate the code as the models discussed in the objectives section above (the evaporative cooler designs) will be modelled. Relative humidity and temperature distribution will be analyzed where efficiency will be used as a basis to compare configurations. The chapter will conclude with contributions and future steps in the project.
- *Chapter 6*: The thesis is summarized, the contributions of the thesis are stated, and future recommendations are made.

Chapter 2 - Governing Equations

2.1 Introduction

In this chapter, the governing equations for fluid flow, energy and mass transport in an arbitrary porous medium are presented. Next, the definitions and theorems that pertain to the volume-averaging method introduced in the previous chapter are presented and utilized to develop the volume-averaged equations for the conservation of mass, momentum, energy and species. The equations in this form will be left in terms of pore level spatial deviations, where closure is given from heuristic methods.

It is necessary when studying flow through porous media using a volume averaging approach, to invoke certain assumptions about the transport in the domain. The first is that the fluid being modeled is both incompressible and Newtonian. This assumption is a valid one, as most working fluids in the applications of cooling or conditioning, are air or refrigerant. The porous domain is also assumed to be spatially periodic and isotropic at the pore level. Furthermore, the assumption of constant porosity will be made. With material of roughly the same geometry, this estimate is a valid one. The previous three assumptions allow the use of the spatially-periodic boundary conditions on a representative unit cell within the domain, which are important for closing the equations. In reality, porous domains do not have perfectly periodic flow, but by properly choosing the unit cell, these assumptions lead to a good approximation of the flow characteristics. It will also be assumed that the ratio of conductive to convective resistance within the solid, characterized by the Biot number,

is quite low. The effect of this assumption for both mass and heat transfer is that the resistance to conduction/diffusion within the solid is much less than the resistance to convection across the fluid boundary layer, therefore leading to a more uniform distribution within the solid.

2.2 Governing equations in Fluid Region

The conservation of mass in the fluid region of the system assuming that the fluid is incompressible, is of the form

$$\frac{\partial \rho_f}{\partial t} + \nabla \cdot (\rho_f \mathbf{v}) = 0 . \tag{2.1}$$

Although we have considered the fluid to be incompressible, and this assumption usually warrants the transient term of equation 2.1 being neglected, this is not the case in this derivation as the density of the atmospheric air has the ability to vary mainly as a function of species content and temperature. Also, the velocity of equation 2.1 corresponds to the mass average velocity of the mixture.

The conservation of momentum for a Newtonian fluid is described by the well know Navier-Stokes equations, given in all three dimensions as

$$\frac{\partial \rho_f \mathbf{v}}{\partial t} + \nabla \cdot (\rho_f \mathbf{v}\mathbf{v}) = -\nabla p + \mu \nabla^2 \mathbf{v} + \rho_f f , \tag{2.2}$$

where ρ_f is the density of the fluid, $\mathbf{v}$ the vector of velocity, p represents the fluid pressure, μ is its dynamic viscosity, and f representing a body force per unit mass on the fluid.

Air in the atmosphere can be represented as a mixture of nitrogen, oxygen, argon, carbon dioxide, water vapour, and variations in other contaminates such as dust. Dry air refers only to the components of the gas when the contaminants and water vapour have been removed. Since the variations of these gases in the atmosphere, generally remain constant, it is convenient to treat atmospheric air solely as a mixture of dry air and water vapour with an error in this assumption of 0.2% [25]. The conservation of this binary mixture is given as

$$\frac{\partial \rho_f Y_A}{\partial t} + \nabla \cdot \left(\rho_f Y_A \mathbf{v}\right) = \nabla \cdot \left(\rho_f \mathcal{D}_{AB} \nabla Y_A\right) + S_{Y,A}\,, \tag{2.3}$$

and

$$\frac{\partial \rho_f Y_B}{\partial t} + \nabla \cdot \left(\rho_f Y_B \mathbf{v}\right) = \nabla \cdot \left(\rho_f \mathcal{D}_{BA} \nabla Y_B\right) + S_{Y,B}\,, \tag{2.4}$$

where Y_A and Y_B are the amount of water vapour and dry air present in the mixture, $\mathcal{D}_{AB} = \mathcal{D}_{BA}$, which is the binary diffusion coefficient and $S_{Y,i}$ represents the volumetric rate of production of component A or B. In a single phase, the source term will sum to zero, seen by $\sum_{i=1}^{n} S_{Y,i} = 0$. As it is only required to have two equations to solve the species and overall continuity equations, it is convenient to work with the first of the two equations, the conservation of species A, as well as overall continuity in the medium, equations 2.1, and 2.3.

Finally, considering the thermal energy equation for the fluid phase, it is desirable to refer to the works of Bird et al [26] or the work of Slattery [2,3], where it

is shown for a multi-species system, the form of the equation neglecting compressional work and viscous dissipation is

$$\frac{\partial}{\partial t}\left(\sum_{i=1}^{n}\rho_f Y_i\overline{h_i}\right)+\nabla\cdot\left(\sum_{i=1}^{n}\rho_f Y_i\mathbf{v}_i\overline{h_i}\right) \tag{2.5}$$

$$=-\nabla\cdot q_f+\sum_{i=1}^{n}\rho_i\mathbf{u}_i\cdot f_i-\rho_f\frac{D}{Dt}\sum_{i=1}^{n}\frac{1}{2}\frac{\rho_i}{\rho_f}u_i^2$$

$$+S_{energy}\,.$$

The last term in the above equation represents any possible sources of energy. Also, the second last two terms on the right side of the equation, representing the diffusive body force rate of work and the time rate of change of the diffusive kinetic energy can be safely neglected due to their magnitude, and this is given as

$$\sum_{i=1}^{n}\rho_i\mathbf{u}_i\cdot f_i=\rho_f\frac{D}{Dt}\sum_{i=1}^{n}\frac{1}{2}\frac{\rho_i}{\rho_f}u_i^2=0\,. \tag{2.6}$$

Therefore, the final form of equation 2.5 is

$$\frac{\partial}{\partial t}\left(\sum_{i=1}^{n}\rho_f Y_i\overline{h_i}\right)+\nabla\cdot\left(\sum_{i=1}^{n}\rho_f Y_i\mathbf{v}_i\overline{h_i}\right)=-\nabla\cdot q_f+S_{energy}\,. \tag{2.7}$$

Decomposing the species velocity ($\mathbf{v}_i$) into a diffusive velocity ($\mathbf{u}_i$) subtracted from the bulk velocity ($\mathbf{v}$) given as

$$\mathbf{v}_i=\mathbf{v}-\mathbf{u}_i\,, \tag{2.8}$$

along with the continuity equation and the definition

$$\rho_f h_f = \sum_{i=1}^{n} \rho_f Y_i \overline{h_i}\,, \tag{2.9}$$

equation 2.7 can be manipulated algebraically, to yield

$$\frac{\partial}{\partial t}(\rho_f h_f) + \nabla \cdot (\rho_f \mathbf{v} h_f) \tag{2.10}$$
$$= -\nabla \cdot q_f - \nabla \cdot \left(\sum_{i=1}^{n} \rho_f Y_i \mathbf{u}_i \overline{h_i} \right) + S_{energy}\,,$$

with the second last term of 2.10 representing the energy transfer associated with the species diffusion. Unlike the continuity equation, this term will not sum to zero when summed over all species due to the differing enthalpies of specie 'i'. Throughout this analysis, the assumption will be made that all enthalpy is independent of pressure, given as

$$h = h(T)\,, \tag{2.11}$$

and that the heat capacities of the fluid are constant. This latter assumption is reasonable for dry air and water vapour over a temperature range of 263.15 [K] to 323.15 [K], as it yields an error of less than 0.2% [25]. With these assumptions made, now enthalpy can be represented by

$$h = C_P T + h^{\circ}\,, \tag{2.12}$$

allowing equation 2.10, with the further use of Fourier's law, to be expressed as

$$(c_p)_f\left\{\frac{\partial}{\partial t}(\rho_f T_f)+\nabla\cdot(\rho_f \mathbf{v} T)\right\} \tag{2.13}$$

$$= k_f\nabla^2 T_f - \nabla\cdot\left(\sum_{i=1}^{n}\rho_f Y_i \mathbf{u}_i \overline{h_i}\right) - h_o\frac{\partial}{\partial t}(\rho_f Y_f)$$

$$+ S_{energy}\,.$$

where the mixture specific heat, is expressed as the product of each species specific heat and the content of the individual species in the flow, seen as

$$(c_p)_f = \sum_{i=1}^{n}\frac{\rho_i}{\rho_f}(\overline{c_p})_i = Y_A(\overline{c_p})_A + Y_B(\overline{c_p})_B\,, \tag{2.14}$$

and the term associated with the energy transfer due to diffusion of species, simplified with the use of Fick's law for binary mixtures, is given as

$$-\nabla\cdot\left(\sum_{i=1}^{n}\rho_f Y_i \mathbf{u}_i \overline{h_i}\right) = -\nabla\cdot\left(\sum_{i}^{n} -\rho_f D_i \overline{h_i}\nabla Y_i\right) \tag{2.15}$$

$$= \nabla\cdot\left(\rho_f\left(D_{AB}\overline{h_A}\nabla Y_A + D_{AB}\overline{h_B}\nabla Y_B\right)\right).$$

This gives the final form of equation 2.12 as,

$$(c_p)_f\left\{\frac{\partial}{\partial t}(\rho_f T_f)+\nabla\cdot(\rho_f \mathbf{v} T)\right\} \tag{2.16}$$

$$= k_f\nabla^2 T_f$$

$$+ \nabla\cdot\left(\rho_f\left(D_{AB}\overline{h_A}\nabla Y_A + D_{AB}\overline{h_B}\nabla Y_B\right)\right)$$

$$- h_o\frac{\partial}{\partial t}(\rho_f Y_f) - \nabla\cdot(\rho_f \mathbf{v} h_o) + S_{energy}\,.$$

In the solid region, the energy and species equations take the form of;

$$\frac{\partial \rho_f Y_S}{\partial t} = \nabla \cdot (\rho_s \mathcal{D}_s \nabla Y_S) + S_{Y,S}\,, \tag{2.17}$$

and

$$(c_p)_s \frac{\partial}{\partial t}(\rho_s T_s) \tag{2.18}$$

$$= k_s \nabla^2 T_s + \nabla \cdot \left(\sum_i^n \rho_s D_s \overline{h_S} \nabla (Y_i)_s \right) + S_{energy}\,,$$

where the species diffusion term may or may be included or not, depending on the application. Neglecting this term leads to

$$\frac{\partial \rho_f Y_S}{\partial t} = S_{Y,S}\,, \tag{2.19}$$

and

$$(c_p)_s \frac{\partial}{\partial t}(\rho_s T_s) = k_s \nabla^2 T_s + S_{energy}\,. \tag{2.20}$$

Separate equations govern transport for species content and energy in each region such that the process of volume averaging may include the effects of local non equilibrium.

2.3 Governing Equations in Porous Region

2.3.1 Volume Averaging

Volume averaging is a method whereby the differential equations given above, equations 2.1, 2.2, 2.3, 2.18, 2.19, and 2.20 are scaled such that they are representative of bulk flow through the porous region of the domain. This method was derived by Whitaker [2] and Slattery [3] independently in 1967. In the method of volume

averaging, an averaging volume $\mathcal{V}$ within the porous domain is associated with every point (both fluid and solid phases) in space, and allows an average value to be defined at every point in space. An example of an averaging volume is shown in figure 2.1a, where there exists an average value of property ψ_f assigned to its centroid, located by position vector x_f, and integration over the volume is carried out with respect to the position vector y_f which will be represented as,

$$\psi_f|_{x_f} = \frac{1}{\mathcal{V}} \int_{\mathcal{V}_f} \psi_f(x_f + y_f)\, d\mathcal{V}|_{x_f+y_f}, \tag{2.21}$$

or in a form that is more convenient to write,

$$\langle \psi_f \rangle = \frac{1}{\mathcal{V}} \int_{\mathcal{V}_f} \psi_f d\mathcal{V} \tag{2.22}$$

which represents the superficial average of property ψ_f. In the latter notation, it is implied the average of quantity $\langle \psi_f \rangle$ within the volume is associated with the volume centroid and that its integration is carried forward with respect to the position vector $x_f + y_f$ given in the former definition. Also, it must be mentioned that the averaging volume is to be much smaller than the overall system being studied in order to resolve macroscopic changes and not lead to artificial smoothing. However, the averaging volume must be large enough such that any further increases in the volume do not lead to rapid changing of property ψ_f, yielding a stationary average. This procedure of selecting an appropriate average is shown in figure 2.1b, where it is seen that the average value $\langle \psi_f \rangle$ varies less as the averaging volume increases.

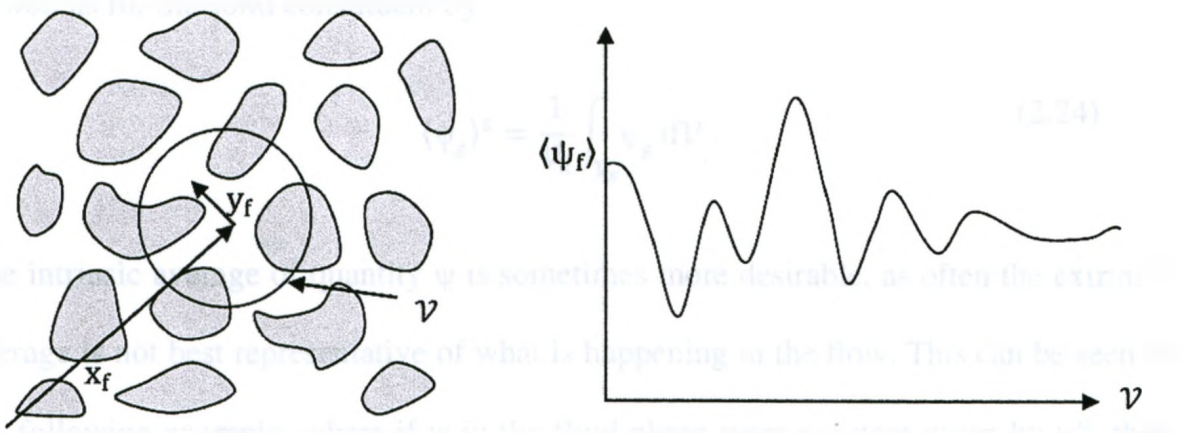

Figure 2-1 a) control volume associated with averaging and position vector located with its location b) plot of averaging quantity $\langle\psi_f\rangle$ with increasing averaging volume $\mathcal{V}$

Once again, a notable mention with regards to the above definition, is that the volume average of a transport variable (equation 2.22), is associated with the centroid of the volume. Therefore integration in the volume is carried out with respect to the components of relative position vector $x_f + y_f$, and cannot generally be considered constant within the averaging volume. This is mentioned as it relates to the evaluation of spatial averages of volume averaged quantities.

In developing the set of volume averaged transport equations, the introduction of the following theorems and definitions are necessary. To begin, the extrinsic or superficial average of a variable in the fluid phase is defined in equation 2.22. An extrinsic average of a quantity in the solid phase can be defined following a similar definition and will be represented by $\langle\psi_s\rangle$. Another type of average is the intrinsic average, defined for the fluid as

$$\langle\psi_f\rangle^f = \frac{1}{\mathcal{V}_f}\int_{\mathcal{V}_f}\psi_f \, d\mathcal{V}\,, \tag{2.23}$$

undesirable to have the volume average of the gradient or divergence operator and is more favourable to be presented with the derivative of the averaged quantity. Therefore, it is useful to present the following spatial averaging theorem [2], which can be shown in two forms, first to transform the average of the gradient

$$\langle \nabla \psi_f \rangle = \nabla \langle \psi_f \rangle + \frac{1}{\mathcal{V}} \int_{\mathcal{A}_{fs}} \psi_f \mathbf{n} d\mathcal{A} \tag{2.29}$$

and secondly, to alter the average of the divergence operator such that it becomes the divergence of the average value, seen as

$$\langle \nabla \cdot \psi_f \rangle = \nabla \cdot \langle \psi_f \rangle + \frac{1}{\mathcal{V}} \int_{\mathcal{A}_{fs}} \psi_f \cdot \mathbf{n} d\mathcal{A} \,. \tag{2.30}$$

In general ψ_f in equations 2.29, and 2.30 can be a scalar, vector or tensor of second order. The unit normal **n** given by definition is defined to be from the fluid phase directed at the solid phase. Again, the above definitions can also be applied to the solid phase.

When volume averaging the given transport equations, it is undesirable to volume average the product of multiple variables which may appear. In order to accommodate this difficulty and move forward, it is useful to follow the type of analysis used in turbulent transport, where in time averaging, velocity is decomposed into a time average and temporal deviation [2]. Therefore using a similar analogy, it is useful to decompose each transport quantity when volume averaging a product into the sum of its intrinsic average and a deviation from that average, which will be declared as $\tilde{\psi}_f$. This can be stated for a general variable in the fluid region as

$$\psi_f = \langle \psi_f \rangle^f + \tilde{\psi}_f , \tag{2.31}$$

and is identically defined in the solid region. The decomposition is then used in the volume average of the product of two variables ψ_{f1}, and ψ_{f2} to give

$$\langle \psi_{f1} \psi_{f2} \rangle = \langle \langle \psi_{f1} \rangle^f \langle \psi_{f2} \rangle^f \rangle + \langle \langle \psi_{f1} \rangle^f \tilde{\psi}_{f2} \rangle + \langle \tilde{\psi}_{f1} \langle \psi_{f2} \rangle^f \rangle + \langle \tilde{\psi}_{f1} \tilde{\psi}_{f2} \rangle . \tag{2.32}$$

Using equation 2.25 the first term of 2.32 is represented as

$$\langle \psi_{f1} \rangle^f \langle \psi_{f2} \rangle^f \big|_{x_f} = \frac{1}{\mathcal{V}} \int_{\mathcal{V}_f} \langle \psi_{f1} \rangle^f \langle \psi_{f2} \rangle^f \big|_{x_f + y_f} d\mathcal{V}|_{x_f + y_f} , \tag{2.33}$$

and if we ignore the intrinsic average of the variable within the averaging volume, we obtain

$$\langle \psi_{f1} \rangle^f \langle \psi_{f2} \rangle^f \big|_{x_f} = \langle \psi_{f1} \rangle^f \langle \psi_{f2} \rangle^f \langle 1 \rangle = \langle \psi_{f1} \rangle^f \langle \psi_{f2} \rangle^f \varepsilon . \tag{2.34}$$

Under similar length scale constraints of $\ell \ll L$, equation 2.32 becomes

$$\langle \psi_{f1} \psi_{f2} \rangle = \langle \psi_{f1} \rangle^f \langle \psi_{f2} \rangle^f \varepsilon + \langle \psi_{f1} \rangle^f \langle \tilde{\psi}_{f2} \rangle + \langle \tilde{\psi}_{f1} \rangle \langle \psi_{f2} \rangle^f + \langle \tilde{\psi}_{f1} \tilde{\psi}_{f2} \rangle . \tag{2.35}$$

It is consistent with this simplification to set the average of the spatial deviation equal to zero, seen as $\langle \tilde{\psi}_{f2} \rangle = 0$ [2]. Therefore in its final form, equation 2.35 becomes

$$\langle \psi_{f1} \psi_{f2} \rangle = \langle \psi_{f1} \rangle^f \langle \psi_{f2} \rangle^f \varepsilon + \langle \tilde{\psi}_{f1} \tilde{\psi}_{f2} \rangle , \tag{2.36}$$

which is written in terms of intrinsic averages. A similar expression is stated in terms of the macroscopic averages of ψ_{f1}, ψ_{f2} , where with the use of equation 2.27, equation 2.36 is manipulated to become

$$\langle \psi_{f1}\psi_{f2}\rangle = \langle \psi_{f1}\rangle\langle \psi_{f2}\rangle\frac{1}{\varepsilon} + \langle \widetilde{\psi}_{f1}\widetilde{\psi}_{f2}\rangle . \tag{2.37}$$

The preceding theorems and definitions allow volume averaging of the transport equations to be accomplished. The following sections will now derive the equations for transport of mass, momentum, energy and species in a porous domain given the above averaging techniques.

2.3.2 Volume Averaging of Continuity, Species and Momentum

To obtain the continuity equation, we will apply the averaging theorems above to the mixture continuity (equation 2.1), where the possibility of a mass source exists in the fluid region as we consider the solid region to be colloidal, meaning the surface contains moisture in a thin layer. Therefore

$$\left\langle \frac{\partial \rho_f}{\partial t} \right\rangle + \langle \nabla \cdot (\rho_f \mathbf{v}) \rangle = 0 \tag{2.38}$$

and examining each term individually, gives

$$\left\langle \frac{\partial \rho_f}{\partial t} \right\rangle = \frac{\partial \langle \rho_f \rangle}{\partial t} - \frac{1}{\mathcal{V}} \int_{\mathcal{A}_{fs}} \rho_f \mathbf{w} \cdot n_{fs} \, d\mathcal{A} , \tag{2.39}$$

where $\mathbf{w} \cdot n_{fs}$ represents the speed of displacement of the bulk fluid and solid interface. Furthermore, the convective term becomes

$$\langle \nabla \cdot (\rho_f \mathbf{v}) \rangle = \nabla \cdot \langle \rho_f \mathbf{v} \rangle + \frac{1}{\mathcal{V}} \int_{\mathcal{A}_{fs}} n_{fs} \cdot (\rho_f \mathbf{v}) \, d\mathcal{A} , \tag{2.40}$$

and combining the two yields

$$\frac{\partial\langle\rho_f\rangle}{\partial t} + \nabla\cdot\langle\rho_f\mathbf{v}\rangle + \frac{1}{\mathcal{V}}\int_{\mathcal{A}_{fs}} \rho_f(\mathbf{v}-\mathbf{w})\cdot n_{fs}\, d\mathcal{A} = 0\,. \tag{2.41}$$

The superficial average of density in the accumulation term is then re-arranged using equation 2.27 to give

$$\langle\rho_f\rangle = \varepsilon\langle\rho_f\rangle^f \tag{2.42}$$

and the convective transport term decomposed by using equation 2.31 to give

$$\rho_f = \langle\rho_f\rangle^f + \tilde{\rho}_f\,, \text{and} \tag{2.43a}$$

$$\mathbf{v}_f = \langle\mathbf{v}_f\rangle^f + \tilde{\mathbf{v}}_f\,, \text{and finally} \tag{2.43b}$$

$$\frac{\partial\varepsilon\langle\rho_f\rangle^f}{\partial t} + \nabla\cdot\langle\rho_f\rangle^f\langle\mathbf{v}\rangle + \nabla\cdot\langle\tilde{\rho}_f\tilde{\mathbf{v}}_f\rangle + \frac{1}{\mathcal{V}}\int_{\mathcal{A}_{fs}} \rho_f(\mathbf{v}-\mathbf{w})\cdot n_{fs}\, d\mathcal{A}. \tag{2.43c}$$

It is mentioned that the convective term is expressed in terms of the superficial average velocity, according to the following analysis:

$$\langle\langle\rho_f\rangle^f\langle\mathbf{v}\rangle^f\rangle = \langle\rho_f\rangle^f\langle\mathbf{v}\rangle^f\langle 1\rangle = \langle\rho_f\rangle^f\langle\mathbf{v}\rangle^f\varepsilon = \langle\rho_f\rangle^f\langle\mathbf{v}\rangle \tag{2.44}$$

The quantity $\tilde{\rho}_f\tilde{\mathbf{v}}_f$ is known as the dispersive flux of mass, and while the dispersion terms are often considered to be important in the species continuity equations, this term will be neglected in the total continuity [27]. The interface is assumed to be rigid as we will neglect any shrinkage due to water loss. Using this along with the no slip

condition, $v = 0$ on the interface, the integral term in equation 2.43c simplifies to zero. Therefore, in its final form, the mixture continuity is represented as

$$\frac{\partial \varepsilon \langle \rho_f \rangle^f}{\partial t} + \nabla \cdot \langle \rho_f \rangle^f \langle \mathbf{v} \rangle = \langle \dot{m} \rangle^{fs}, \tag{2.45}$$

where $\langle \dot{m} \rangle^{fs}$ in this work represents a source term due to the surface of the solid containing a thin non-varying film of vapour.

Next we will use volume averaging on the species continuity equation (equation 2.3) and this is given as;

$$\left\langle \frac{\partial \rho_f Y_A}{\partial t} \right\rangle + \langle \nabla \cdot (\rho_f Y_A \mathbf{v}) \rangle = \langle \nabla \cdot (\rho_f \mathcal{D}_{AB} \nabla Y_A) \rangle + \langle S_{Y,A} \rangle . \tag{2.46}$$

Once again, we will address each term individually, where the transient term of equation 2.46 is manipulated similarly to the transient term in the total continuity equation, becoming

$$\left\langle \frac{\partial \rho_f Y_A}{\partial t} \right\rangle = \varepsilon \frac{\partial \langle \rho_f \rangle^f \langle Y_A \rangle^f}{\partial t}, \tag{2.47}$$

and again it is assumed the interface displacement is zero. Next, we will examine the convective term, where volume averaging leads to

$$\langle \nabla \cdot (\rho_f Y_A \mathbf{v}) \rangle = \nabla \cdot \langle \rho_f Y_A \mathbf{v} \rangle + \frac{1}{\mathcal{V}} \int_{\mathcal{A}_{fs}} n_{fs} \cdot (\rho_f Y_A \mathbf{v}) \, d\mathcal{A}, \tag{2.48}$$

and the spatial decomposition for density, mass fraction, and velocity are used to yield

$$\langle \nabla \cdot (\rho_f Y_A v) \rangle \tag{2.49}$$

$$= \nabla \cdot \left(\varepsilon \langle \rho_f \rangle^f \langle Y_A \rangle^f \langle \mathbf{v} \rangle^f \right) + \nabla \cdot \left(\langle \rho_f \rangle^f \langle \widetilde{Y}_A \tilde{v} \rangle \right) + \nabla$$

$$\cdot \left(\langle \tilde{\rho}_f \tilde{v} \rangle \langle Y_A \rangle^f \right) + \frac{1}{\mathcal{V}} \int_{\mathcal{A}_{fs}} n_{fs} \cdot \left(\rho_f Y_A v \right) d\mathcal{A} .$$

Finally, the diffusive term of equation 2.46 will be examined giving

$$\langle \nabla \cdot \left(\rho_f \mathcal{D}_{AB} \nabla Y_A \right) \rangle \tag{2.50}$$

$$= \nabla \cdot \langle \rho_f \mathcal{D}_{AB} \nabla Y_A \rangle + \frac{1}{\mathcal{V}} \int_{\mathcal{A}_{fs}} n_{fs} \cdot \left(\rho_f \mathcal{D}_{AB} \nabla Y_A \right) d\mathcal{A}$$

and with use of the decomposition of density for the first term on the right side of the equal sign, this gives

$$\langle \rho_f \mathcal{D}_{AB} \nabla Y_A \rangle = \langle \langle \rho_f \rangle^f \mathcal{D}_{AB} \nabla Y_A \rangle + \langle \tilde{\rho}_f \mathcal{D}_{AB} \nabla Y_A \rangle , \tag{2.51}$$

where the variations of $\langle \rho_f \rangle^f$ and $\mathcal{D}_{AB}$ are neglected within the averaging volume [27], in order to obtain

$$\langle \rho_f \mathcal{D}_{AB} \nabla Y_A \rangle = \langle \rho_f \rangle^f \mathcal{D}_{AB} \langle \nabla Y_A \rangle + \langle \tilde{\rho}_f \mathcal{D}_{AB} \nabla Y_A \rangle . \tag{2.52}$$

It must be clarified that although the variation of $\mathcal{D}_{AB}$ and $\langle \rho_f \rangle^f$ are neglected within the averaging volume, these parameters are not necessarily constant, as this simplification does allow variations over the macroscopic region. The averaging theorem is then used on the first term to the right of the equal sign of equation 2.52 to obtain

$$\langle \rho_f \rangle^f \mathcal{D}_{AB} \langle \nabla Y_A \rangle = \langle \rho_f \rangle^f \mathcal{D}_{AB} \left(\nabla \langle Y_A \rangle + \frac{1}{\mathcal{V}} \int_{\mathcal{A}_{fs}} n_{fs} Y_A \, d\mathcal{A} \right), \tag{2.53}$$

where once again using the decomposition leads to

$$\langle \rho_f \rangle^f \mathcal{D}_{AB} \langle \nabla Y_A \rangle = \langle \rho_f \rangle^f \mathcal{D}_{AB} \left(\nabla \langle Y_A \rangle + \frac{1}{\mathcal{V}} \int_{\mathcal{A}_{fs}} n_{fs} \widetilde{Y}_A \, d\mathcal{A} \right) \tag{2.54}$$

and finally, the terms above are combined giving

$$\begin{aligned} &\langle \rho_f \mathcal{D}_{AB} \nabla Y_A \rangle \\ &= \langle \rho_f \rangle^f \mathcal{D}_{AB} \left(\nabla \langle Y_A \rangle + \frac{1}{\mathcal{V}} \int_{\mathcal{A}_{fs}} n_{fs} \widetilde{Y}_A \, d\mathcal{A} \right) \\ &+ \langle \tilde{\rho}_f \mathcal{D}_{AB} \nabla Y_A \rangle . \end{aligned} \tag{2.55}$$

Decomposing the last term in equation 2.55, and invoking certain length scale constraints [27] gives

$$\langle \tilde{\rho}_f \mathcal{D}_{AB} \nabla Y_A \rangle = \langle \tilde{\rho}_f \mathcal{D}_{AB} \nabla \widetilde{Y}_A \rangle , \tag{2.56}$$

where Whitaker and Carbonel [28] show that

$$\nabla \widetilde{Y}_A \leq O\left(\nabla \langle Y_A \rangle^f\right) \tag{2.57}$$

and that it is also plausible to assume that the spatial deviation density is constrained by

$$\tilde{\rho}_f \ll \langle \rho_f \rangle^f . \tag{2.58}$$

With equation 2.57 and 2.58, equation 2.56 becomes

$$\langle \rho_f \rangle^f \mathcal{D}_{AB} \nabla \langle Y_A \rangle \gg \langle \tilde{\rho}_f \mathcal{D}_{AB} \nabla \widetilde{Y}_A \rangle , \tag{2.59}$$

where finally $\langle \rho_f \mathcal{D}_{AB} \nabla Y_A \rangle$ is simplified to

$$\langle \rho_f \mathcal{D}_{AB} \nabla Y_A \rangle = \langle \rho_f \rangle^f \mathcal{D}_{AB} \left(\nabla \langle Y_A \rangle + \frac{1}{\mathcal{V}} \int_{\mathcal{A}_{fs}} n_{fs} \widetilde{Y}_A \, d\mathcal{A} \right). \tag{2.60}$$

The final form of the complete diffusion term from equation 2.50 is simplified to be

$$\begin{aligned} &\langle \nabla \cdot \left(\rho_f \mathcal{D}_{AB} \nabla Y_A \right) \rangle \\ &= \nabla \cdot \langle \rho_f \rangle^f \mathcal{D}_{AB} \left(\nabla \langle Y_A \rangle + \frac{1}{\mathcal{V}} \int_{\mathcal{A}_{fs}} n_{fs} \widetilde{Y}_A \, d\mathcal{A} \right) \\ &+ \frac{1}{\mathcal{V}} \int_{\mathcal{A}_{fs}} n_{fs} \cdot \left(\rho_f \mathcal{D}_{AB} \nabla Y_A \right) d\mathcal{A} . \end{aligned} \tag{2.61}$$

The surface reaction known as absorption/desorption is represented in the last term of equation 2.61 and will be designated given as $\langle \dot{m} \rangle^{fs}$. The total continuity of species A with the no-slip condition applied, as in total continuity, is expressed as

$$\begin{aligned} &\varepsilon \frac{\partial \langle \rho_f \rangle^f \langle Y_A \rangle^f}{\partial t} + \nabla \cdot \left(\varepsilon \langle \rho_f \rangle^f \langle Y_A \rangle^f \langle \mathbf{v} \rangle^f \right) \\ &= \nabla \\ &\cdot \Bigg(\langle \rho_f \rangle^f \mathcal{D}_{AB} \nabla \langle Y_A \rangle + \frac{\langle \rho_f \rangle^f \mathcal{D}_{AB}}{\mathcal{V}} \int_{\mathcal{A}_{fs}} n_{fs} \widetilde{Y}_A \, d\mathcal{A} \\ &- \langle \rho_f \rangle^f \langle \widetilde{Y}_A \tilde{v} \rangle - \langle \tilde{\rho}_f \tilde{v} \rangle \langle Y_A \rangle^f \Bigg) + \langle \dot{m} \rangle^{fs} \end{aligned} \tag{2.62}$$

where written in its final form, similar to the expression developed by Kaviany [4]

$$\begin{aligned} &\varepsilon \frac{\partial \langle \rho_f \rangle^f \langle Y_A \rangle^f}{\partial t} + \nabla \cdot \left(\varepsilon \langle \rho_f \rangle^f \langle Y_A \rangle^f \langle \mathbf{v} \rangle^f \right) \\ &= \nabla \cdot D_{eff,A} \langle \rho_f \rangle^f \cdot \nabla \langle Y_A \rangle + \langle \dot{m} \rangle^{fs} . \end{aligned} \tag{2.63}$$

$D_{eff,A}$ represents the total effective mass diffusivity tensor, and represents the combined effects of the effective diffusivity and dispersion in the fluid, represented by

$$D_{eff,A} = D_{AB,eff} + D_{AB}^{dispersion} . \tag{2.64}$$

The continuity for species A within the solid constituent is found similarly to equation 2.63, and given as

$$\varepsilon \frac{\partial \langle \rho_f \rangle^s \langle Y_A \rangle^s}{\partial t} = \nabla \cdot D_{efs,A} \langle \rho_f \rangle^s \cdot \nabla \langle Y_A \rangle^s - \langle \dot{m} \rangle^{fs} . \tag{2.65}$$

Finally, volume averaging of the momentum equations (equation 2.2) leads to

$$\left\langle \frac{\partial \rho_f \mathbf{v}}{\partial t} \right\rangle + \langle \nabla \cdot (\rho_f \mathbf{v}\mathbf{v}) \rangle = -\langle \nabla p \rangle + \langle \mu \nabla^2 \mathbf{v} \rangle + \langle \rho_f f \rangle, \tag{2.66}$$

and again noting that the solid constituent is rigid and given the constraints of the density and velocity deviations, the transient term, similar to the species continuity equation is re-written as

$$\left\langle \frac{\partial \rho_f \mathbf{v}}{\partial t} \right\rangle = \frac{\partial \langle \rho_f \rangle^f \langle \mathbf{v} \rangle}{\partial t} . \tag{2.67}$$

Next, averaging the convective term with the use of the spatial decomposition leads to

$$\langle \nabla \cdot (\rho_f \mathbf{v}\mathbf{v}) \rangle = \nabla \cdot \left(\langle \rho_f \rangle^f \langle \mathbf{v} \rangle \langle \mathbf{v} \rangle^f \right) + \nabla \cdot \left(\langle \rho_f \rangle^f \langle \tilde{\mathbf{v}}\tilde{\mathbf{v}} \rangle \right), \tag{2.68}$$

where the last term on the right of equation 2.68 only exists, if a macroscopic gradient in the flow field is present. This is the case near bounding walls, where the macroscopic convective term does not capture the additional momentum transport of the interaction of the pore level deviations with themselves.

Volume averaging the pressure term, and expressing the pressure in terms of the intrinsic average leads to

$$\langle \nabla p \rangle = \varepsilon \nabla \langle p \rangle^f + \frac{1}{\mathcal{V}} \int_{\mathcal{A}_{fs}} n_{fs} p \, d\mathcal{A} \, . \tag{2.69}$$

Once again, the spatial decomposition for pressure is used for the integral term

$$\langle \nabla p \rangle = \varepsilon \nabla \langle p \rangle^f + \frac{1}{\mathcal{V}} \int_{\mathcal{A}_{fs}} n_{fs} \langle p \rangle^f \, d\mathcal{A} + \frac{1}{\mathcal{V}} \int_{\mathcal{A}_{fs}} n_{fs} \tilde{p} \, d\mathcal{A} \tag{2.70}$$

and using the length scale constraints that l<<L, then

$$\langle \nabla p \rangle = \varepsilon \nabla \langle p \rangle^f + \frac{\langle p \rangle^f}{\mathcal{V}} \int_{\mathcal{A}_{fs}} n_{fs} \, d\mathcal{A} + \frac{1}{\mathcal{V}} \int_{\mathcal{A}_{fs}} n_{fs} \tilde{p} \, d\mathcal{A} \, , \tag{2.71}$$

where it can be shown by setting $\psi = 1$ that the fist integral term simplifies to zero, assuming no variation in porosity and making use of the spatial averaging theorem of equation 2.29. This is shown as;

$$\langle \nabla 1 \rangle = \nabla \langle 1 \rangle + \frac{1}{\mathcal{V}} \int_{\mathcal{A}_{fs}} (1) \mathbf{n} d\mathcal{A} \tag{2.72}$$

Or with further simplification,

$$\frac{1}{\mathcal{V}} \int_{\mathcal{A}_{fs}} (1) \mathbf{n} d\mathcal{A} = 0 \, . \tag{2.73}$$

The pressure term in the momentum equation is now expressed as

$$\langle \nabla p \rangle = \varepsilon \nabla \langle p \rangle^f + \frac{1}{\mathcal{V}} \int_{\mathcal{A}_{fs}} n_{fs} \tilde{p} \, d\mathcal{A} \, . \tag{2.74}$$

The last term on the right side of equation 2.74 represents the effect of pore level deviations causing an additional pressure force. The viscous term is handled similarly to the diffusive term in the species equation, which leads to

$$\langle \mu \nabla^2 \mathbf{v} \rangle = \mu \nabla^2 \langle \mathbf{v} \rangle + \frac{\mu}{\mathcal{V}} \int_{\mathcal{A}_{fs}} n_{fs} \cdot \nabla \tilde{\mathbf{v}} \, d\mathcal{A} \, , \tag{2.75}$$

where the integral term accounts for the additional viscous forces at the fluid solid interface due to the no-slip condition, and the first term accounts for the macroscopic velocity gradients due to, for example, macroscopic boundary layers. Therefore the momentum equation is stated as

$$\begin{aligned} &\frac{\partial \langle \rho_f \rangle \langle \mathbf{v} \rangle}{\partial t} + \frac{1}{\varepsilon} \nabla \cdot \left(\langle \rho_f \rangle \langle \mathbf{v} \rangle \langle \mathbf{v} \rangle \right) + \nabla \cdot \left(\langle \rho_f \rangle^f \langle \tilde{\mathbf{v}} \tilde{\mathbf{v}} \rangle \right) \\ &\quad = -\varepsilon \nabla \langle p \rangle^f + \mu \nabla^2 \langle \mathbf{v} \rangle \\ &\quad + \frac{1}{\mathcal{V}} \int_{\mathcal{A}_{fs}} n_{fs} \{ -\mathbf{I} \tilde{p} + \mu \nabla \tilde{\mathbf{v}} \} \, d\mathcal{A} \, , \end{aligned} \tag{2.76}$$

where **I** represents the unit vector.

2.3.3 Volume Averaging of Energy Equations

The energy equations will now be averaged for both the fluid and solid constituent. The equations are volume averaged with many of the theories and simplifications demonstrated in the continuity, species and momentum equations and are averaged under the same length scale restrictions. With the use of equation 2.16, this leads to

$$\left\langle \frac{\partial}{\partial t}\left(\rho_f h_f\right)\right\rangle + \left\langle \nabla \cdot \left(\rho_f \mathbf{v} h_f\right)\right\rangle \tag{2.77}$$

$$= -\langle \nabla \cdot q_f \rangle - \left\langle \nabla \cdot \left(\sum_{i=1}^{n} \rho_f Y_i \mathbf{u}_i \overline{h_i} \right) \right\rangle + \langle S_{energy} \rangle .$$

As in the governing equations for the fluid above, the enthalpies are represented using the form of equations 2.9, and 2.12. Therefore the transient term with a rigid interface becomes

$$\left\langle \frac{\partial}{\partial t}\left(\rho_f h_f\right)\right\rangle = \sum_{i}^{n} \frac{\partial}{\partial t} \langle \rho_{f,i} \left(c_p\right)_{f,i} T_f \rangle + \sum_{i}^{n} \frac{\partial}{\partial t} \langle h_i^{\circ} \rho_{f,i} \rangle \tag{2.78}$$

where the last term on the right of equation 2.78 represents the sum of each species reference state enthalpy. Noting that the heat capacity and reference enthalpy of species 'i' remains constant, the first term is re-arranged using the spatial decomposition to yield

$$\sum_{i}^{n} \frac{\partial}{\partial t} \langle \rho_{f,i} \left(c_p\right)_{f,i} T_f \rangle \tag{2.79}$$

$$= \sum_{i}^{n} \varepsilon \left(c_p\right)_{f,i} \frac{\partial}{\partial t} \langle \rho_{f,i} \rangle^f \langle T_f \rangle^f + \sum_{i}^{n} \left(c_p\right)_{f,i} \frac{\partial}{\partial t} \langle \tilde{\rho}_{f,i} \widetilde{T}_f \rangle ,$$

where the final form of the transient term is

$$\left\langle \frac{\partial}{\partial t}\left(\rho_f h_f\right)\right\rangle \tag{2.80}$$

$$= \sum_{i}^{n} \left(\varepsilon \left(c_p\right)_{f,i} \frac{\partial}{\partial t} \left(\langle \rho_{f,i} \rangle^f \langle T_f \rangle^f \right) + \varepsilon h_i^{\circ} \frac{\partial}{\partial t} \langle \rho_{f,i} \rangle^f \right.$$

$$\left. + \left(c_p\right)_{f,i} \frac{\partial}{\partial t} \langle \tilde{\rho}_{f,i} \widetilde{T}_f \rangle \right) .$$

The convective component with the no slip condition at the fluid solid interface is now manipulated to give

$$\langle \nabla \cdot (\rho_f \mathbf{v} h_f) \rangle = \sum_i^n \nabla \cdot \langle \rho_{f,i} \mathbf{v} (c_p)_{f,i} T_f \rangle + \sum_i^n \nabla \cdot \langle h_i^o \rho_{f,i} \mathbf{v} \rangle , \tag{2.81}$$

where the specific heat, as well as the reference enthalpy of species i may be taken out of the integral to yield

$$\langle \nabla \cdot (\rho_f \mathbf{v} h_f) \rangle = \sum_i^n (c_p)_{f,i} \nabla \cdot \langle \rho_{f,i} \mathbf{v} T_f \rangle + \sum_i^n h_i^o \nabla \cdot \langle \rho_{f,i} \mathbf{v} \rangle . \tag{2.82}$$

Using the spatial decomposition, and keeping in mind that deviation terms are constrained by

$$\tilde{T}_f \ll \langle T_f \rangle^f \qquad \tilde{\rho}_f \ll \langle \rho_f \rangle^f \qquad \tilde{\mathbf{v}} \leq O(\langle \mathbf{v} \rangle^f) , \tag{2.83}$$

the convective term becomes

$$\begin{aligned} &\langle \nabla \cdot (\rho_f \mathbf{v} h_f) \rangle \\ &= \sum_i^n \Big\{ (c_p)_{f,i} \nabla \\ &\quad \cdot \left(\langle \rho_{f,i} \rangle^f \langle \mathbf{v} \rangle \langle T_f \rangle^f + \langle \rho_{f,i} \rangle^f \langle \tilde{T}_f \tilde{\mathbf{v}} \rangle + \langle \tilde{\rho}_{f,i} \tilde{\mathbf{v}} \rangle \langle T_f \rangle^f \right) \\ &\quad + h_i^o \nabla \cdot \left(\langle \rho_{f,i} \rangle^f \langle \mathbf{v} \rangle + \langle \tilde{\rho}_{f,i} \tilde{\mathbf{v}} \rangle \right) \Big\} . \end{aligned} \tag{2.84}$$

The conduction term is averaged and presented as

$$\langle \nabla \cdot q_f \rangle = \langle k_f \nabla^2 T_f \rangle \tag{2.85}$$

$$= \nabla \cdot k_f \left(\nabla \langle T_f \rangle + \frac{1}{\mathcal{V}} \int_{\mathcal{A}_{fs}} n_{fs} \widetilde{T}_f \, d\mathcal{A} \right)$$

$$+ \frac{1}{\mathcal{V}} \int_{\mathcal{A}_{fs}} n_{fs} \cdot (k_f \nabla T_f) \, d\mathcal{A} \, ,$$

with the last term in equation representing the conduction per unit volume through the fluid solid interface. Finally, the energy associated with the diffusion of each species is given as

$$\langle \nabla \cdot \left(\sum_{i=1}^{n} \rho_{f,i} \mathbf{u}_i \overline{h_i} \right) \rangle \tag{2.86}$$

$$= \sum_{i=1}^{n} \left\{ (c_p)_i \nabla \cdot \langle \rho_{f,i} \mathbf{u}_i T_f \rangle + h_i^o \nabla \cdot \langle \rho_{f,i} \mathbf{u}_i \rangle \right\}$$

$$+ \sum_{1}^{n} \left\{ \frac{1}{\mathcal{V}} \int_{\mathcal{A}_{fs}} n_{fs} \cdot \left((c_p)_i \left(\rho_{f,i} \mathbf{u}_i T_f \right) \right) d\mathcal{A} \right.$$

$$\left. + \frac{1}{\mathcal{V}} \int_{\mathcal{A}_{fs}} n_{fs} \cdot \left(h_i^o \left(\rho_{f,i} \mathbf{u}_i \right) \right) d\mathcal{A} \right\} ,$$

where the last two terms in equation 2.86 represent the diffusion of energy per unit volume through the fluid solid interface due to species transfer. The second term after the equal sign of equation 2.86, within the first summation bracket is identical to the diffusion term in the species continuity equation (equation 2.63) and volume averaging it will not be re-iterated. The first term following the equal sign within the summation bracket of equation 2.86 is decomposed to give

$$\langle \rho_{f,i} \mathbf{u}_i T_f \rangle = \langle \rho_{f,i} \mathbf{u}_i \langle T_f \rangle^f \rangle + \langle \rho_{f,i} \mathbf{u}_i \widetilde{T}_f \rangle \, . \tag{2.87}$$

Each term on the right side of equation 2.87 will now be examined individually, where Fick's law will be made use of to simplify $\rho_{f,i}\mathbf{u}_i$. Ignoring the variation of $\langle T_f \rangle^f$ within the averaging volume due to length scale constraints, the first term becomes

$$\langle \rho_{f,i}\mathbf{u}_i \langle T_f \rangle^f \rangle = \langle \rho_{f,i}\mathbf{u}_i \rangle \langle T_f \rangle^f = \langle \rho_f \mathcal{D}_{AB} \nabla Y_i \rangle \langle T_f \rangle^f . \tag{2.88}$$

Using the same arguments as in the species continuity equation (equation 2.87), equation 2.88 is simplified to

$$\begin{aligned} &\langle \rho_f \mathcal{D}_{AB} \nabla Y_i \rangle \langle T_f \rangle^f \\ &= \mathcal{D}_{AB} \left\{ \langle \rho_f \rangle^f \left(\nabla \langle Y_i \rangle + \frac{1}{\mathcal{V}} \int_{\mathcal{A}_{fs}} n_{fs} \widetilde{Y}_i \, d\mathcal{A} \right) \langle T_f \rangle^f \right. \\ &\left. + \langle \tilde{\rho}_f \nabla \widetilde{Y}_i \rangle \langle T_f \rangle^f \right\} . \end{aligned} \tag{2.89}$$

The second term in equation 2.87 is again converted using Fick's law to be

$$\langle \rho_{f,i}\mathbf{u}_i \widetilde{T}_f \rangle = \langle \rho_f \mathcal{D}_{AB} \nabla Y_i \widetilde{T}_f \rangle. \tag{2.90}$$

The spatial decomposition of density is now needed, where neglecting the deviation of $\langle \rho_f \rangle^f$ and $\mathcal{D}_{AB}$ within the averaging volume once again gives

$$\langle \rho_f \mathcal{D}_{AB} \nabla Y_i \widetilde{T}_f \rangle = \mathcal{D}_{AB} \left(\langle \rho_f \rangle^f \langle \nabla Y_i \widetilde{T}_f \rangle + \langle \tilde{\rho}_f \nabla Y_i \widetilde{T}_f \rangle \right) . \tag{2.91}$$

This process is repeated once more for the gradient of the mass fraction to give

$$\langle \rho_f \mathcal{D}_{AB} \nabla Y_i \widetilde{T}_f \rangle \tag{2.92}$$

$$= \mathcal{D}_{AB} \left(\langle \rho_f \rangle^f \nabla \langle Y_i \rangle^f \langle \widetilde{T}_f \rangle + \langle \rho_f \rangle^f \langle \nabla \widetilde{Y}_i \widetilde{T}_f \rangle \right.$$

$$\left. + \langle \tilde{\rho}_f \widetilde{T}_f \rangle \nabla \langle Y_i \rangle^f + \langle \tilde{\rho}_{f_f} \nabla \widetilde{Y}_i \widetilde{T}_f \rangle \right).$$

The two components of equation 2.88 are re-assembled and this takes the form

$$\langle \rho_{f,i} \mathbf{u}_i T_f \rangle = \mathcal{D}_{AB} \left\{ \langle \rho_f \rangle^f \left(\nabla \langle Y_i \rangle + \frac{1}{\mathcal{V}} \int_{\mathcal{A}_{fs}} n_{fs} \widetilde{Y}_i \, d\mathcal{A} \right) \langle T_f \rangle^f \right. \tag{2.93}$$

$$\left. + \langle \tilde{\rho}_{f_f} \nabla \widetilde{Y}_i \rangle \langle T_f \rangle^f \right\}$$

$$+ \mathcal{D}_{AB} \{ \langle \rho_f \rangle^f \nabla \langle Y_i \rangle^f \langle \widetilde{T}_f \rangle + \langle \rho_f \rangle^f \langle \nabla \widetilde{Y}_i \widetilde{T}_f \rangle + \langle \tilde{\rho}_f \widetilde{T}_f \rangle \nabla \langle Y_i \rangle^f$$

$$+ \langle \tilde{\rho}_f \nabla \widetilde{Y}_i \widetilde{T}_f \rangle \}.$$

Using the constraint on deviations terms, given by

$$\widetilde{T}_f \ll \langle T_f \rangle^f \qquad \tilde{\rho}_f \ll \langle \rho_f \rangle^f \qquad \nabla \widetilde{Y}_i \leq O\left(\nabla \langle Y_i \rangle^f \right) \tag{2.94}$$

allows equation 2.93 to be simplified to

$$\langle \rho_{f,i} \mathbf{u}_i T_f \rangle = \mathcal{D}_{AB} \left\{ \langle \rho_f \rangle^f \left(\nabla \langle Y_i \rangle + \frac{1}{\mathcal{V}} \int_{\mathcal{A}_{fs}} n_{fs} \widetilde{Y}_i \, d\mathcal{A} \right) \langle T_f \rangle^f \right\}. \tag{2.95}$$

Finally, the energy term associated with the diffusion of species is given as

$$\langle \nabla \cdot \left(\sum_{i=1}^{n} \rho_{f,i} \mathbf{u}_i \overline{h_i} \right) \rangle \tag{2.96}$$

$$= \mathcal{D}_{AB} \sum_{i=1}^{n} \nabla$$

$$\cdot \left[(c_p)_{f,i} \langle \rho_f \rangle^f \nabla \langle Y_i \rangle \langle T_f \rangle^f + \frac{(c_p)_{f,i} \langle \rho_f \rangle^f \langle T_f \rangle^f}{\mathcal{V}} \int_{\mathcal{A}_{fs}} n_{fs} \widetilde{Y}_i \, d\mathcal{A} + h_i^o \langle \rho_f \rangle^f \nabla \langle Y_A \rangle \right.$$

$$\left. + \frac{h_i^o \langle \rho_f \rangle^f}{\mathcal{V}} \int_{\mathcal{A}_{fs}} n_{fs} \widetilde{Y}_i \, d\mathcal{A} \right]$$

$$+ \sum_{1}^{n} \left\{ \frac{1}{\mathcal{V}} \int_{\mathcal{A}_{fs}} n_{fs} \cdot \left((c_p)_i \left(\rho_{f,i} \mathbf{u}_i T_f \right) \right) d\mathcal{A} + \frac{1}{\mathcal{V}} \int_{\mathcal{A}_{fs}} n_{fs} \cdot \left(h_i^o \left(\rho_{f,i} \mathbf{u}_i \right) \right) d\mathcal{A} \right\}.$$

The energy equation for the fluid phase is now presented in its volume averaged form as

(2.97)

$$\sum_{i}^{n} \left(\varepsilon (c_p)_{f,i} \frac{\partial}{\partial t} \left(\langle \rho_{f,i} \rangle^f \langle T_f \rangle^f \right) + \varepsilon h_i^o \frac{\partial}{\partial t} \langle \rho_{f,i} \rangle^f \right) + \sum_{i}^{n} \left\{ (c_p)_{f,i} \nabla \cdot \left(\langle \rho_{f,i} \rangle^f \langle \mathbf{v} \rangle \langle T_f \rangle^f \right) \right.$$

$$\left. + h_i^o \nabla \cdot \left(\langle \rho_{f,i} \rangle^f \langle \mathbf{v} \rangle \right) \right\}$$

$$= \nabla$$

$$\cdot \left(\varepsilon k_f \nabla \langle T_f \rangle^f + \frac{k_f}{\mathcal{V}} \int_{\mathcal{A}_{fs}} n_{fs} \widetilde{T}_f \, d\mathcal{A} - (c_p)_{f,i} \langle \rho_{f,i} \rangle^f \langle \widetilde{T}_f \widetilde{\mathbf{v}} \rangle - (c_p)_{f,i} \langle \widetilde{\rho}_{f,i} \widetilde{\mathbf{v}} \rangle \langle T_f \rangle^f \right.$$

$$\left. - h_i^o \langle \widetilde{\rho}_{f,i} \widetilde{\mathbf{v}} \rangle \right)$$

$$+ \sum_{i=1}^{n} \nabla \cdot \left[\varepsilon \mathcal{D}_{AB} (c_p)_{f,i} \langle \rho_f \rangle^f \nabla \langle Y_i \rangle^f \langle T_f \rangle^f + \frac{\mathcal{D}_{AB} (c_p)_{f,i} \langle \rho_f \rangle^f \langle T_f \rangle^f}{\mathcal{V}} \int_{\mathcal{A}_{fs}} n_{fs} \widetilde{Y}_i \, d\mathcal{A} \right.$$

$$\left. + \varepsilon \mathcal{D}_{AB} h_i^o \langle \rho_f \rangle^f \nabla \langle Y_i \rangle^f + \frac{\mathcal{D}_{AB} h_i^o \langle \rho_f \rangle^f}{\mathcal{V}} \int_{\mathcal{A}_{fs}} n_{fs} \widetilde{Y}_i \, d\mathcal{A} \right] + \frac{1}{\mathcal{V}} \int_{\mathcal{A}_{fs}} n_{fs} \cdot (k_f \nabla T_f) \, d\mathcal{A}$$

$$+ \sum_{1}^{n} \left\{ \frac{1}{\mathcal{V}} \int_{\mathcal{A}_{fs}} n_{fs} \cdot \left((c_p)_{f,i} \left(\rho_{f,i} \mathbf{u}_i T_f \right) \right) d\mathcal{A} + \frac{1}{\mathcal{V}} \int_{\mathcal{A}_{fs}} n_{fs} \cdot \left(h_i^o \left(\rho_{f,i} \mathbf{u}_i \right) \right) d\mathcal{A} \right\},$$

where the constraints of the temperature and density deviation have been used to reduce the transient term. The same procedure in volume averaging the solid phase energy equation is preformed and given as,

$$\sum_{i}^{n}\left((1-\varepsilon)(c_p)_{s,i}\frac{\partial}{\partial t}\left(\langle\rho_{s,i}\rangle\langle T_s\rangle^s\right)+(1-\varepsilon)h_i^o\frac{\partial}{\partial t}\langle\rho_{s,i}\rangle^s\right) \tag{2.98}$$

$$= \nabla\cdot\left((1-\varepsilon)k_s\nabla\langle T_s\rangle^s-\frac{k_s}{\mathcal{V}}\int_{\mathcal{A}_{fs}}n_{fs}\widetilde{T}_s\,d\mathcal{A}\right)$$

$$+\sum_{i=1}^{n}\nabla$$

$$\cdot\left[(1-\varepsilon)\mathcal{D}_{AB}\rho_s(c_p)_{s,i}\nabla\langle Y_i\rangle^s\langle T_s\rangle^s-\frac{\mathcal{D}_{AB}\rho_s(c_p)_{s,i}\langle T_s\rangle^s}{\mathcal{V}}\int_{\mathcal{A}_{fs}}n_{fs}\widetilde{Y}_i\,d\mathcal{A}\right.$$

$$\left.+(1-\varepsilon)\mathcal{D}_{AB}\rho_s h_i^o\nabla\langle Y_i\rangle^s-\frac{\mathcal{D}_{AB}h_i^o\rho_s}{\mathcal{V}}\int_{\mathcal{A}_{fs}}n_{fs}\widetilde{Y}_i\,d\mathcal{A}\right]-\frac{1}{\mathcal{V}}\int_{\mathcal{A}_{fs}}n_{fs}\cdot(k_s\nabla T_s)\,d\mathcal{A}$$

$$-\sum_{1}^{n}\left\{\frac{1}{\mathcal{V}}\int_{\mathcal{A}_{fs}}n_{fs}\cdot\left((c_p)_{s,i}\left(\rho_{s,i}u_iT_s\right)\right)d\mathcal{A}\right.$$

$$\left.+\frac{1}{\mathcal{V}}\int_{\mathcal{A}_{fs}}n_{fs}\cdot\left(h_i^o\left(\rho_{s,i}u_i\right)\right)d\mathcal{A}\right\}$$

where the fluctuations in total density are not considered within the solid phase and it is mentioned that the direction of the normal n_{fs}, is represented in the negative sign in front of integral terms.

2.4 Closed form of equations

Although the equations presented in the above sections are volume averaged, they are not yet useful for a macro-scale computational model as terms exist that require pore level resolution. Heuristic closure is studied in the works of [2, 4, 5, 6, 7] where these terms may be grouped together and correlations used to represent them.

This is not the aim of this work, however the closed form of the equations will be needed for chapter 3, and therefore all equations in the porous region are given as:

$$\frac{\partial \varepsilon \langle \rho_f \rangle^f}{\partial t} + \nabla \cdot \langle \rho_f \rangle^f \langle \mathbf{v} \rangle = \langle \dot{n}_i \rangle^{fs} \tag{2.98}$$

$$\varepsilon \frac{\partial \langle \rho_f \rangle^f \langle Y_A \rangle^f}{\partial t} + \nabla \cdot \left(\langle \rho_f \rangle^f \langle Y_A \rangle^f \langle \mathbf{v} \rangle \right) = \nabla \cdot \mathcal{D}_{eff,f} \langle \rho_f \rangle^f \cdot \nabla \langle Y_A \rangle + \langle \dot{n}_i \rangle^{fs} \tag{2.99}$$

$$\begin{aligned} &\frac{\varepsilon\, \partial \langle \rho_f \rangle^f \langle \mathbf{v} \rangle}{\partial t} + \frac{1}{\varepsilon} \nabla \cdot \left(\langle \rho_f \rangle^f \langle \mathbf{v} \rangle \langle \mathbf{v} \rangle \right) \\ &\quad = -\varepsilon \nabla \langle p \rangle^f + \mu_B \nabla^2 \langle \mathbf{v} \rangle - \frac{\varepsilon \mu_B}{K} \langle \mathbf{v} \rangle - \frac{\varepsilon \langle \rho_f \rangle^f C_E}{\sqrt{K}} |\langle \mathbf{v} \rangle| \langle \mathbf{v} \rangle \\ &\quad + \varepsilon \langle \rho_f \rangle^f \mathbf{f} \end{aligned} \tag{2.100}$$

$$\begin{aligned} &\sum_i^2 \left(\varepsilon (c_p)_{f,i} \frac{\partial}{\partial t} \left(\langle \rho_{f,i} \rangle^f \langle T_f \rangle^f \right) + \varepsilon h_i^o \frac{\partial}{\partial t} \langle \rho_{f,i} \rangle^f \right) \\ &\quad + \sum_i^2 \left\{ (c_p)_{f,i} \nabla \cdot \left(\langle \rho_{f,i} \rangle^f \langle \mathbf{v} \rangle \langle T_f \rangle^f \right) \right. \\ &\left. + h_i^o \nabla \cdot \left(\langle \rho_{f,i} \rangle^f \langle \mathbf{v} \rangle \right) \right\} \\ &\quad = \nabla \cdot \left(\varepsilon k_{eff,f} \nabla \langle T_f \rangle^f \right) \\ &\quad + \sum_{i=1}^2 \nabla \cdot \left[\mathcal{D}_{eff,f} (c_p)_{f,i} \langle \rho_f \rangle^f \nabla \langle Y_i \rangle^f \langle T_f \rangle^f + \mathcal{D}_{eff,f} h_i^o \langle \rho_f \rangle^f \nabla \langle Y_i \rangle^f \right] \\ &\quad + h_{fs} A_{fs} \left(\langle T_f \rangle_P^s - \langle T_f \rangle_P^f \right) - h_A A_{fs} \langle \dot{n}_i \rangle^{fs}, \end{aligned} \tag{2.101}$$

$$(1 - \varepsilon) \frac{\partial \langle \rho_f \rangle^s \langle Y_A \rangle^s}{\partial t} = \nabla \cdot \mathcal{D}_{eff,S} \langle \rho_s \rangle^s \cdot \nabla \langle Y_A \rangle^s - \langle \dot{n}_i \rangle^{fs} \tag{2.102}$$

$$\sum_{i}^{2}\left((1-\varepsilon)(c_p)_{s,i}\frac{\partial}{\partial t}\left(\langle\rho_{s,i}\rangle^s\langle T_s\rangle^s\right)+(1-\varepsilon)h_i^o\frac{\partial}{\partial t}\langle\rho_{s,i}\rangle^s\right) \tag{2.103}$$
$$=\nabla\cdot\left((1-\varepsilon)k_{eff,s}\nabla\langle T_s\rangle^s\right)$$
$$+\sum_{i=1}^{2}\nabla\cdot\Big[(1-\varepsilon)D_{eff,s}\langle\rho_{s,i}\rangle^s(c_p)_{s,i}\nabla\langle Y_i\rangle^s\langle T_s\rangle^s$$
$$+(1-\varepsilon)\mathcal{D}_{eff,s}\langle\rho_{s,i}\rangle^s h_i^o\nabla\langle Y_i\rangle^s-h_{fs}A_{fs}(\langle T_f\rangle_P^s-\langle T_f\rangle_P^f)+h_A A_{fs}\langle\dot{n}_i\rangle^{fs}\Big]$$

where momentum has been heuristically closed using the familiar Darcy and Forchheimer terms, and the effective components k_{eff} and $\mathcal{D}_{eff}$ in the species and energy equations account for the stagnant portion of diffusion and may also account for the effects of dispersion. This formulation of the governing equations is limited to applications where correlations for the effective properties and the additional coefficients have been studied, as heuristic closure determines these parameters.

2.5 Summary

A complete set of equations for continuity, species, momentum and energy conservation have now been presented for the fluid, porous and solid regions. In full form, the equations contain terms that require information about pore level fluctuations which is not the goal of this work nor is desirable. In fact, the method of volume averaging was developed to avoid computations of pore level flow and thus, these terms must be eliminated. The method used to close these terms is described in the literature review section where the equations are shown to be heuristically closed. The next chapter shows the numerical implementation of the closed form of the transport equations presented in this section.

Chapter 3 - Numerical Methods

3.1 Introduction

This chapter describes the numerical methods selected to solve for the governing equations derived in the previous chapter. Initially, the discretization of a general transport equation, including the transient, convective, and diffusive terms will be addressed using a finite volume technique. Additionally, volumetric source terms may exist in these equations and their general discretization will be presented. The finite volume implementation is chosen as a discretization method, as it has the advantage of being fully conservative. It is assumed that the generalized form of the discrete equation presented up to this point is developed under the assumption of a known velocity field; however in general, the solution procedure requires that the flow field be computed. To solve for this field, the continuity and momentum equations are also developed using the general finite volume discretization, however the development of these equations require special attention as both pressure and velocities are unknown. This special treatment is demonstrated through the concept of pressure-velocity coupling, as it is used to maintain coupling between the continuity and momentum equations.

Having established a finite volume approach for a general transport equation, this methodology is utilized to discretize the mass, momentum, energy, and species conservation equations. Each transport equation is presented in its discrete form for the pure fluid, porous, and pure solid domain types, where focus is brought to any additional terms not seen in previous models. These terms are attributed to the water vapour component of the air mixture.

To conclude this chapter, the solution approach to the system of equations is presented, focusing mainly on any modifications encountered due to the addition of a mass fraction equation. In this section, explanation on how the assembled matrices are solved is given. Additionally, it is shown how parameters dependent on the solution field are re-computed, and finally tolerance criteria that govern the solutions are explained.

3.2 Discretization of a General Transport Equation

The computational fluid dynamics model implemented is based upon the finite volume discretization described by Patankar [29]. This method subdivides the domain into multiple control volumes that do not overlap. The transport equations listed in the previous chapter are integrated over a control volume and solved at discrete locations, as opposed to all locations in the domain. There are benefits to choosing this method over other finite techniques. One benefit being is that there is integral conservation of all quantities over each control volume, each group of control volumes, and the entire domain irrespective of the number of control volumes used. In this work, the domain is subdivided into orthogonal hexahedron elements, and is discretized using a structured grid framework shown for two dimensions in figure 3.1.

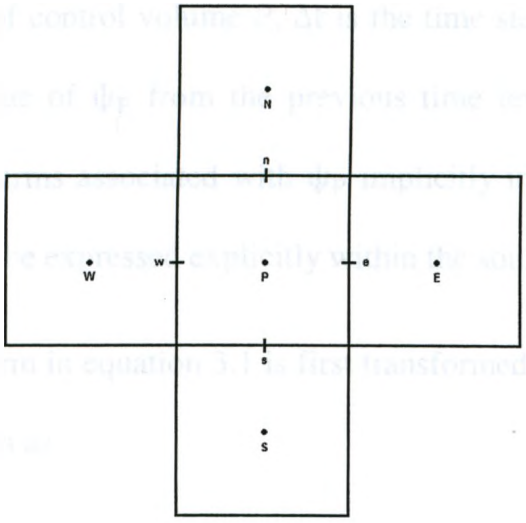

Figure 3-1 Discretization of a two-dimensional structured grid, where the central grid 'P' is neighboured by West ('W') ,East('E'), North('N'), and South('S') nodes. Common faces are classified as integration points denoted by smaller case .

To begin, a general transport equation is given as

$$\underbrace{\frac{\partial \rho_f \psi}{\partial t}}_{1} + \underbrace{\nabla \cdot (\rho_f \psi \mathbf{v})}_{2} = \underbrace{\nabla \cdot (\Gamma \nabla \psi)}_{3} + \underbrace{S_V}_{4}, \tag{3.1}$$

where ρ_f represents the mixture density of the transported fluid, ψ represents a generic transport variable (for example Y_i, T_i), Γ represents the diffusion coefficient, and S_V characterizes any volumetric sources. Beginning with the transient term of equation 3.1, the implementation of a first order backwards difference is used. The result is integrated over a discrete volume V, where it assumed that the value ψ is represented at the centroid of the volume V_P, and is constant over that volume. This procedure is given as,

$$\int_{V_P} \frac{\partial \rho_f \psi}{\partial t} dV = \rho_f \frac{\psi_P - \psi_P^{old}}{\Delta t} V_P = M_{VP} \frac{\psi_P - \psi_P^{old}}{\Delta t} \tag{3.2}$$

where M_{VP} is the mass of control volume P, Δt is the time step, and superscript 'old' represent the former value of ψ_P from the previous time level. It is noted that the discretization will treat terms associated with ψ_P implicitly in the coefficient matrix, and remaining terms will be expressed explicitly within the source term.

The convective term in equation 3.1 is first transformed from a volume integral to a surface integral, given as

$$\int_{V_P} \nabla \cdot (\rho_f \psi \mathbf{v})\, dV = \int_S (\rho_f \psi \mathbf{v}) \cdot \mathbf{n}\, dS\,. \tag{3.3}$$

The surface integral is now integrated over all external faces of the hexahedral control volume V_P stated as

$$\int_S (\rho_f \psi \mathbf{v}) \cdot \mathbf{n}\, dS = \sum_{i=1}^{nf} \dot{m}_i \psi_i\,, \tag{3.4}$$

where $\dot{m}_i$ represents the mass flux through each of the integration points. In the case of the grid structure chosen in this work, 'nf' (number of faces or integration points) corresponds to the 'e, w, n, s, t, b' faces, and this was illustrated in two dimensional form and previously shown in figure 3.1. The value of ψ in equation 3.4 at the integration point must be approximated using an advection scheme. A first order upwinding scheme is selected as an implicit method of predicting ψ at the integration point, as it is stable and therefore well suited for the advected values. This is shown for the east face of the control volume as

$$\psi_e = \frac{1+\alpha_e}{2}\psi_P + \frac{1-\alpha_e}{2}\psi_E \qquad (3.4)$$

where α_e is a parameter used to determine the upwinding direction of the flow at integration point 'e'. This scheme does lead to erroneous results under certain conditions, and in this work, higher order schemes are used to improve accuracy, and reduce errors associated with upwinding. Many higher order advection schemes have been formulated to predict integration point values in computational problems [30, 31, 32, 33, 34]. Advection schemes of particular interest due to convergence properties, and spatial accuracy of up to second order, are total variation diminishing (TVD) schemes. These schemes are desirable for stability and non-oscillatory behaviour because they have been designed to be preserve monotonicity. Monotonicity preserving schemes are such that the total variation of the discrete solution should diminish with time and these schemes ensure this by the use of limiter functions. TVD Schemes that have been implemented in this work follow the limiters developed by Van Albada [32] and also Venkatakrishnan [33]. While these schemes were found to give stable non-oscillatory solutions, the monotone upstream-centred scheme for conservation laws (MUSCL) limiter was chosen, as it produced comparable results at a lower computational cost [34]. The MUSCL limited scheme is defined for the east face as,

$$\psi_e = \psi_P + \Phi\frac{(\psi_E - \psi_P)}{\Delta x_{PE}} \qquad \text{for } \dot{m}_P > 0 \qquad (3.5)$$

$$\psi_e = \psi_E - \Phi \frac{(\psi_P - \psi_E)}{\Delta x_{PE}} \qquad \text{for } \dot{m}_P < 0 \tag{3.6}$$

where the limiter is a function of the Sweby factor (r) at the integration point. The Sweby factor is defined as a ratio of upstream to downstream gradients. The limiter is defined as

$$\Phi = \Phi(r|_e) = \frac{r + |r|}{1 + |r|} \tag{3.7}$$

for the MUSCL scheme. The implementation of higher order improvements to the first order implicit scheme is implemented through the use of a deferred correction (DC_i), where the difference between the higher order and first order estimate is calculated and added explicitly to the system of equations. This method is utilized to avoid the possibility of calculating negative active coefficients in the discretization. It is shown for the east face as

$$\dot{m}_e\psi_e = \dot{m}_e\psi_e^{UDS} + \beta\dot{m}_e(\psi_e^{HOS} - \psi_e^{UDS}), \tag{3.8}$$

where the explicit correction for the east face is

$$DC_e = \beta\dot{m}_e(\psi_e^{HOS} - \psi_e^{UDS}). \tag{3.9}$$

The variable β is used as a blending factor if needed, and superscripts HOS and UDS represent the value of ψ_i at the integration point predicted using both the higher order and upwind difference schemes, respectively.

The diffusion term will now be discretized using the finite volume method. The divergence theorem is used once again in the diffusion term to convert the volume integral into a surface integral, given as

$$\int_V \nabla \cdot (\Gamma \nabla \psi)\, dV = \int_S (\Gamma \nabla \psi) \cdot n\, dS = \sum_{i=1}^{nf} A_{nf}[(\Gamma \nabla \psi) \cdot n]|_{nf} \,. \tag{3.10}$$

It is important to note that A_{nf} is the area of the face at the integration point. The gradients at the integration points are easily computed in regions of similar type (example; pure fluid), however this term will be discussed further in section 4, where values at the interface of multiple domain types (example; fluid-porous) are computed.

The final term of the general transport equation (equation 3.1), represents volumetric sources. This term is discretized by directly integrating the volumetric source over the control volume, given by

$$\int_V S_V dV = V_P S_V \,. \tag{3.11}$$

Each transport equation is discretized over finite volumes in domains of similar type (pure fluid, porous, and solid), and this is shown in figure 3.2.

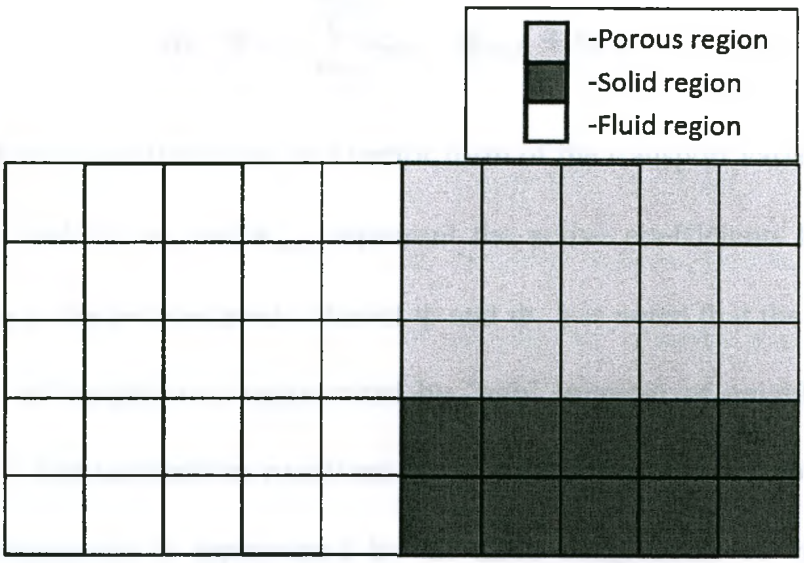

Figure 3-2 Discretization strategy in domains of similar type (pure fluid, porous, solid), where each region is discretized as a continuum

Unlike the general transport equation presented in equation 3.1, the momentum equations also contain pressure terms. Pressure and velocity will be detailed more carefully in the following pressure-velocity coupling section, however at this point, the pressure term is treated as a source term, and is discretized following the procedure of equation 3.11, which leads to

$$\int_V \nabla p dV = (\nabla p)|_P \, V_P \, . \tag{3.12}$$

The discretization of all terms in the general transport equation leads to the general formation of the discrete equation, given as

$$a_P \psi_P = \sum_{i=1}^{nnb} a_{nnb} \psi_{nnb} + b_P \tag{3.13}$$

or,

$$\mathbf{a}_P \cdot \boldsymbol{\psi}_P = \sum_{i=1}^{nnb} \mathbf{a}_{nnb} \cdot \boldsymbol{\psi}_{nnb} + b_P \,, \tag{3.14}$$

where ψ and $\boldsymbol{\psi}$ represent the scalar and vector form of the transport variable. Similarly a_P, and a_{nnb}; as well as $\mathbf{a}_P$, and $\mathbf{a}_{nnb}$ represent the active coefficients both in scalar and matrix form at the cell centered value of ψ and $\boldsymbol{\psi}$. It is noted that the summation is performed over all neighbours; represented by 'nnb' (number of neighbours), of the central 'p' node. The momentum equations are a special form of the above systems as $\boldsymbol{\psi}_P$ in three dimensions is represented by all three components of velocity and a pressure term. This system is underdetermined as no equation for pressure exists. Therefore in order to seek a solution, the continuity equation is made to contain pressure and this leads into the topic of pressure velocity coupling.

3.3 Pressure-Velocity Coupling

As stated in section 3.2, the continuity equation and momentum equations are coupled and maintaining this coupling is important as the pressure term for incompressible flows does not appear directly in the continuity equation. Therefore, pressure must be expressed in the continuity equation appropriately. To explain this idea further, the pressure field is correct when it drives velocity such that mass is conserved. It is noted that even with pressure being included in the mass conservation, care must be taken when specifying where the values of pressure and velocity are defined. For instance, if both are specified at the same location; the centroid of a control volume, the possibility exists that a highly non-uniform pressure field could appear as a uniform field in the discretized momentum equations without being

detected. Methods have been developed to maintain the coupling between the continuity and momentum equations.

One such method is the staggered grid approach developed by Harlow and Welch [29]. This concept is to solve the scalar variables such as pressure, temperature, etc., at standard volume nodal points while solving for velocity components on a staggered grid centred about integration points. This method is well established however it requires extra indexing and geometric information about the velocity components, and additional interpolations regarding these components. The additional parameters obviously make two and three dimensional problems quite complex as an additional cost is presented in storage of these staggered quantities.

Another method is that of Rhie and Chow, where coupling is maintained using a collocated grid. Essentially, the advected velocity $\dot{m}_e u_e$ in the x-direction is obtained from a different equation than the advecting velocity $\dot{m}_e = \rho A_e \hat{u}_e$. Where the east face velocity u_e is obtained similar to any advected scalar and $\hat{u}_e$ is obtained from a special momentum equation. Although these two parameters come from different equations, it is desirable that they solve to be approximately equal to each other $u_e \approx \hat{u}_e$. On collocated grids, a direct solution where pressure and velocity are solved as a coupled set; or a segregated solution, where each are solved separately, may be formulated. In this work, the direct solution method is chosen to solve the coupled set of equations. For the formulation of collocated method, the partially discretized equations for continuity and momentum in the fluid region are presented as;

$$\frac{(\rho_{f,P} - \rho_{f,P}{}^{o})V_P}{\Delta t} + \sum_{i=1}^{nf} \dot{m}_i = 0 \tag{3.15}$$

$$\frac{(\mathbf{u}_P - \mathbf{u}_P^o)\rho_{f,P}V_P}{\Delta t} + \sum_{i=1}^{nf} \dot{m}_i (\mathbf{u}_i - \mathbf{u}_P) \tag{3.16}$$

$$= -(\nabla p)|_P V_P + \sum_{i=1}^{nf} \mu_f \left(A \frac{\partial u}{\partial n}\right)\Big|_i + \rho_{f,P} V_P \mathbf{f}_P ,$$

noting that equation 3.16 is obtained by subtracting equation 3.15 from the discretized form of equation 2.76 to ensure a conservative method.

In developing an expression for $\hat{u}_e$, momentum must be conserved over a virtual volume, centered about the integration points within the domain. Beginning with the conservation of momentum for the 'x' velocity component, equation 3.13 for the 'P' node is written as

$$a_P u_P = \underbrace{\sum_{i=1}^{nnb} a_{nnb} u_{nnb} + b_P}_{\breve{u}_P} - \frac{\partial p}{\partial x}\Big|_P V_P \tag{3.17}$$

and likewise for the neighbouring volume,

$$a_E u_E = \breve{u}_E - \frac{\partial p}{\partial x}\Big|_E V_E . \tag{3.18}$$

By analogy, the advecting velocity at the integration point is found using a similar expression,

$$a_e \hat{u}_e = \breve{u}_e - \frac{\partial p}{\partial x}\Big|_e V_e \tag{3.19}$$

where a_e, and V_e are the active coefficient and volume associated with the virtual volume. The inverse distancing approximation is then made for regions of similar types (fluid, or porous) that,

$$\breve{u}_e = \left(\frac{\Delta x_{eE}}{\Delta x_{PE}}\breve{u}_P + \frac{\Delta x_{Pe}}{\Delta x_{PE}}\breve{u}_E\right) \tag{3.20}$$

It is also approximated that $a_e = \frac{1}{2}(a_P + a_E)$ and $V_e = \frac{1}{2}(V_P + V_E)$ and finally simplifying that $a_P \approx a_E \approx a_e$ and $V_P \approx V_E \approx V_e$, the final form of equation 3.19 becomes

$$\hat{u}_e = \left(\frac{\Delta x_{eE}}{\Delta x_{PE}}u_P + \frac{\Delta x_{Pe}}{\Delta x_{PE}}u_E\right) - \frac{V_e}{a_e}\left[\frac{\partial p}{\partial x}\bigg|_e - \left(\frac{\Delta x_{eE}}{\Delta x_{PE}}\frac{\partial p}{\partial x}\bigg|_P + \frac{\Delta x_{Pe}}{\Delta x_{PE}}\frac{\partial p}{\partial x}\bigg|_E\right)\right]. \tag{3.21}$$

Or in more concise notation [6],

$$\hat{u}_e = u_e^{ID} - \frac{V_e}{a_e}\left[\frac{\partial p}{\partial x}\bigg|_e - \frac{\partial p}{\partial x}\bigg|_e^{ID}\right] \tag{3.22}$$

where superscript 'ID' represents an inverse distancing approximation. Here, the first pressure gradient term is approximated using the values surrounding the east integration point and is treated implicitly in equation 3.15, whereas the second gradient is deferred and approximated using the inverse distance of cell centered values at nodes P and E. These two methods of representing the pressure gradient will be almost equal in a converged solution however they serve to smooth out any oscillations as the solution procedure progresses.

Similarly, this method carried out in the porous region, noting that the discretized momentum equations in this region differ in form than that of in the pure fluid region (equations 2.15, and 2.16). This is presented as;

$$\frac{\varepsilon\left(\langle\rho_f\rangle_P^f - \langle\rho_f\rangle_P^{f,o}\right)V_P}{\Delta t} + \sum_{i=1}^{nf} \dot{m}_i = V_P\langle\dot{n}_i\rangle^{fs} \tag{3.23}$$

$$\frac{(\langle\mathbf{u}\rangle_P - \langle\mathbf{u}\rangle_P^o)\langle\rho_f\rangle_P^f V_P}{\Delta t} + \sum_{i=1}^{nf} \frac{\dot{m}_i}{\varepsilon}(\langle\mathbf{u}\rangle_i - \langle\mathbf{u}\rangle_P) \tag{3.24}$$

$$= -\varepsilon\left(\nabla\langle p\rangle^f\right)\Big|_P V_P + \sum_{i=1}^{nf} \mu_f\left(A\frac{\partial\langle\mathbf{u}\rangle}{\partial n}\right)\Big|_i - \frac{\varepsilon\mu_f V_P}{K}\langle\mathbf{u}\rangle_P$$

$$-\frac{\varepsilon\langle\rho_f\rangle_P^f V_P c_E}{K}|\langle\mathbf{u}\rangle_P|\langle\mathbf{u}\rangle_P + \langle\rho_f\rangle_P^f V_P \mathbf{f}_P$$

where $\hat{u}_e$ in $\dot{m}_i$ is replaced with $\langle\hat{u}\rangle_e$ and equation 3.17 with

$$a_P\langle u\rangle_P = \langle\breve{u}\rangle_P - \varepsilon\frac{\partial\langle p\rangle^f}{\partial x}\Big|_P V_P . \tag{3.25}$$

Using the same procedure implemented to derive equation 3.22, gives an approximation for the advecting velocity in the porous region [6], seen as

$$\langle\hat{u}\rangle_e = \langle u\rangle_e^{ID} - \frac{\varepsilon V_e}{a_e}\left[\frac{\partial\langle p\rangle^f}{\partial x}\Big|_e - \frac{\partial\langle p\rangle^f}{\partial x}\Big|_e^{ID}\right] \tag{3.26}$$

where the correction term is multiplied by a factor of porosity.

3.4 Discrete Form of all Transport Equations

To complete the set of discretized equations, the closed form of the species and energy equations specific to each region of the domain, are discretized. All discrete

equation presented, have been treated similarly to momentum, where the continuity equation multiplied by the transport variable at the P node are subtracted from the discretized equation. This is presented in final form as:

Fluid Region

$$\frac{(Y_P - Y_P^o)\rho_{f,P}V_P}{\Delta t} + \sum_{i=1}^{nf} \dot{m}_i (Y_i - Y_P) = \sum_{i=1}^{nf} D_f \left(\rho_f A \frac{\partial u}{\partial n}\right)\Big|_i \tag{3.27}$$

$$\frac{\rho_{f,P}V_P}{\Delta t} \sum_{\gamma=1}^{ns} \left\{(c_p)_{f,\gamma} Y_{\gamma,P}(T_P - T_P^o) + h_\gamma^o (Y_{\gamma,P} - Y_{\gamma,P}^o)\right\} \tag{3.28}$$

$$+ \sum_{\gamma=1}^{ns} \left[\sum_{i=1}^{nf} \dot{m}_i \left\{(c_p)_{f,\gamma} Y_{\gamma,P}(T_i - T_P) + h_\gamma^o (Y_{\gamma,i} - Y_{\gamma,P})\right\}\right]$$

$$= \sum_{i=1}^{nf} \left\{k_f \left(A \frac{\partial T}{\partial n}\right)\Big|_i + \sum_{\gamma=1}^{ns} D_f \left(A \rho_f h_\gamma^o \frac{\partial Y_\gamma}{\partial n}\right)\Big|_i\right\}$$

Porous Region

$$\frac{\varepsilon\left(\langle Y_A\rangle_P^f - \langle Y_A\rangle_P^{f,o}\right)\langle\rho_f\rangle_P^f V_P}{\Delta t} + \sum_{i=1}^{nf} \dot{m}_i \left(\langle Y_A\rangle_i^f - \langle Y_A\rangle_P^f\right) \tag{3.29}$$

$$= \sum_{i=1}^{nf} D_{f,eff} \left(A \langle\rho_f\rangle^f \frac{\partial \langle Y_A\rangle^f}{\partial n}\right)\Big|_i + V_P \langle \dot{n}_A\rangle^{fs}$$

$$\frac{\varepsilon V_P \langle \rho_f \rangle^f}{\Delta t} \sum_{\gamma=1}^{ns} \left\{ \left(c_p\right)_{f,\gamma} \langle Y_\gamma \rangle_P^f \left(\langle T_f \rangle_P^f - \langle T_f \rangle_P^{f,o} \right) + h_\gamma^o \left(\langle Y_\gamma \rangle_P^f - \langle Y_\gamma \rangle_P^{f,o} \right) \right\} \tag{3.30}$$

$$+ \sum_{\gamma=1}^{ns} \left[\sum_{i=1}^{nf} \dot{m}_i \left\{ \left(c_p\right)_{f,\gamma} \langle Y_\gamma \rangle_P^f \left(\langle T_f \rangle_i^f - \langle T_f \rangle_P^f \right) \right.\right.$$

$$\left.\left. + h_\gamma^o \left(\langle Y_\gamma \rangle_i^f - \langle Y_\gamma \rangle_P^f \right) \right\} \right]$$

$$= \sum_{i=1}^{nf} \left\{ k_{f,eff} \left(A \frac{\partial \langle T_f \rangle^f}{\partial n} \right) \Big|_i + \sum_{\gamma=1}^{ns} D_{f,eff} \left(A \langle \rho_f \rangle^f h_\gamma^o \frac{\partial \langle Y_\gamma \rangle^f}{\partial n} \right) \Big|_i \right\}$$

$$+ h_{fs} A_{fs} V_P \left(\langle T_f \rangle_P^s - \langle T_f \rangle_P^f \right) - h_A V_P \langle \dot{n}_A \rangle^{fs}$$

$$\frac{(1-\varepsilon)\left(\langle Y_A \rangle_P^s - \langle Y_A \rangle_P^{s,o} \right) \langle \rho_f \rangle_P^s V_P}{\Delta t} \tag{3.31}$$

$$= \sum_{i=1}^{nf} D_{s,eff} \left(A \langle \rho_f \rangle^s \frac{\partial \langle Y_A \rangle^s}{\partial n} \right) \Big|_i - V_P \langle \dot{n}_A \rangle^{fs}$$

$$\sum_{\gamma=1}^{ns} \frac{(1-\varepsilon)\langle \rho_f \rangle^s V_P}{\Delta t} \left\{ \left(c_p\right)_{s,\gamma} \langle Y_\gamma \rangle_P^s \left(\langle T_s \rangle_P^s - \langle T_s \rangle_P^{s,o} \right) \right. \tag{3.32}$$

$$\left. + h_\gamma^o \left(\langle Y_\gamma \rangle_P^s - \langle Y_\gamma \rangle_P^{s,o} \right) \right\}$$

$$= \sum_{i=1}^{nf} \left\{ k_{s,eff} \left(A \frac{\partial \langle T_s \rangle^s}{\partial n} \right) \Big|_i \right.$$

$$\left. + \sum_{\gamma=1}^{ns} D_{s,eff} \left(A \langle \rho_s \rangle^s h_\gamma^o \frac{\partial \langle Y_\gamma \rangle^s}{\partial n} \right) \Big|_i \right\}$$

$$- h_{fs} A_{fs} V_P \left(\langle T_f \rangle_P^s - \langle T_f \rangle_P^f \right) - h_A V_P \langle \dot{n}_A \rangle^{fs}$$

A variety of reaction types can be defined in the reaction term $\langle \dot{n}_A \rangle^{fs}$. As stated in the previous chapter, this work considers only a heterogeneous surface reaction between

the two constituents present (solid and fluid). Models tend to assume that the solid surface reaction rate is kinetically controlled [10], meaning concentration of species 'A' is approximately uniform and there is negligible diffusion resistance of that species reaching the surface. In keeping a general derivation, for the purpose of looking at lower velocities or larger particle size in the case of food storage, where $\langle Y_A \rangle_P^{fs}$ differs substantially from $\langle Y_A \rangle_P^{s}$ and the deviation of $\langle Y_A \rangle_P^{s}$ is under investigation, the surface reaction is given as [4, 35, 36];

$$\langle \dot{n}_A \rangle^{fs} = \frac{1}{\frac{1}{\langle \dot{n} \rangle_D^{fs}} + \frac{1}{\langle \dot{n} \rangle_\kappa^{fs}}}. \tag{3.33}$$

Equation 3.33 represents a parallel resistance model for the surface reaction, where the kinetic component $\langle \dot{n} \rangle_\kappa^{fs}$, is;

$$\langle \dot{n} \rangle_\kappa^{fs} = -\langle \rho_f \rangle^f \kappa_A A_{fs} \langle Y_A \rangle^f, \tag{3.34}$$

And the diffusion component $\langle \dot{n} \rangle_D^{fs}$, analogous to heat transfer is given as,

$$\langle \dot{n} \rangle_D^{fs} = \langle \rho_f \rangle^f h_{m,fs} A_{fs} \left(\langle Y_A \rangle_P^{fs} - \langle Y_A \rangle_P^{f} \right). \tag{3.35}$$

Here, $h_{m,fs}$ represents the mass transfer coefficient, and A_{fs} denotes the specific surface area associated with the fluid solid boundary.

Solid

Energy transport is the only form of exchange in the solid region, and is governed by a transient diffusion equation presented as

$$\frac{\rho_s V_P c_s (T_P - T_P^o)}{\Delta t} = \sum_{i=1}^{nf} k_s \left(A \frac{\partial T}{\partial n} \right)\Big|_i , \tag{3.36}$$

where the density ρ_s, specific heat c_s, and thermal conductivity k_s are parameters of the solid medium.

The discrete forms of the transport equations have now been presented for regions of fluid, porous and solid regions. Although the flow is incompressible, variations in properties such as density are still caused by temperature, species and pressure variations and therefore the derivation considers this. Furthermore, density of the fluid is also affected by the exchange of water vapour in the porous media. These variations increase the complexity of the systems being solved.

3.5 Solution Procedure

The numerical procedure for this system requires additional attention as variations in parameters with temperature, pressure and species content (content of water vapour) occur. Furthermore, calculation of parameters not computed directly by the discrete form of the transport equations (equations 3.15, 3.16, 3.23, 3.24, 3.27-3.32), such as vapour pressure and relative humidity becomes important when initializing the solution, maintaining boundary conditions, and determining mass transfer rate within the porous medium.

Equations 3.27 and 3.29 represent the transport of the mass fraction of water vapour in the mixture composition throughout the domain. Although this equation format is more suitable for representing each component of a mixture and species diffusion, it is not the best representation of the composition of humid air in a domain.

This is because mass fraction is not easily measured directly in practice. In fact, for applications involving humid air, the ratio of the amount of water vapour in the air to amount of dry air on a mass basis is defined. This is defined as the specific humidity ω_{spec} of the air, and is shown as a ratio of masses or with the ideal gas law, a ratio of pressures given as;

$$\omega_{spec} = \frac{m_v}{m_a} = \frac{p_V V/R_V T}{p_a V/R_a T} = \frac{p_V/R_V}{p_a/R_a}. \tag{3.37}$$

Here, m_v, and m_a are the mass of the water vapour and air, p_v, and p_a the partial pressure of the vapour and air, V the volume occupied, and R_V, and R_a the specific gas constants of the vapour and air components. Their exists two bounds to the range of ω_{spec}, the first occurs when the mixture consists solely of dry air, represented by a specific humidity of zero. The second of these bounds being the maximum amount of moisture the air can hold, classified as saturated air. These limits are scaled better with the definition of relative humidity, which is the ratio of the amount of vapour in the air to the maximum amount of vapour air can hold (m_g) at a given temperature, again defined in mass or pressure basis as

$$\omega_{rel} = \frac{m_v}{m_g} = \frac{p_v}{p_g}, \tag{3.38}$$

where the p_g is equal to the saturation pressure of water at the temperature of the vapour. The saturation pressure is found by using saturated water tables or more conveniently, by a temperature based correlation [25]. Expressions 3.37, and 3.38 are related, and with the use of Dalton's law this gives

$$\omega_{spec} = \frac{R_a/R_V\, \omega_{rel} p_g}{p_{tot} - \omega_{rel} p_g}. \tag{3.39}$$

In practice, the relative and specific humidity's are traditionally measured by a sling psychrometer or more recently, by an electronic sensor. ω_{spec}, ω_{rel} and the mass fraction of vapour Y_A are interchangeable by considering the sum of the individual components ($\sum_{i=1}^{n} Y_i = 1$), which gives

$$Y_A = \frac{1}{\frac{1}{\omega_{spec}} + 1}. \tag{3.40}$$

With the relation between specific humidity, relative humidity, and mass fraction established, the system may be initialized for the iterative solution process.

Also important for the system, is the proper declaration of boundary conditions. Although this is problem dependent, it must be clarified that similar to the domain, it is important to implement conditions that make use of measurable parameters. This is of concern in the mass fraction equation, where an inlet relative humidity is generally specified as it is known, yet what is needed is an input mass fraction for the solution procedure. As shown, converting from relative humidity to mass fraction is accomplished with the use of equations 3.39, and 3.40 however when using a Dirichlet type condition for a prescribed value, it is noticed that the pressure in equation 3.39 is not generally known. In fact, defining a constant inlet boundary pressure does lead to oscillation at the inlet, because pressure is allowed to develop through the domain and is not known at the inlet. Therefore, in order to create a specified inlet relative humidity, a Dirichlet condition at the inlet is imposed where pressure must be extrapolated. This is given for a west inlet as;

$$Y_{inlet} = \frac{1}{\frac{1}{\frac{R_a/R_V\,\omega_{rel}p_g}{p_{tot,in} - \omega_{rel}p_g}} + 1} \tag{3.40}$$

with the pressure term at the west face being constructed as

$$p_{tot,in} = p_E - \left.\frac{\partial p}{\partial x}\right|_{e,E} \Delta x_{inE} \,. \tag{3.41}$$

Here p_E is the pressure at the node just east of the inlet, the gradient term in the x direction is evaluated at the east face of the E node, and the Δx_{inE} represents the distance to the inlet face. It is also mentioned that $p_{tot,in}$ also on the scale of atmospheric pressure, as this is the defined outlet condition.

Assuming the boundary and initial conditions of the system have been computed, and the domain was a medium of similar type, the active coefficients would be assembled and the solution procedure could be initiated. However this work is developed for conjugate domains and this requires special attention at interfaces. Chapter 4 will explain how to treat interfaces in the discrete domain.

At this point, it will be assumed that the interface corrections have been performed and the active coefficient matrices assembled for all transport equations. The matrix is sparse in structure and in this work, is represented as

$$Ax = b \tag{3.42}$$

Where A is the global coefficient matrix, b is the constant vector and x represents the solution vector. The solution to the system of discrete equations is carried forward using a software package named PETSc (Portable, Extension Toolkit for Scientific

computation) [37, 38, 39]. This package contains Krylov subspace iterative solvers which are used to solve the large matrix structures in this work. The system is also preconditioned in the PETSc environment to accelerate the solution procedure. Preconditioning is performed on the matrix as

$$M_L^{-1}Ax = M_L^{-1}b\,, \tag{3.43}$$

where the preconditioning procedure is assumed to be from the left only. Preconditioning is performed such that $M_L^{-1}A$ is better conditioned than A alone. Once again, multiple preconditioning techniques are possible with this toolkit and further information regarding this package is presented in [37].

The solutions to the discrete equations are solved using a sequential method. This means that although velocities, pressures, temperatures, and mass fractions are not all solved simultaneously, they are solved at each non-linear iteration. Once computed, the solutions of these fields allow parameters that are influenced by temperature, pressure, and mass fraction to be re-computed at each subsequent iteration. This includes updates on a cell by cell basis to mixture density, partial pressures, relative humidity, and saturation pressure. Also in terms of any porous section in the domain, this method allows updates to the additional drag, dispersion, and fluid-solid exchange terms. These variations in parameters and properties do lead to an increase in the non-linearity of the system; however it is observed in this work that the sequential method does converge without any need for relaxation.

Determining convergence is accomplished by computing a normalized residual value at every iteration, over the domain across each control volume. To define the convergence criterion for the non linear problem, we manipulate equation 3.13 as

$$R_P = a_P\psi_P + b_P - \sum_{nnb} a_{nnb}\psi_{nnb}\,, \tag{3.44}$$

where the residual is computed after each coefficient update. This represents a single volume residual or local residual. To obtain a good representation for global convergence, the maximum local residual is found over all control volumes. The magnitude of the residual value is dependent on the transport variable associated with it. To eliminate this problem, the residual is normalized such that the magnitude of ψ is of no influence. Convergence is obtained for the non-linear loops when the maximum value of the normalized residual meets an assigned tolerance of $R_P < 10^{-5}$.

3.6 Summary

In this chapter, the descretization of a general transport equation across a three dimensional orthogonal structured finite volume domain was presented. Additionally, the concept of pressure-velocity coupling was presented, where a scheme was implemented for collocated grids. Furthermore, a complete set of transport equations for mass, momentum, energy, and species was presented in discrete form for conjugate fluid, porous, and solid domains. The solution procedure for a system of this type was covered where a brief mention of convergence was covered. In this chapter, it was assumed that interfaces between mediums were already discretized. Chapter four will

address the problems encountered at these interfaces, and develop methods of avoiding oscillations across, and in the vicinity of these interfaces.

Chapter 4 - Interfaces Encountered in the Domain

4.1 Introduction

The code development in this work is for applications that contain conjugate fluid/porous/solid domains, and it must be noted that the treatment of the interfaces between differing regions requires additional consideration above that of the general form of the conservation equations for a single medium. At an interface, the forms of the governing equations often differ, and the goal in the numerical treatment of these interfaces is to have physically reasonable estimates for advection, conduction, and pressure in the regions where rapid geometrical changes occur. These estimates will apply to all regions where the domain type changes, for example, fluid-solid, fluid-porous, and porous-solid. The subsequent sub-sections in this chapter will address the mathematical approach to distributing transport quantities at the interface; and the computational methods associated with the interface. The overall goal is to establish conditions that are physically reasonable and monotonically convergent.

4.2 Mathematical Model at Interfaces

As stated, a conjugate domain contains multiple medium types, and in order for the solution across the full domain to be computed, the mathematical treatment at interfaces between domains must be considered. This special treatment is seen at interfaces between differing regions, where the possibility exists for having discontinuities in the governing equations. The goal of this section is to develop

interface conditions which are used to match the transport equations in neighbouring domains so that the discretized form of the equations, which will be explained in section 4.3, reflects the physical properties of conservation. It is noted that in the following sections, the transport variables directly next to a porous region (in the solid or fluid), are not necessarily the point values, and due to length scale constraints, a volume average cannot be taken directly on the porous side next to an interface. However, these values can be considered as a local average over the area of the interface which reduces to a classic point or volume average at short distances from that interface. Thus, the discretized transport equations utilizing the mathematical conditions still reflect the physical principles of conservation.

4.2.1 Interface Joining Pure fluid and Pure Porous regions

Conditions at the interface between a pure fluid and a porous region have been extensively studied for the flow of fluid [4, 6, 40]. This work will assume the condition of continuity of the velocity at the interface, and this is what is imposed. This is represented by;

$$\boldsymbol{u}_f = \langle \boldsymbol{u} \rangle_{por} \tag{4.1}$$

where it is noted that the velocity in equation 4.1 is the mass fraction averaged velocity of the mixture. This differs slightly from the works reference above, however still represents a physically reasonable condition. Furthermore, referring to the different forms of equations 3.16 and 3.24, it is seen that the stress at the interface must also be addressed. Therefore, it is reasonable to enforce the continuity of interface stress on the pure fluid side with the intrinsic average of the stress on the porous side. These

conditions have also been well-established, and are presented in similar form to [6, 41] as;

$$(\mathbf{n}\cdot\mathbf{t}\cdot\sigma)_f = \left(\mathbf{n}\cdot\mathbf{t}\cdot\langle\sigma\rangle^f\right)_{por} \tag{4.2}$$

for the shear stress component, and

$$(\mathbf{n}\cdot\mathbf{n}\cdot\sigma)_f = \left(\mathbf{n}\cdot\mathbf{n}\cdot\langle\sigma\rangle^f\right)_{por} \tag{4.3}$$

for the normal component of stress. It is noted that **n** is an outward unit normal and **t** represents a tangent unit vector. Also, subscripts 'f' and 'por' represent the distribution on the pure fluid and porous sides of the interface. The stress tensors represented in equations 4.2 and 4.3 are given by;

$$\sigma_{ij} = \mu_f\left(\frac{\partial u_i}{\partial x_j} + \frac{\partial u_j}{\partial x_i}\right) - p\delta_{ij} \tag{4.4}$$

$$\langle\sigma\rangle_{ij} = \frac{\mu_B}{\varepsilon}\left(\frac{\partial\langle u_i\rangle}{\partial x_j} + \frac{\partial\langle u_j\rangle}{\partial x_i}\right) - \langle p\rangle^f\delta_{ij} \tag{4.5}$$

where μ_B is the Brinkman viscosity, and δ_{ij} is the Kronecker delta function. Equations 4.4 and 4.5 show that a fraction of the total stress on the fluid side is carried into the fluid constituent of the porous side. This implies that the remainder of the total stress is balanced by the solid constituent of the porous medium. The parameter that governs the division of stress into both constituents is porosity which is defined by equation 2.26. Finally, it is insisted that the pressure at the interface be continuous, and this is given as

$$p_f = \langle p \rangle^f_{por} . \qquad (4.6)$$

Although equation 4.6 means that pressure is represented by a single value at the interface, it can be seen through equations 3.16, and 3.24, that due to the differing forms of the advecting velocity, there must be an allowance for a rapid change in pressure in the pure fluid region at the interface which is associated with the dynamic pressure effects [6]. It is important that pressure transitions smoothly in the cells surrounding interfaces, as any oscillation will not only influence the mass and momentum equations, but also affect the convective terms in the remaining transport equations; and alter terms that are affected by partial pressures.

The species transport equation that is used to govern the transport of the water vapour component of the mixture is now considered at the fluid-porous interface. The transport of species through a fluid-porous interface may include effects of excess surface accumulation, diffusion, convection and other processes. Many studies have been devoted to modelling the species equation in a pure fluid or pure porous region, however only few have looked at transport through both regions joined by an interface [9, 42]. One characteristic that makes mass transfer complex to study is the possibility that discontinuities may exist at interfaces separating regions of differing concentrations. Another complexity is that there are many forms of mass transfer between differing media types such as absorption, adsorption, and forms of surface reaction.

It is important at this point to develop a general method of modelling interfaces, but also to tailor the derivation to suit interfaces found in the applications encountered

in this work. In these applications, the diffusion of vapour within the solid constituent across the macroscopic porous domain is not considered to be of high influence to the vapour transport in the system. This means that the diffusion term in equation 3.30 and the energy associated with these terms in equation 3.32 are neglected. This assumption is made for both the air conditioning processes and the modeling of bulk foods. The reason for this assumption in evaporative cooling is that the porous material is assumed to be kept saturated at all times by an external water source and therefore internal diffusion of the water component can be neglected. In bulk food storage, the porous modelling technique is used to simplify large domains of whole food items. Although within a food item there may be diffusive transport, this is not represented by the diffusive term in the macroscopic species transport equation for the solid. Therefore, to achieve a continuous distribution through the interface, species A in the fluid region is taken to be continuous with the intrinsic average of species A in the porous region, given as;

$$Y_{A,f} = \langle Y \rangle_{A,por}\,, \tag{4.7}$$

where $Y_{A,f}$ represents the content of species A (the water vapour component) in the fluid region and $\langle Y \rangle_{A,por}$ the volumetric average of species A in the porous region. At this point, for a general derivation, it is also insisted that a species flux balance through the interface is enforced, given as

$$\left(-D_{AB}\rho\frac{\partial Y_A}{\partial n}\right)_f \tag{4.8}$$

$$= \left(-D_{eff,f}\langle\rho_f\rangle^f\frac{\partial\langle Y_A\rangle^f}{\partial n}\right.$$

$$\left. - D_{eff,s}\langle\rho_s\rangle^s\frac{\partial\langle Y_A\rangle^s}{\partial n}\right).$$

Further simplifications to this conservation expression based on the above assumptions will be carried out in section 4.3.3.

The energy equations must also be resolved at the interface. Therefore, a physically reasonable method of ensuring a proper distribution of heat through the interface from the pure fluid to the fluid-solid constituents of the porous region must be established. In this work, the temperature on the pure fluid side of the fluid-porous interface is taken to be continuous with the total average temperature on the porous side for the thermal equilibrium of the interface [40, 6], and this is given as

$$T_f = \langle T\rangle_{por}. \tag{4.9}$$

Additionally it must be considered that energy flux is also balanced across the interface and this is shown as

$$\left(-k_f\frac{\partial T}{\partial n}-\sum_i^n \rho_f D_i \overline{h_i}\nabla Y_i\right)_f \tag{4.10}$$

$$=\left(-k_{f,eff}\frac{\partial\langle T_f\rangle^f}{\partial n}-k_{s,eff}\frac{\partial\langle T_s\rangle^s}{\partial n}\right.$$

$$-\sum_i^{ns} D_{f,eff}\langle\rho_f\rangle^f h_{ns}^o\frac{\partial\langle Y_{ns}\rangle^f}{\partial n}$$

$$\left.-\sum_i^{ns} D_{s,eff}\langle\rho_s\rangle^s h_{ns}^o\frac{\partial\langle Y_{ns}\rangle^s}{\partial n}\right)_{por}$$

where energy balance at the interface must consider the energy associated with conduction and the enthalpy associated with species diffusion.

4.2.2 Interfaces Joining with solid regions

The conditions enforced at interfaces that join with solid regions are that which are enforced at impermeable boundaries. That is, the pressures are extrapolated from the interior of the domain to the interface, and the no slip, no penetration velocity conditions are enforced at the interface. This also applies to the mass fraction transport equation as it is considered that the solid boundaries are rigid and do not contain any water vapour, nor are they capable of accumulating or transporting vapour. Therefore, for simplicity, the amount of water vapour is extrapolated from the interior of the domain to the solid interface.

The conditions for the energy equation are constructed similarly as the interface conditions given in equations 4.9 and 4.10. At the fluid/solid interface, the continuity of temperature and an energy balance give;

$$T_{sol} = \langle T \rangle_f \text{, and} \tag{4.11}$$

$$\left(-k_{sol}\frac{\partial T}{\partial n}\right)_{sol} = \left(-k_f\frac{\partial T_f}{\partial n}\right)_f. \tag{4.12}$$

Also, between the pure solid and pure porous region similar conditions apply, giving:

$$T_{sol} = \langle T \rangle_{por} \tag{4.13}$$

$$\left(-k_{sol}\frac{\partial T}{\partial n}\right)_{sol} = \left(-k_{f,eff}\frac{\partial \langle T_f \rangle^f}{\partial n} - k_{s,eff}\frac{\partial \langle T_s \rangle^s}{\partial n}\right)_{por}. \tag{4.14}$$

4.3 Computational Treatment at Interfaces

At volumes adjacent to the interfaces encountered throughout the domain, it is important to obtain accurate estimates of the terms governed by the discretized equations. This is done by utilizing the interface conditions developed in section 4.1 for fluid/porous, fluid/solid, and porous/solid regions. An example of a structured two dimension case of this type of domain is given in figure 4.1.

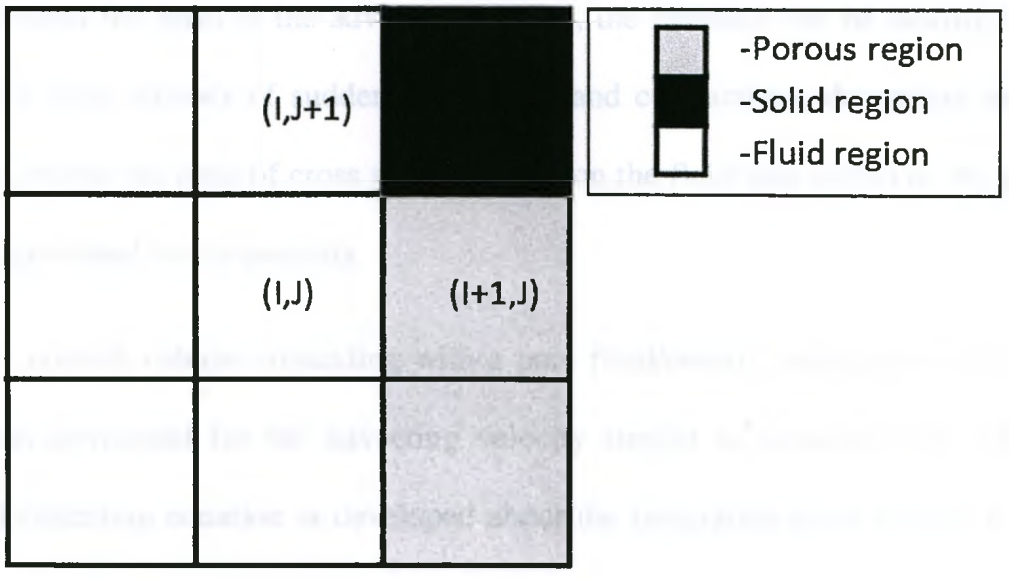

Figure 4-1 Two dimensional structured finite-volume grid for a conjugate domain. (I,J) represents the labelling scheme for the 'P' node, (I+1,J) for the 'E' node, and (I,J+1) for the 'N' node.

4.3.1 Advected Velocity

In the pure fluid volume adjacent to the interface (volume 'I,J'), the advective terms in the discrete forms of the momentum, energy, and species equations must be modified. It is required that these terms be continuous through the interface that separates the pure fluid, and porous regions. To accomplish this, the intrinsic fluid velocity, temperature, and mass fraction are taken to be advected. If the east face is considered, the discretized advected terms that correspond to this in the momentum, energy and mass fraction equations are given as;

$$\text{Momentum: } \dot{m}_e \frac{\langle u \rangle_e}{\varepsilon} \tag{4.15}$$

$$\text{Species: } \dot{m}_e \langle Y \rangle_e^f \tag{4.16}$$

$$\text{Energy: } \sum_{\gamma=1}^{ns} \left[\dot{m}_e \left\{ (c_p)_{f,\gamma} \langle Y_\gamma \rangle_P^f \langle T_f \rangle_e^f + h_\gamma^o \langle Y_\gamma \rangle_e^f \right\} \right]. \tag{4.17}$$

To understand the form of the advected velocity, the interface can be idealized as an array of a large number of sudden expansions and contractions, depending on flow direction, where the ratio of cross sectional area on the fluid side to that of the porous side is represented by the porosity.

A control volume coinciding with a pure fluid/porous interface must have an expression developed for the advecting velocity similar to equation 3.22, where a special momentum equation is developed about the integration point on the 'e' face. This is given as;

$$\langle \hat{u} \rangle_e = \frac{1}{2}\left(\frac{a_P}{a_e} u_P + \frac{a_E}{a_e}\langle u \rangle_E\right) \tag{4.18}$$

$$-\frac{V_e}{a_e}\left[\underbrace{\left(\frac{\partial p}{\partial x}\right)\Big|_e}_{1} - \frac{1}{2}\left(\frac{V_P}{V_e}\frac{\partial p}{\partial x}\Big|_{P+} + \frac{\varepsilon V_P}{V_e}\frac{\partial \langle p \rangle^f}{\partial x}\Big|_{E-}\right)\right],$$

where the pressure term labelled as '1' is

$$\left(\frac{\partial p}{\partial x}\right)\Big|_e = \frac{1}{V_e}\left[\frac{V_P}{2}\frac{\partial p}{\partial x}\Big|_{P+} + \frac{\varepsilon V_E}{2}\frac{\partial \langle p \rangle^f}{\partial x}\Big|_{E-}\right]. \tag{4.19}$$

Unlike the development of equation 3.22, the assumption $a_P \approx a_E \approx a_e$ is not made as due to source terms, these coefficients may differ significantly [6]. Also, the behaviour of pressure is quite different in neighbouring regions to an interface. Therefore the pressure gradient terms given above must be developed for half volumes surrounding the interface, given as the P+ (a volume from node 'P' to integration point 'e') and E- (a volume from integration point 'e' to node 'E') regions.

4.3.2 Pressure Term

In order to compute the pressure gradient terms, an approximation of pressure at the interface is to be constructed. Standard approximation methods normally used in the fluid region are not accurate at the interface due to the Darcy and Forchheimer terms present in the discrete equations within the porous region. Also, as stated, rapid velocity changes occur at the interface which also complicate the estimate. Therefore, the approximation imposed is that developed by [6], and is made by considering the momentum balance of a control volume (figure 4.22) on a simple volume next to the interface.

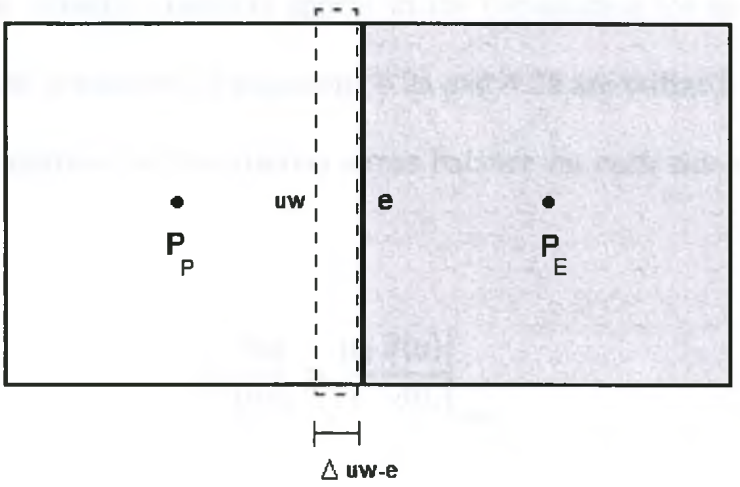

Figure 4-2 Control volume next to an interface: 'uw' defines the upwind west face of the control volume, 'e' is the integration point along the face separating the P and E nodes, and P_E and P_W represent the pressure of each node

With the assumption that Δ_{uw-e} is much smaller the distance from 'P' to the integration point 'e', the mass flux tangent to the interface may be neglected. Also, it is assumed the viscous stresses balance separately and furthermore, that $u_{uw} = u_e = \langle u \rangle_e$ which leads to an estimation for pressure, given as

$$\langle P\rangle_e^f = P_e \approx P_{UW} - \left(\frac{1-\varepsilon}{\varepsilon}\right)\frac{\dot{m}_e\langle u\rangle_e}{A_e}, \tag{4.20}$$

where the upwind pressure P_{UW} is found by an extrapolation to the interface. This estimate is then averaged with an estimate of interface pressure from the porous side, also obtained by extrapolation from the 'E' node to the integration point 'e'. More details of this implementation are found in the work of Betchen et al. [6].

4.3.3 Diffusive and Advective terms

It is seen in the discretized form of the momentum equations (equations 3.16, and 3.24), that only portions of the viscous stresses involving the face-normal components of the velocity gradients appear in the formulation for an incompressible fluid. Therefore, the conditions of equations 4.2a and 4.2b are utilized, but modified to require that these portions of the viscous stress balance on each side of the interface, given as

$$\mu_f \left.\frac{\partial u}{\partial n}\right|_f = \frac{\mu_B}{\varepsilon}\left.\frac{\partial\langle u\rangle}{\partial n}\right|_{por}. \tag{4.21}$$

If the east face of the fluid volume is examined in figure 4.1, it is seen that the conditions 4.2-4.3 place the proper requirements on normal stress at the interface, but the shear stress conditions differ, where

$$\mu_f\left(\frac{\partial u}{\partial y}+\frac{\partial v}{\partial x}\right)\Big|_f = \frac{\mu_B}{\varepsilon}\left(\frac{\partial\langle u\rangle}{\partial y}+\frac{\partial\langle v\rangle}{\partial x}\right)\Big|_{por} \tag{4.22}$$

is now given as

$$\mu_f \left(\frac{\partial v}{\partial x}\right)\Big|_f = \frac{\mu_B}{\varepsilon}\left(\frac{\partial \langle v \rangle}{\partial x}\right)\Big|_{por} \tag{4.23}$$

The conditions required to match the species and energy equation at the interface are given by equations 4.7 and 4.8, where it is assumed that there is a diffusive and conductive balance of mass fraction and energy respectively, across the interface. To accomplish this, a similar approach to that used for heat transfer given in [43, 6] is applied, where the interface is simplified using a one-dimensional resistance model, shown in figure 4.3.

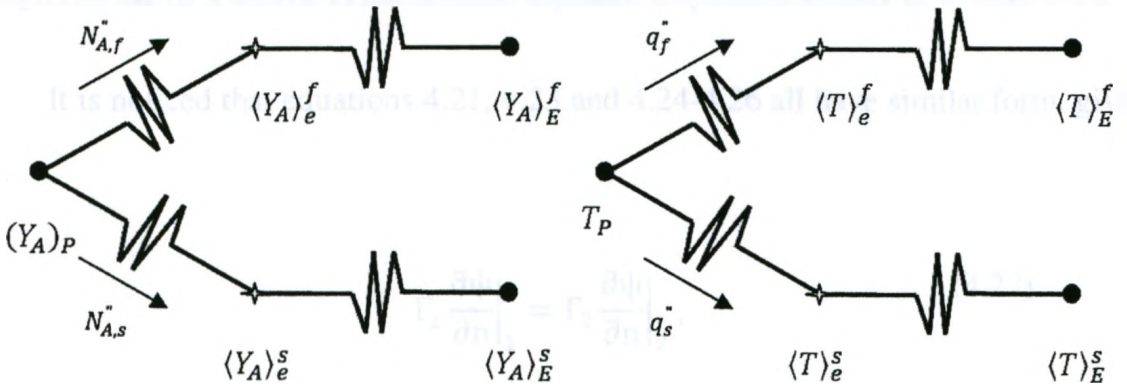

Figure 4-3 Resistance models for Mass fraction diffusion (left), and Heat transfer conduction (right)

This leads to discrete balances through the interface of;

$$N''_f = \varepsilon D_{AB} \frac{\langle Y_A \rangle_e^f - (Y_A)_P}{\Delta x_{Pe}} = D_{f,eff} \frac{\langle Y_A \rangle_E^f - \langle Y_A \rangle_e^f}{\Delta x_{Pe}} \tag{4.24}$$

$$q''_f = \varepsilon k_f \frac{\langle T \rangle_e^f - T_P}{\Delta x_{Pe}} = k_{f,eff} \frac{\langle T \rangle_E^f - \langle T \rangle_e^f}{\Delta x_{Pe}} \tag{4.25}$$

$$q_s'' = (1-\varepsilon)k_s \frac{\langle T\rangle_e^s - T_P}{\Delta x_{Pe}} = k_{s,eff} \frac{\langle T\rangle_E^s - \langle T\rangle_e^s}{\Delta x_{Pe}}. \qquad (4.26)$$

It is noticed that the diffusion of species into the solid is neglected even though it is represented in figure 4.3. This is due mainly to the assumptions stated in section 4.1, where it is mentioned that the diffusion of species at the interface is presented in general form, however the model itself is tailored to be application specific. Furthermore, for applications that involve a discontinuity in the mass fraction equations at the surface of the solid constituent in the porous domain, this is dealt with through the use of a source in the discrete equation explained further in section 4.3.3.

It is noticed that equations 4.21, 4.23 and 4.24-4.26 all have similar form, given by

$$\Gamma_1 \left.\frac{\partial \psi}{\partial n}\right|_1 = \Gamma_2 \left.\frac{\partial \psi}{\partial n}\right|_2, \qquad (4.27)$$

where Γ_1 and Γ_2 are the diffusion coefficients. If the diffusion coefficients have abrupt changes, as seen in the derived interface conditions, a simple arithmetic mean may not capture the flux conditions. A better method of approximating the flux is needed, and this is shown by first discretizing equation 4.27 at the interface of volume I,J (figure 4.1) as follows:

$$\Gamma_1 \frac{\psi_e - \psi_P}{\Delta x_{Pe}} = \Gamma_2 \frac{\psi_E - \psi_e}{\Delta x_{eE}}. \qquad (4.28)$$

Isolating for ψ_e, an estimate for the interface value is found to be

$$\psi_e = \left(1 + \frac{\Delta x_{Pe}}{\Delta x_{eE}} \frac{\Gamma_2}{\Gamma_1}\right)^{-1} \psi_P + \left(1 + \frac{\Delta x_{eE}}{\Delta x_{Pe}} \frac{\Gamma_1}{\Gamma_2}\right)^{-1} \psi_E \,. \tag{4.29}$$

If expression 4.29 is substituted into either side of equation 4.28, this yields an estimate to the diffusive flux at the interface of the form

$$\Gamma_i \left.\frac{\partial \psi}{\partial n}\right|_i \approx \frac{\psi_E - \psi_P}{\frac{\Delta x_{Pe}}{\Gamma_1} + \frac{\Delta x_{eE}}{\Gamma_2}}. \tag{4.30}$$

This expression, similar to that developed by Patankar [29], representing the diffusion coefficient at the interface by using a harmonic mean. Also, equation 4.30 provides a physically based estimate for the advected momentum, mass fraction and temperature interface terms.

As stated earlier, at an interface between a pure fluid and porous region, additional complications may exist. This would occur where a pure fluid volume joins with the solid constituent of a porous volume. Although temperature is taken to be continuous across interfaces, this may not be the case for the mass fraction field. Examples of this are seen when thin films of mass on solid's surface exist, or the solid itself is composed of a high content of the transported species, or also if there is a heterogeneous surface reaction.

If the transfer rate is to be determined in this region, then some estimation of the surface value of the transported variable is to be made. This may require the use of Henry's law, which relates the mole fraction of species A in a solid or liquid to the partial pressure outside of this phase. Alternatively if surface reaction occurs, the use of an equation similar to equation 3.33 may be needed. However, as stated in section

4.1, the applications considered in this work consider only evaporation from a saturated surface of the solid constituent in the porous media [figure 4.4].

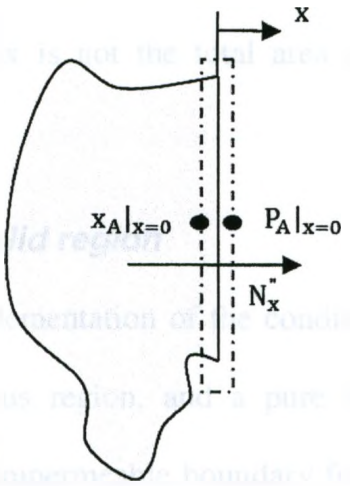

Figure 4-4 Representation of interface between for species transport

Therefore with this assumption and the earlier assumption of the gas mixture being ideal, Raoult's law may be utilized [44] to estimate the value of the partial pressure of species A (the water vapour component) on the fluid side of the interface. This is given as

$$P_A|_{x=0} = (c_A|_{x=0})P_{A,sat}\,, \qquad (4.30)$$

where it is assumed that the mole fraction is essentially unity for evaporative cooling, the application of interest in chapter 5, and that there exists a thin film of this water. The saturation pressure at the interface is required to calculate the partial pressure of the water vapour at the interface, however this is not yet known. To estimate this pressure, once again a temperature based correlation is used where the interface temperature is estimated from equation 4.29. Additionally, specifying a surface mass fraction at the interface is done similarly to specifying an inlet relative humidity (equation 3.40). The pressure at the interface must be approximate and this is done

using the procedure described in section 4.3.2. It is noted that the additional diffusion away from the surface is added as a source/sink term in the discrete equations for the (I,J) volume of figure 4.1. Additionally, it is mentioned that the saturated surface area considered for this surface flux is not the total area of the integration face, but a fraction 'ε' of it.

4.3.4 Interface with pure solid region

The computational implementation of the conditions encountered at interfaces between a pure fluid or porous region, and a pure solid region the same as the conditions implemented at an impermeable boundary for the fluid flow problem. The conditions implemented for the energy equation between a pure fluid and solid are well developed and may be implemented using equation 4.29. Finally, at the interface between a pure solid and porous region, a similar thermal resistance model given by figure 4.3 and equations 4.25 and 4.26 is implemented to govern the conduction transfer.

4.4 Summary

In this chapter, a mathematical model for the interfaces separating differing domain types was discussed. These conditions are developed to be continuous across the interfaces, where there is still allowance for rapid changes near the interface. The interface conditions are then developed numerically, where it is shown that the discrete equations developed in chapter 3 require additional attention when considering advection, diffusion, conduction and pressure. Finally, the species equation is discussed where the numerical procedure for representing saturated surfaces at the pure fluid/porous interfaces are discussed.

Chapter 5 - Results and Discussion

5.1 Introduction

This chapter presents three test cases to study the finite volume code developed in previous chapters. First, two validation cases are presented, where these cases are used to verify and validate the extensions made to the in-house computational code. The first case is the investigation of a direct evaporative cooling cycle. In this test scenario, adiabatic boundary conditions are imposed and the incoming fluid mixture is allowed to saturate through the porous media. The model is utilized to predict the mixture temperature at the outlet of the cooler, and verify the interface conditions at the pure fluid/porous regions. In the second case, an indirect evaporative cooling cycle is modelled. This case not only investigates the principles involved in indirect evaporative cooling, but also allows the numerical code to be tested in a conjugate pure fluid, porous, and solid environment. In the indirect cooling cycle, the simulated results are used to predict the wet bulb effectiveness of the cooling configuration. More recently, there have been novel developments in evaporative cooling cycles, mainly in the area of dual-stage evaporative cooling. One notable development is the Maisotsenko evaporative cooling cycle. This configuration; described further in section 5.3, not only claims to reduce the temperature of the conditioned air to its inlet wet-bulb temperature without adding moisture, but also claims that the air being conditioned approaches due point temperature of the inlet air. The final test case investigated in this work is a simplified Maisotsenko cycle. This case utilizes all

The configuration of the fluid and porous regions in the channel are presented in figure 5.1, where the dimensions are taken to be consistent with the previous studies single phase flow though a porous plug. The relevant flow parameters are given as: $\varepsilon = 0.7$, $\mu_B = \mu_f$, and a Reynolds number based on the channel height of $Re_H = 1$. The inertia coefficient in the momentum equations is calculated by the given relation [4]

$$C_E = \frac{1.75\varepsilon}{\sqrt{150\varepsilon^5}} = 0.2440\,. \qquad (5.1)$$

The boundary conditions imposed for velocity are:

- Inlet conditions: A fully developed velocity profile is imposed on the x = 0 plane; this is given for a channel flow as;

$$u(0,y) = \frac{6Uy}{H}\left[1 - \frac{y}{H}\right] \quad \text{and} \quad v(0,y) = 0\,, \qquad (5.2)$$

  where U is the average axial velocity in the channel. The inlet fluid temperature is arbitrarily chosen to be T_f = 25 degrees Celsius [298.15 K], with a relative humidity of $\omega_{rel} = 40\%$, which is converted to a proper mass fraction for the inlet boundary in equation 3.30 with equation 3.40. The pressure at the inlet plane is extrapolated from the interior of the domain.

- Outlet conditions: Zero derivative conditions in the x direction are imposed for both components (u and v) of velocity on the outlet plane (x = 8H). A constant uniform pressure is set at the outlet, which in this case is equal to atmospheric pressure as the value of the pressure chosen is important because it serves as a datum for pressure and affects the temperature and mass fraction fields inside

the domain. Finally, zero derivative conditions for temperature and mass fraction are assumed at the outlet.

- Wall conditions: No slip, no penetration conditions are imposed on the wall boundaries ($y = 0, \text{and } y = H$). Furthermore, adiabatic wall conditions are enforced in the energy equation and both mass fraction and pressure are extrapolated to the walls from inside the domain assuming a constant gradient.

As noted, this simulation is performed to also test the forms of the energy and species equations developed in the proposed model, and therefore additional parameters are needed for these equations. It will be assumed that the porous material in this case is aluminum with a fluid and solid phase effective conductivity of $k_{f,eff} = 0.0237\ {}^{W}/_{m}\,K$, and $k_{s,eff} = 6.46\ {}^{W}/_{m}\,K$ [45]. The effective fluid phase diffusivity is given to be $D_{f,eff} = 1.5 \times 10^{-4}\ {}^{m^2}/_{s}$ [46]. Also the pore diameter and ligament diameter are given as $d_p = 3.8$ mm and $l_D = 0.55$ mm and that $\mu_B = \mu_f$.

As this is a multi-component mixture, one might expect the mixture thermal conductivity, and dynamic viscosity to change based on the composition. Previous works focussed on determining the mixture thermal conductivity and dynamic viscosity 'ζ_{mix}' of humid air have suggested correlations, such as [47, 48]

$$\zeta_{mix} = \zeta_V \left(\frac{P_V}{P}\right) + \zeta_A \left(1 - \frac{P_V}{P}\right), \tag{5.3}$$

where ζ_V, ζ_A are the properties of the water vapour and air, and P_V/P the specific humidity. As the temperature range is limited in evaporative cooling, and these

properties vary little over the operating conditions (0-50 degrees Celsius), and due to the magnitude of the specific humidity's encountered in this range, the thermal conductivity and dynamic viscosity are taken to that of air at 300 [K] (table 5.1).

Table 5-1 Properties of mixture for test case 1

Properties of air [300 K]	
Specific heat [J/kgK]	1005
Properties of water vapour [300 K]	
Specific heat[J/kgK]	1820
Latent heat [J/kgK]	2500.9 x 10^3
Properties of mixture [300 K]	
Thermal Conductivity [W/mk]	0.0255
Binary Diffusion Coefficient [m^2/s]	2.6 x 10^-5
Dynamic Viscosity [Ns/m^2]	1.843 x 10^-5

The convective interfacial heat and mass transfer coefficients within the plug are calculated by utilizing equivalent Nusselt and Sherwood correlations [45], given as $Nu_{sur} = C_T Re_{ld}^{0.5} Pr^{0.37} = h_{sur} l_D / k_f$ and analogously $Sh_{sur} = C_m Re_{ld}^{0.5} Sc^{0.37} = h_{m,sur} l_D / D_f$. The coefficients in each of the correlation are taken as $C_T = C_m = 0.52$ [45]. The effects of dispersion are neglected in this study. Finally, as this is an evaporative cooler, the surface conditions in the porous region are assumed to be saturated and remain saturated during the cooling process.

A non-uniform structured grid consisting of 31 control volumes in each x-axis section of the channel (0 - 3H, 3H - 5H, 5H - 8H), and 21 control volumes in the y-direction is found to give accurate results, where a coarse representation of this grid is shown in figure 5.2.

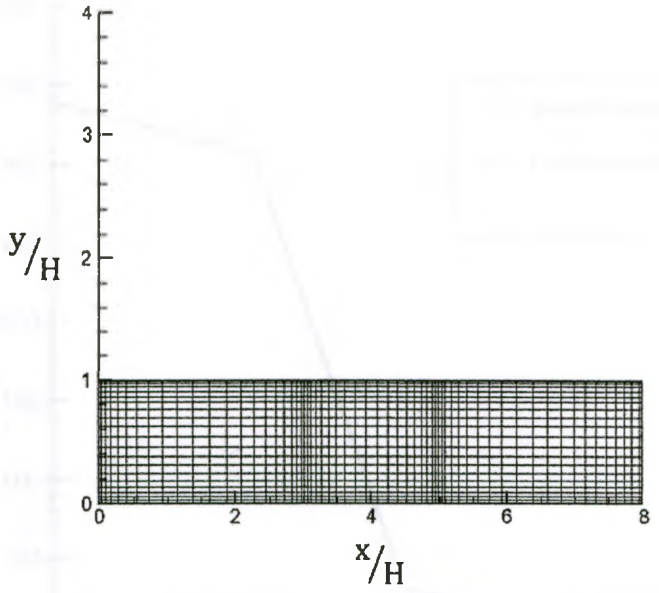

Figure 5-2 Plot showing coarse non-uniform grid used for adiabatic saturator

In previous studies the pressure profile is plotted throughout the domain, as it is used to evaluate the model imposed for the interface conditions in the momentum equations. In this study, pressure is also important for the energy and mass fraction equations, as oscillations in pressure will also cause problems in the temperature and mass fraction fields. Figure 5.3 is a plot of the pressure profile in the domain, which compares the results obtained in this simulation with previously obtained solutions from [6, 40]. This plot is utilized for two reasons; first to show that pressure transitions free of numerical oscillation at the interface, and also to show that grid refinement and grid convergence matched the previous studies. The pressure plot is expected to match the results obtained in previous studies, as the only affect in the mass and momentum equations would be the variation in mixture density, and this was found to be negligible throughout the domain; from 1.192 $^{kg}/_{m^3}$ to 1.212 $^{kg}/_{m^3}$, or 1.67% different.

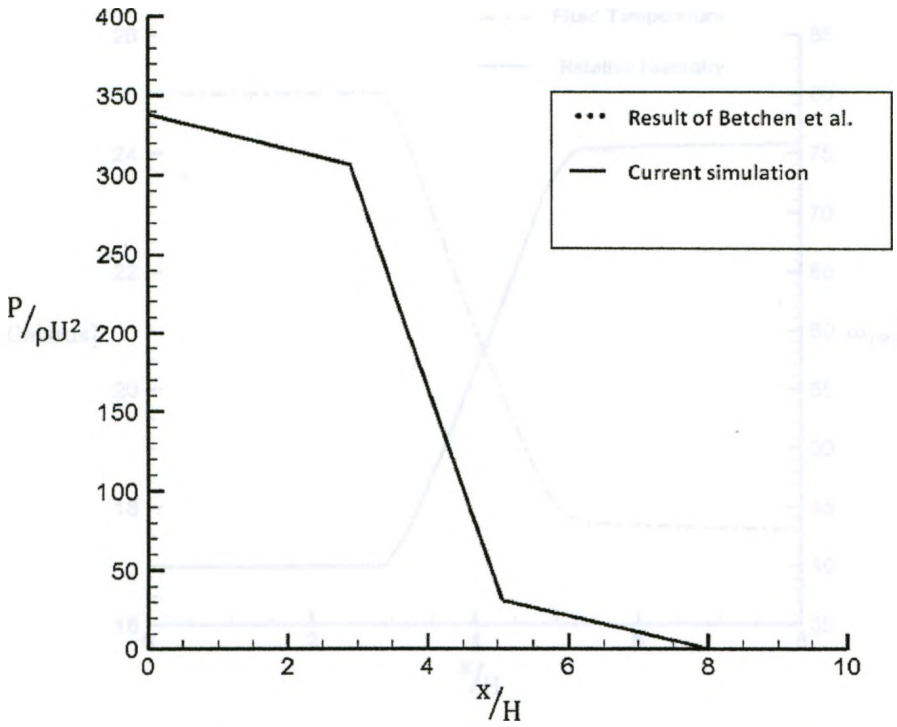

Figure 5-3 Centerline pressure profile through porous plug

Figure 5.4 illustrates the temperature and relative humidity profiles of the inlet mixture as it permeates the porous region in this simulation. The temperature and relative humidity profiles remain almost constant in the regions outside the porous plug ($0 \leq x \leq 3H$ and $5H \leq x \leq 8H$). This is to be expected, as there is no influence from the saturated media. The small increase in the centerline relative humidity past $x = 5H$ is due to the transport of moisture from the walls to the core as the velocity profile re-develops. As the mixture passes through the media ($3H \leq x \leq 5H$), water diffuses into the mixture which directly affects the resulting temperature and relative humidity of the mixture.

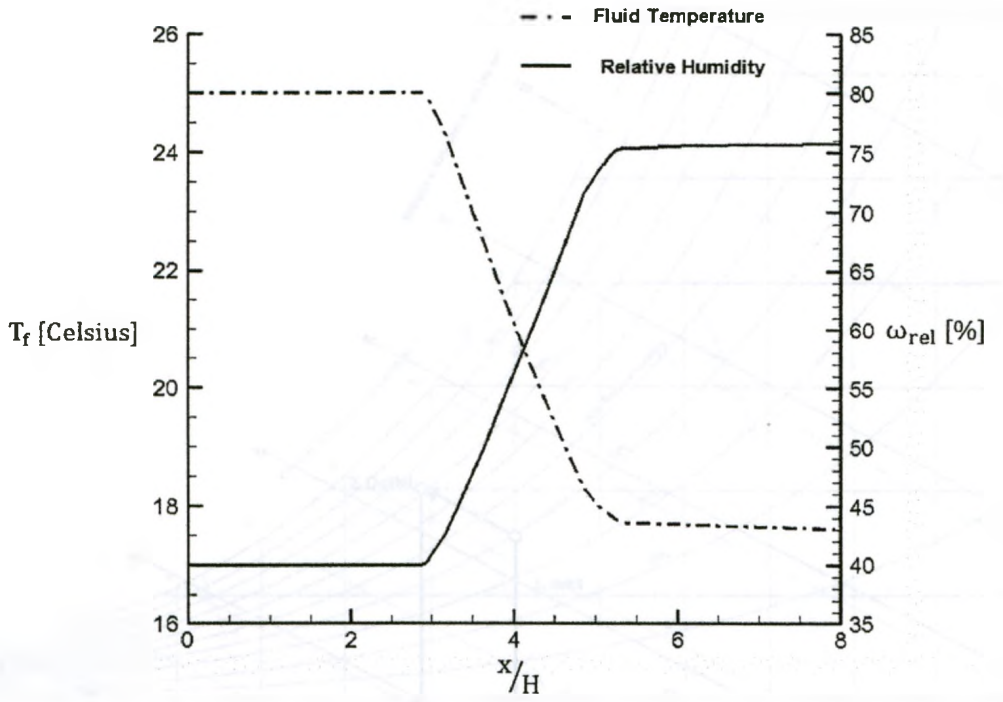

Figure 5-4 Centerline mixture temperature and relative humidity profiles

If an energy balance is taken over the domain shown in Fig. 5.1, and it is assumed that the makeup water saturating the porous medium is at the temperature of the outlet condition, then what is given is similar to an adiabatic saturator. This implies that the enthalpy of the mixture at the inlet is equal to the enthalpy of the mixture at the outlet ($h_{in} = h_{out}$). Utilizing the Psychrometric chart given in figure 5.5, the outlet dry bulb temperature can be predicted. This is performed by locating the inlet state, based on dry bulb temperature and relative humidity (state 1 in figure 5.4), and then following a line of constant enthalpy toward the saturation state. The line is followed until it intersects with the outlet humidity condition predicted from the simulation (state 2 in figure 5.4). The dry bulb temperature is then read off of the chart at this state. The results of the outlet conditions obtained in the simulation are compared with this approach, which is summarized in table 5.2.

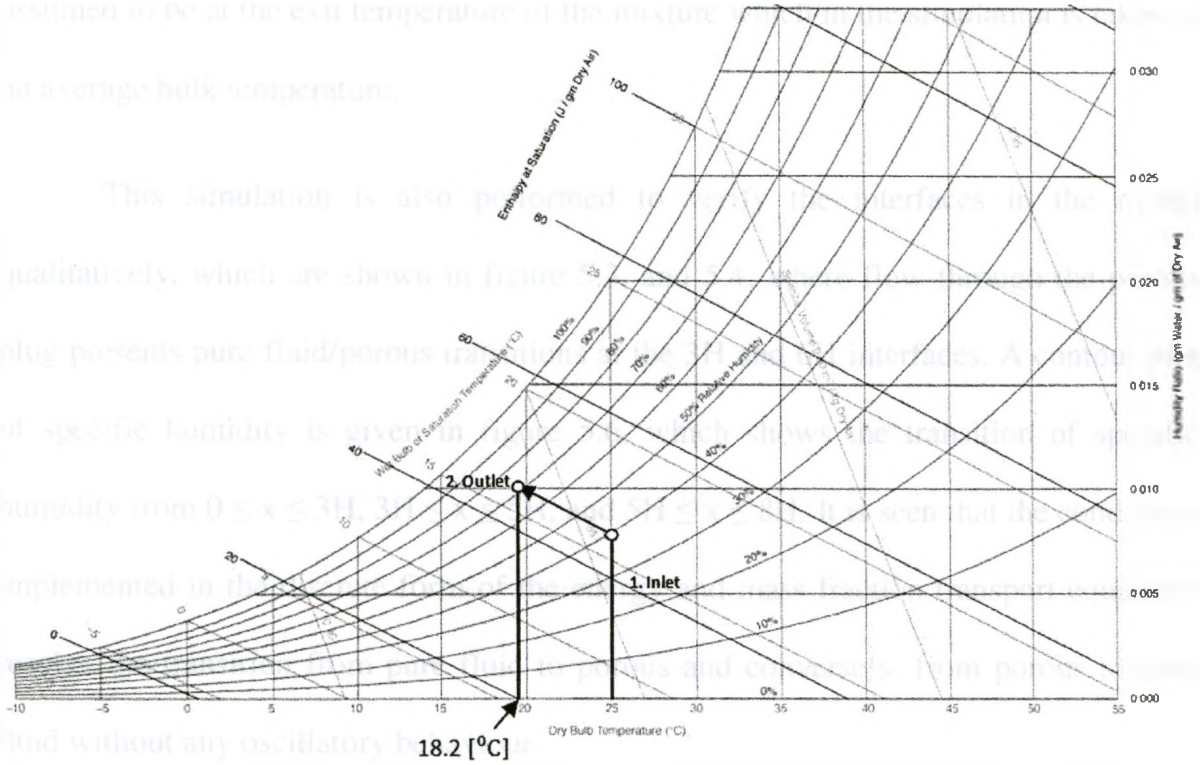

Figure 5-5 Theoretical prediction of outlet temperature from outlet relative humidity found in simulation

Table 5-2 Prediction of outlet temperature from Psycrometric chart compared to numerical results

	Psychrometric Chart	Simulation	% Difference
Inlet Temperature [°C]	25.0	25.0	
Inlet Relative Humidity [%]	40.0	40.0	
Outlet Temperature [°C]	18.2	17.76	2.4%
Outlet Relative Humidity [%]	76.0	76.0	

The difference between the outlet temperature predicted from the psychrometric chart and the outlet temperature predicted in the model is 0.44 degrees Celsius or approximately 2.4%. This is an acceptable result as there will be slight difference due to small density variations, and pressure changes throughout the domain. Also, in order to have adiabatic saturation, the liquid water supplied is

assumed to be at the exit temperature of the mixture which in the simulation is taken as an average bulk temperature.

This simulation is also performed to verify the interfaces in the model qualitatively, which are shown in figure 5.3, and 5.4, where flow through the porous plug presents pure fluid/porous transitions at the 3H and 6H interfaces. A contour plot of specific humidity is given in figure 5.6, which shows the transition of specific humidity from $0 \leq x \leq 3H$, $3H \leq x \leq 5H$, and $5H \leq x \leq 8H$. It is seen that the conditions implemented in the discrete form of the energy and mass fraction transport equations resolve the transition from pure fluid to porous and conversely, from porous to pure fluid without any oscillatory behaviour.

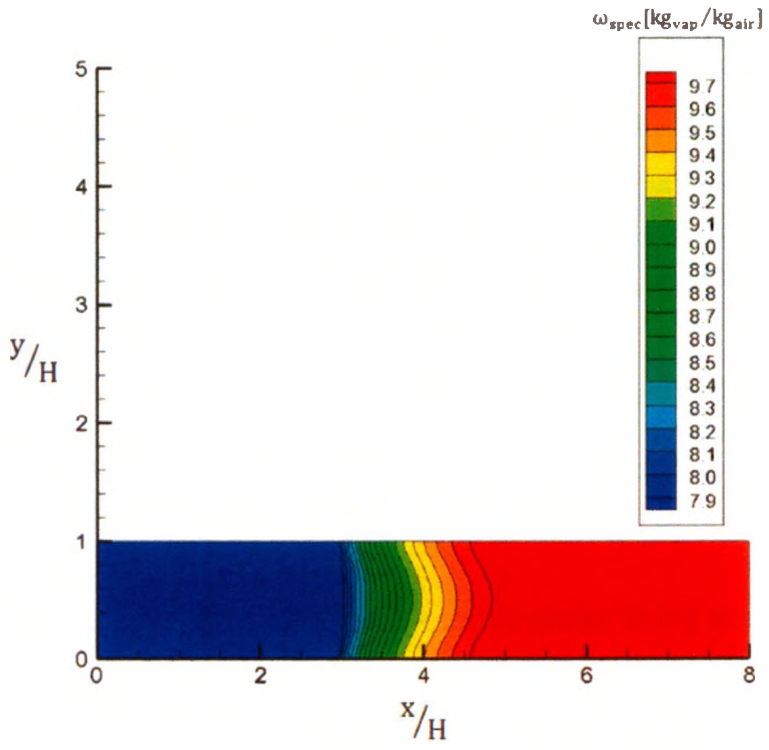

Figure 5-6 Specific Humidity Contours for Adiabatic Porous Plug Saturator

5.3 Test Case 2: Indirect Evaporative Cooling

Indirect evaporative cooling is often chosen over direct evaporative cooling, as the specific humidity of the delivered air is not altered. This allows more control in the comfort level of the air delivered to the conditioned space. In this test case, a two channel counter flow indirect evaporative cooler is simulated (figure 5.7). This is a conjugate pure fluid/porous/solid problem and is used to both validate the interface conditions in all regions of differing domain types, and make a comparison of results to that obtained by Zhan et al [49]. The goal of the simulation is to predict the outlet temperature of the product air stream (the air delivered to the conditioned room).

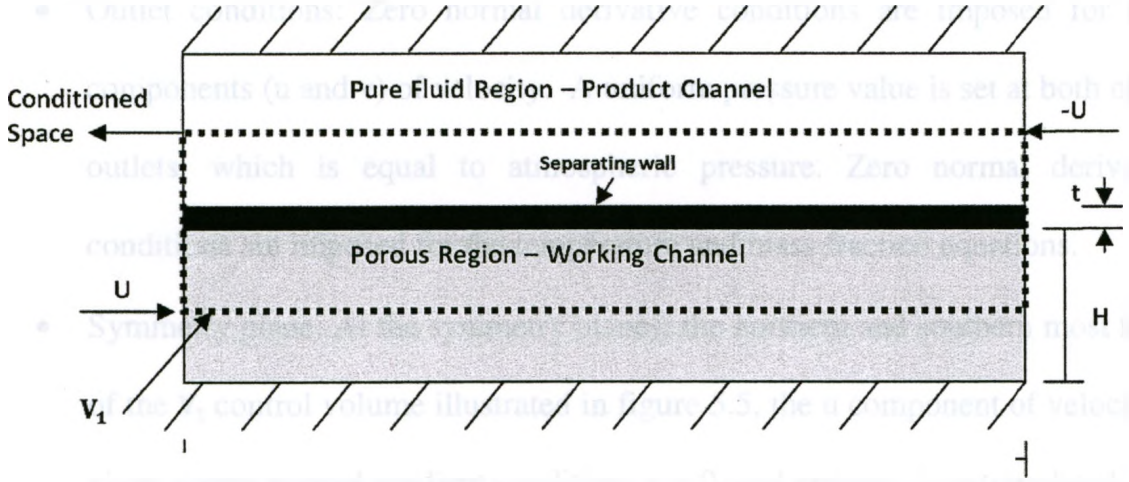

Figure 5-7 top view of counterflow indirect evaporative cooler with 'L' giving the channel length, 'H' the working and dry channel height, and 't' the thickness of the material separating the two channels.

As the complete geometry of the indirect evaporative cooler being analyzed consists of multiple channels similar to figure 5.7 in a stacked arrangement, this allows the domain to be simplified by making symmetry arguments, such that only the domain volume $\mathbf{V_1}$ shown by the dashed line in figure 5.7 is modelled. Also, it will be assumed that the depth of the channel is much longer than the height **H,** and therefore the problem is

additionally simplified to two-dimensions. All boundary conditions imposed must now reflect the domain $\mathbf{V_1}$, and the conditions are given as:

- Inlet conditions: A constant velocity profile is imposed at inlet of the product channel with magnitude U. In the porous region, the inlet velocity is also allowed to develop with a prescribed uniform inlet of U. In the fluid and porous regions, U = 0.4 [m/s], and V = 0 [m/s] at both inlets. The fluid temperature at both inlets is given to be $T_f = 25$ [°C], and the relative humidity's as $\omega_{rel} = 35\%$ consistent with [49]. The pressures at the inlets are extrapolated from the interior of the domain.
- Outlet conditions: Zero normal derivative conditions are imposed for both components (u and v) of velocity. A uniform pressure value is set at both of the outlets, which is equal to atmospheric pressure. Zero normal derivative conditions are imposed for the temperature and mass fraction equations.
- Symmetry plane: At the symmetry planes; the northern and southern most faces of the $\mathbf{V_1}$ control volume illustrated in figure 5.5, the u component of velocity is given a zero normal gradient condition, v = 0, and pressure is extrapolated. The energy and mass fraction equations are also given zero normal gradient boundary conditions.

The porous material in the working channel is modelled using the known properties of the aluminum foam given in test case 1. That is, the fluid and solid phase effective conductivity is given as $k_{f\,eff} = 0.0237\left[{}^{W}/_{m\,K}\right]$, and $k_{s\,eff} = 6.46\left[{}^{W}/_{m\,K}\right]$ [45]. The binary diffusion coefficient is given as $D_{f\,eff} = 1.5 \times 10^{-4}\ \left[{}^{m^2}/_{s}\right]$ [46]. The

pore diameter and ligament diameter are $d_p = 3.8\,\text{mm}$ and $l_D = 0.55\,\text{mm}$. It is assumed that $\mu_B = \mu_f$, and that the fluid properties are taken at the fluid inlet temperature. Dispersion is neglected in this simulation. The convective interfacial heat and mass in the porous region are given as, $Nu_{sur} = C_T Re_{ld}^{0.5} Pr^{0.37} = h_{sur} l_D / k_f$ and $Sh_{sur} = C_m Re_{ld}^{0.5} Sc^{0.37} = h_{m,sur} l_D / D_f$ where $C_T = C_m = 0.52$ [45]. The interior wall with thickness 't' separating the working and dry channels in figure 5.5 is assumed to be aluminum, with thermal conductivity of $k_s = 250.0\,[^{W}/_{m\,K}]$. This is modelled to validate the interface conditions at the pure fluid/porous and pure fluid/solid regions. The remaining properties of the mixture are given by imposing the same arguments in the first test case, and are taken to be that of air at 300[K] (table 5.1). The channel length **L** is 1.4 [m] and both the working and product channel each have a height of **H** = 0.08[m]. Finally, it is assumed that the surface of the porous region is kept saturated, and that the device is operated at steady state conditions.

It is noted that the results presented have been obtained using a grid convergence procedure in the fluid and porous channel regions (table 5.3). In the interior wall, four volumes are used in the y-direction. Results are acceptable when the percentage difference in the bulk outlet temperature of the product channel is less than 5% between consecutive grid refinements. Table 5.3 only indicates the quantity of control volumes used in the x and y direction in the two channels, however it is stated that grid refinement is used at the inlet and outlet, and in regions near the interior wall.

Table 5-3 Grid convergence study for indirect evaporative cooling simulation

Number of volumes (X-direction x Y-direction)	Bulk Temperature of product channel [°C]	% Difference
101 CV x 36 (18 wet channel, 18 dry channel)	23.88	
111 CV x 46 (23 wet channel, 23 dry channel)	22.66	5.1%
121 CV x 56 (28 wet channel, 28 dry channel)	22.14	2.4%

Relative humidity and temperature contour plots of the above conditions in the simulated domain ($\mathbf{V_1}$) of figure 5.7 are given in figure 5.8 and figure 5.9. Although the plots cannot be quantitatively compared to the work of [49], as these results only present the outlet dry bulb temperature, the simulations are qualitatively evaluated.

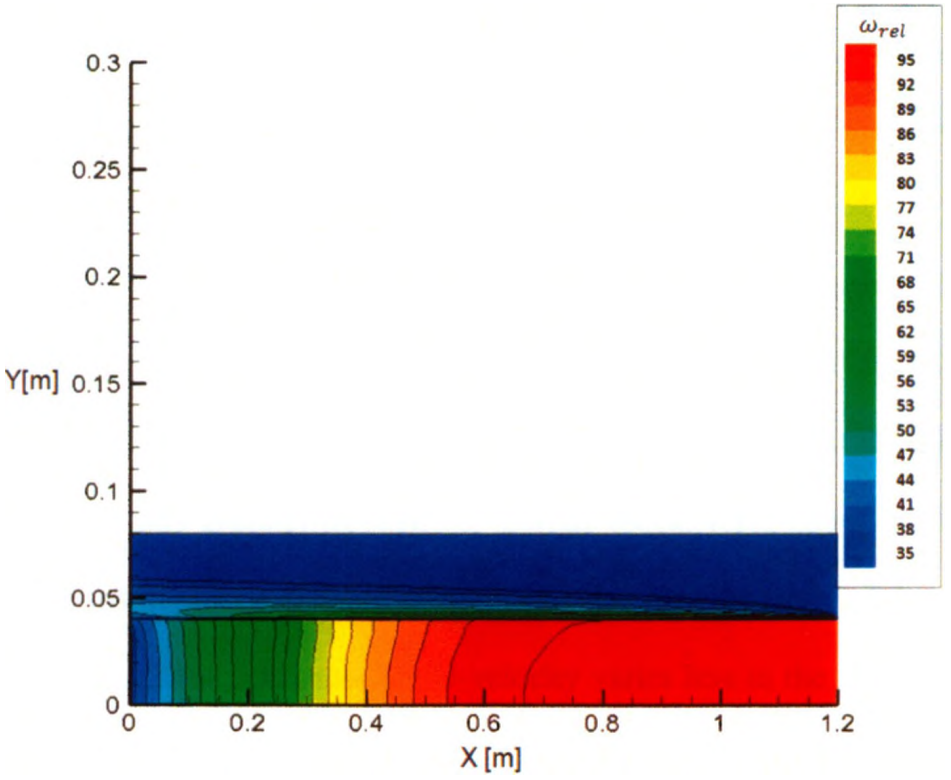

Figure 5-8 Plot showing relative humidity contours of the product and working channels for the case of an indirect evaporative cooler.

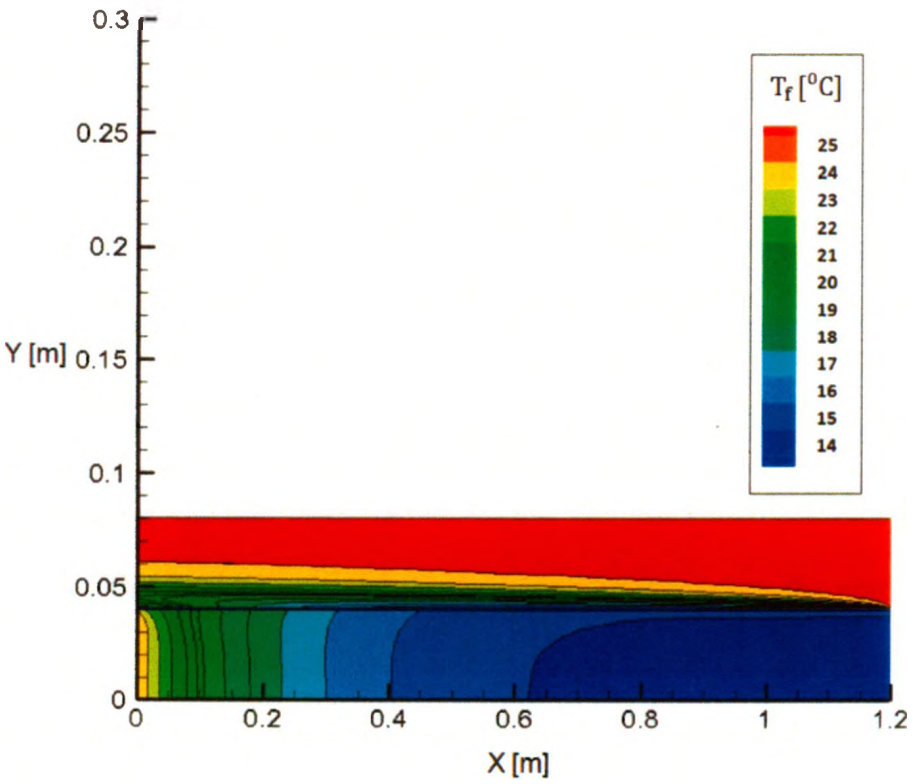

Figure 5.9 - Plot showing temperature contours of the product and working channels for the case of an indirect evaporative cooler.

Qualitatively, the results of the temperature and relative humidity plots correctly simulate the indirect evaporative cooling process. It is viewed that in the wet channel, the humidity increases in the stream-wise direction through the saturated media, from $\omega_{rel} = 35\%$ to $\omega_{rel} = 94.7\%$, which is due to the large wet bulb depression present in the incoming water vapour/air mixture. Also, it is seen that due to the increased drag in this channel through the porous block, represented by the Darcy-Forcheimer terms in the momentum equations, the contour lines of humidity are essentially vertical. This is because the U-velocity varies less in the y-direction of the porous plug than it does in the pure fluid region, as momentum is spread over the channel.

In the product channel, as the flow develops over the plate, it loses sensible energy to the porous side which decreases the temperature of the flow, in the region near the interior wall. As the specific humidity remains constant in this channel, the decrease in temperature of the mixture leads to an increase in relative humidity. This is because the saturation state of the mixture is influenced by temperature.

The interface conditions appear to function correctly through the regions intersecting the solid interior wall as there are no numerical oscillations in the temperature and mass fraction field. To further validate this point; the entrance region of the porous channel and the exit region of the product channel, near the interior wall are examined further. Inspecting figures 5.8 and 5.9, it is noticed that the relative humidity of the product channel increases slightly near the interface of the pure fluid/solid region directly adjacent to the outlet. This is because some of the heat from the inlet of the working channel conducts into the product channel. This results in a slight increase in the fluid temperature next to the interface in the product channel due to the high conductivity of the aluminum. As the temperature increases in this fluid region, the saturation pressure also increases, which ultimately lowers the relative humidity in this region.

The supply air temperature (air exiting the product channel) from the simulation is plotted against the results of Zhan et al. [49, 50], in figure 5.8. Although these two studies are not identical; in that this work utilizes a porous domain to saturate the media rather than a fibre sheet along the working channel wall, the concept is similar and therefore the trends in the data are expected to be similar.

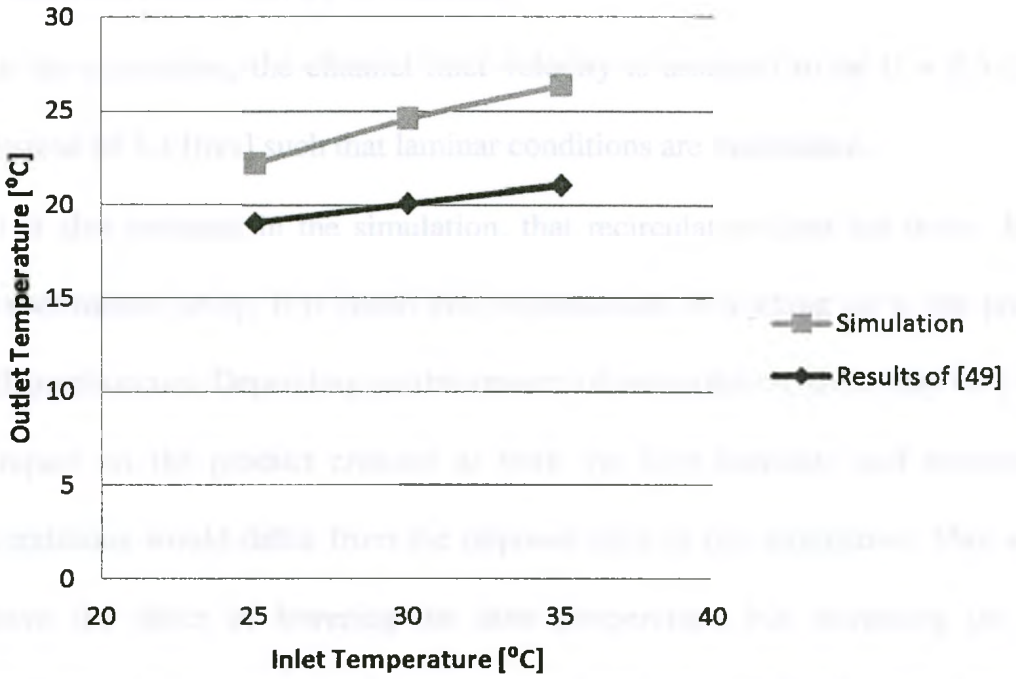

Figure 5-9 Outlet temperature compared with inlet temperature for indirect cooling process

The results obtained from the current numerical work follow a similar trend as the results obtained in [49, 50]. However, it is seen that the outlet temperatures predicted in this simulation are greater than the experimental values. Discrepancies in the data results are expected for the following reasons;

- The sensors utilized in the experimental setup have certain accuracies associated with measurement. In the experiment performed [49, 50], the thermocouples have an accuracy of ± 0.2 [^{0}C] over there 0-100 [^{0}C] operating range, and the hot-wire anemometer is stated to have an accuracy of $\pm 5\%$ in a 0.2-20 [m/s] operation range. Although the magnitude of the temperature accuracy is small within the operation range of the experiment, this is not the

case for the measured velocity, which may introduce some error on the inlet conditions imposed in the simulation.

- In the simulation, the channel inlet velocity is assumed to be U = 0.4 [m/s], instead of 2.4 [m/s] such that laminar conditions are maintained.
- It is also assumed in the simulation, that recirculation does not occur. In the experimental setup, it is stated that recirculation of working air to the product channel occurs. Depending on the amount of recirculation, there may be a large impact on the product channel as both the inlet humidity and temperature conditions would differ from the imposed inlet of this simulation. This would have the effect of lowering the inlet temperature, but increasing the inlet humidity. As the amount of recirculation is not fully defined, this is neglected in the simulation.

The wet bulb effectiveness is a standard measure of the efficiency of an evaporative cooling process. This is defined as

$$\epsilon_{wb} = \frac{T_{i,db} - T_{o,db}}{T_{i,db} - T_{i,wb}}, \qquad (5.4)$$

where $T_{i,wb}$, $T_{i,db}$, $T_{o,db}$ ar the inlet wet bulb, inlet dry bulb, and outlet dry bulb temperatures. In the experimental results, the average wet bulb effectiveness is calculated to be 77%. The simulated cooling cycle gives an average wet bulb effectiveness of 42%. Although the simulated results predict a much lower average wet bulb effectiveness, they seem to better reflect stated values in other literature which claim standard indirect evaporative cooling processes generally obtain between 50-60% wet bulb effectiveness [22].

5.4 Test Case 3: Simplified Maisotsenko Cycle

In the two previous test cases, direct and indirect evaporative cooling was simulated. As stated, the advantage of a direct evaporative cooling process is that the cooling efficiency; defined by equation 5.4, is much higher than an indirect evaporative cooling process. This difference in performance is seen to be even greater in most practical applications, as indirect configurations are generally cross flow oriented. The disadvantage of direct evaporative cooling is that the air being delivered to the working space is generally poorly conditioned, due to the high value of relative humidity. A desired scenario would be to obtain the performance of a direct evaporative cooler, with the configuration of an indirect evaporative cooler.

In this work, a more recent technique of evaporative cooling, called the Maisotsenko evaporative cooling cycle [51] is investigated. This configuration is similar to an indirect evaporative cooler, as both a wet working channel and a dry product channel exist, however a third dry channel is added to the geometry where a simplified version is given in figure 5.10. The addition of the third dry channel is novel in that it provides preconditioning to the inlet air prior to entering the porous section of the working zone. This is further explained after the contour plots in this section. This geometry is said to be more efficient at cooling the product channel over traditional indirect evaporative cooling processes.

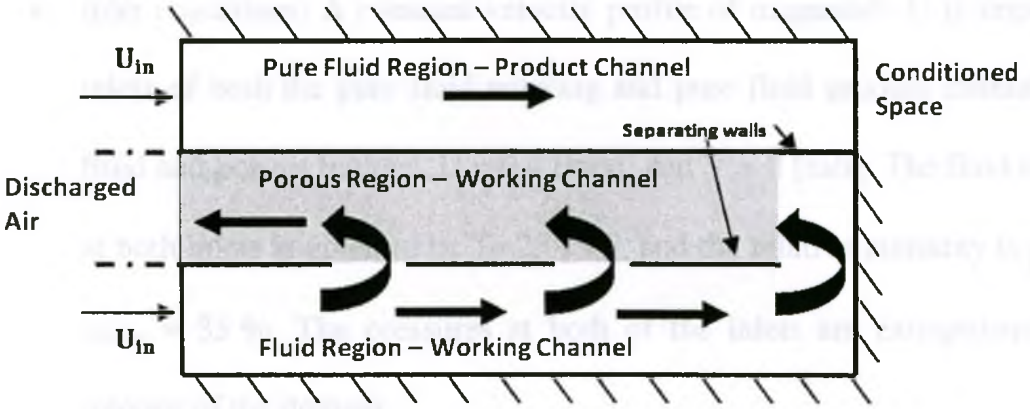

Figure 5-10 The Maisotsenko Evaporative cooling cycle

As very little numerical or experimental data is available to investigate Maisotsenko configurations, the test case proposed will study the cycle qualitatively. Therefore, dimensions similar to the indirect evaporative cooler of the second test case are implemented on the simplified domain; shown in figure 5.10, to simulate this novel cycle.

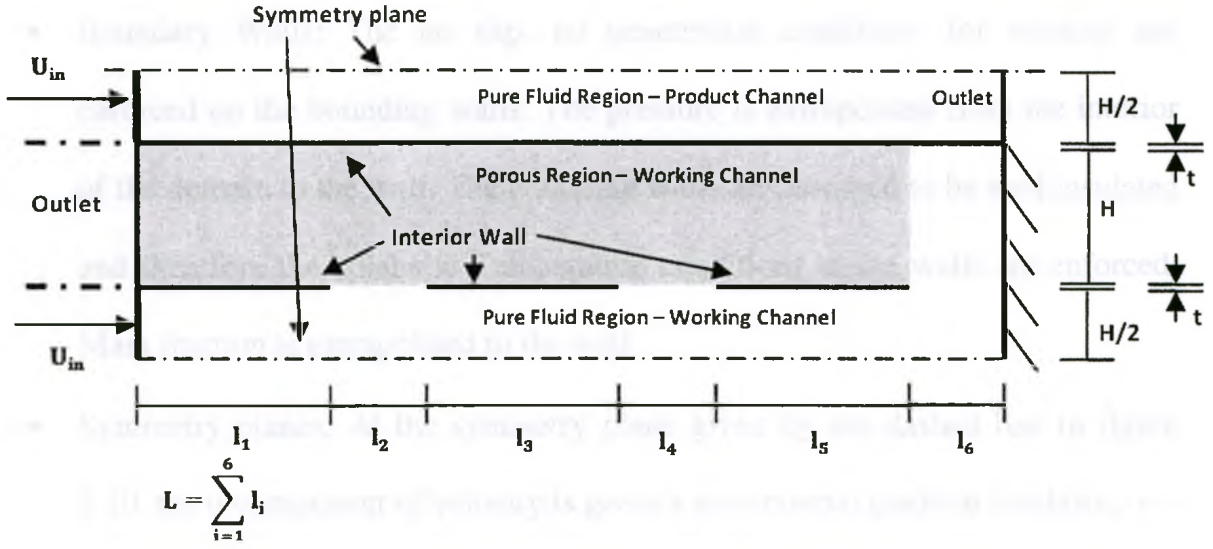

Figure 5-11 Domain conditions for the Maisotsenko evaporative cooling cycle.

The boundary conditions implemented in this test case, with domain represented in figure 5.11, are:

- Inlet conditions: A constant velocity profile of magnitude U is imposed at the inlets of both the pure fluid working and pure fluid product channels. In both fluid and porous regions, U = 0.4 [m/s], and V = 0 [m/s]. The fluid temperature at both inlets is given to be T_f=25 [^oC], and the relative humidity is given to be $\omega_{rel} = 35\ \%$. The pressures at both of the inlets are extrapolated from the interior of the domain.
- Outlet conditions: Zero normal derivative conditions are imposed for the two components (u and v) of velocity at both the pure fluid product channel and the porous working channel outlet. Additionally, a uniform pressure value is set at both of the outlets, which is equal to atmospheric conditions. Finally, zero normal derivative conditions are imposed for the temperature and mass fraction equations.
- Boundary Walls: The no slip, no penetration conditions for velocity are enforced on the bounding walls. The pressure is extrapolated from the interior of the domain to the wall. The bounding walls are assumed to be well insulated and therefore the adiabatic Temperature conditions at the walls are enforced. Mass fraction is extrapolated to the wall.
- Symmetry planes: At the symmetry plane given by the dashed line in figure 5.10, the u component of velocity is given a zero normal gradient condition, v = 0, and pressure is extrapolated. The energy and mass fraction equations are also given zero normal gradient boundary conditions.

The porous material in the working channel is modelled using the properties of the aluminum foam from the indirect evaporative cooling test case (test case 2).

The pore and ligament diameter of the foam are given as, $d_p = 3.8\,[\text{mm}]$ and $l_D = 0.55\,\text{mm}$. The effective binary diffusion coefficient is given as $D_{f,eff} = 1.5 \times 10^{-4}[m^2/s]$ [46]. The fluid and solid phase effective conductivity is given as $k_{f,eff} = 0.0237[W/m\,K]$, and $k_{s,eff} = 6.46[W/m\,K]$ [45]. It is assumed that $\mu_B = \mu_f$, and that the fluid properties are taken at the fluid inlet temperature. Dispersion is once again neglected in this simulation. The convective interfacial heat and mass transfer in the porous calculated by $Nu_{sur} = C_T Re_{ld}^{0.5} Pr^{0.37} = h_{sur} l_D / k_f$ and $Sh_{sur} = C_m Re_{ld}^{0.5} Sc^{0.37} = h_{m,sur} l_D / D_f$ where $C_T = C_m = 0.52$ [45]. The interior wall with thickness 't' separating three channels in figure 5.10 is assumed be aluminum with thermal conductivity of $k_s = 250.0\,[W/m\,K]$. The properties of the water vapour/dry air mixture are taken to be for an inlet temperature of 25 [°C]. The channel length **L** is 1.2 [m], consistent with the indirect evaporative cooling cycle in the second test case. Although the total channel length is defined, the lengths of each interior wall and gap ($l_1, l_2, l_3, l_4, l_5, \text{and } l_6$) separating the two sections of the working channel must be determined. As this case is for pure demonstration, these lengths are chosen arbitrarily, but aimed at maximizing saturation throughout the working channel. These lengths are listed in table 5.4, given as:

Table 5-4 Simplified Maitsosenko Channel Lengths

Section of working channel	Length [m]
l_1	0.46
l_2	0.04
l_3	0.36
l_4	0.04
l_5	0.26
l_6	0.04

The working and product channels each have a height of **H** = 0.08[m], and the thickness of each interior wall is given as **t** = 0.0005 [m]. The surface of the porous region is assumed to be saturated, and the device is operated at steady state conditions. In order to obtain a sufficiently conditioned coefficient matrix, the steady state solutions were obtained by marching in time from an initial condition where all field variables are set to an initial state: this being velocity components set equal to zero, pressure to atmosphere, and temperature and mass fraction to the inlet conditions. Steady state is assumed when the maximum change in the fields, in any volume, between successive time steps falls below 0.01%. A grid of 280 control volumes in the x-direction, and in the y-direction: 30 control volumes over each of the pure fluid region channels, 4 control volumes over each interior wall, and 50 control volumes in the porous region, are found to be grid-converged to within 5% based on the bulk outlet temperature.

The contours of relative humidity and temperature for the domain of figure 5.11 with the given inlet conditions above are presented in Figures 5.12 and 5.13.

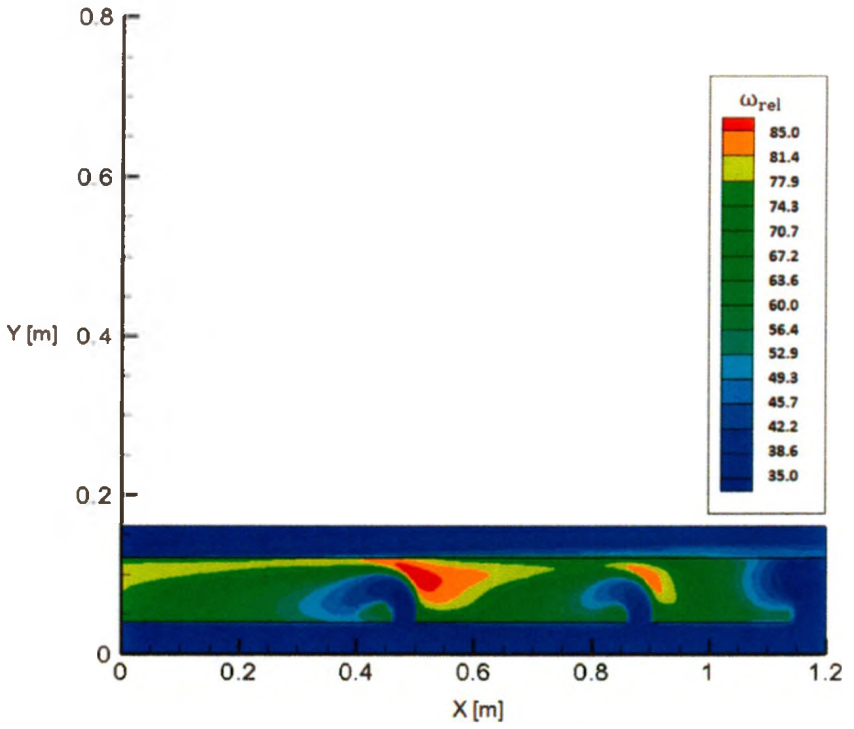

Figure 5-12 Plot showing relative humidity contours of the product and working channels for basic Maisotsenko Cycle

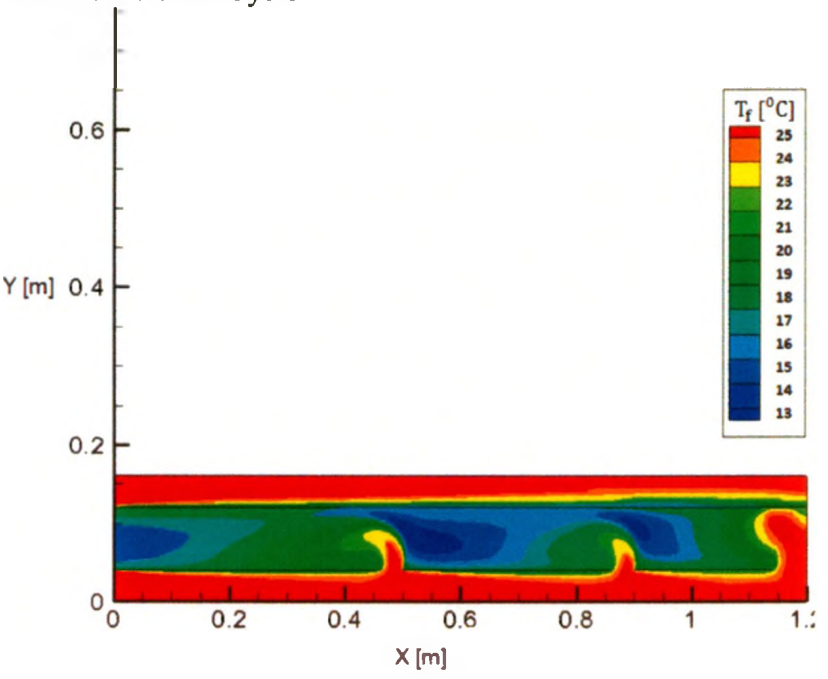

Figure 5-13 Plot showing relative humidity contours of the product and working channels for basic Maisotsenko Cycle

The bulk temperature of the air exiting product channel is 20.88 [°C]. The wet bulb temperature of the intake air to the system is 15.5 [°C]. Although the outlet air is

not at or below the inlet wet bulb temperature, it is exiting at a lower value than the simulated indirect evaporative cooling cycle with similar geometry. Comparing both designs; this configuration yields a wet bulb effectiveness of 44%, whereas using the indirect evaporative cooler with identical inlet conditions gives an effectiveness of 26%. This indicates that the Maisotsenko cycle is more effective at cooling the inlet air when using a similar geometric design as the indirect cooler. Although this example is purely demonstrative, there are relevant qualitative conclusions that can be drawn from the simulation.

The cycle is explained using the psychrometric chart:

Working channel

- 1-2': As the inlet working air travels through the dry side of the working channel (southern most channel), it is cooled similarly to the dry product channel (northern most channel). This is functioning as an indirect evaporative cooler for the working channel and is seen in figures 5.12 and 5.13, as the mixture humidity rises and the mixture temperature lowers, near the interior wall of the dry side of the working channel.
- 2'-3'-3: As the air enters the inlet to the porous region of the domain, it is has been reduced in temperature from the inlet conditions. At this reduced temperature, saturating the air approaches a lower wetbulb temperature then boundary inlet condition (2'-3'). However, as the inlet condition in the product channel is at a higher temperature, some sensible heat is absorbed back into the near saturated working channel (3'-3).

Dry Channel

- 1-4: The product channel is cooled along a similar line as the dry side of the working channel losing sensible heat to the porous section of the working channel. Under ideal conditions, this allows the dry product channel to approach the dew point temperature.

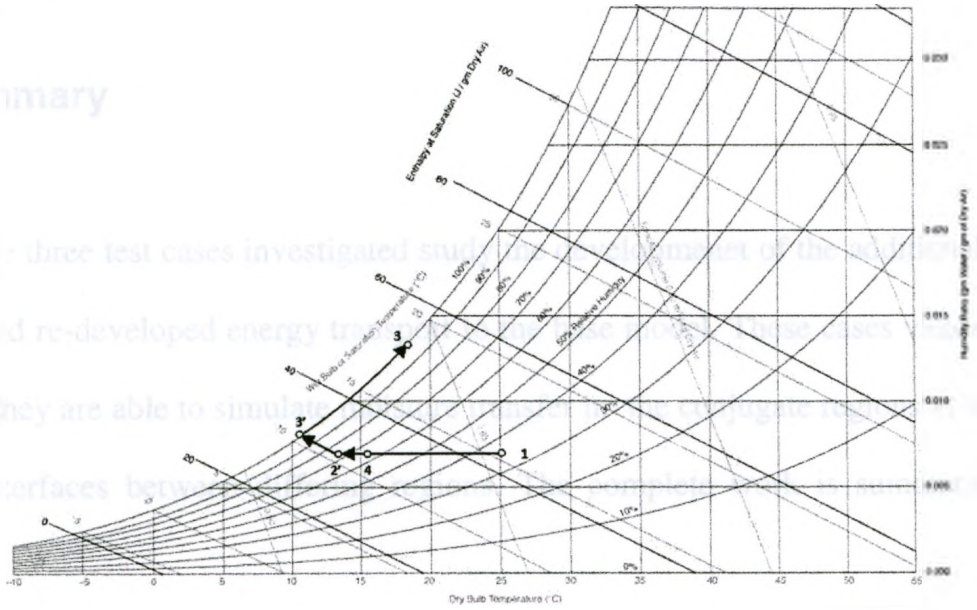

Figure 5-14 Maisotsenko cycle analyzed on Psychrometric chart

Although the product air never reaches the dew point, the process explained above is occurring in the system. The mixture on the dry side of the working channels (sections $0 \leq x \leq 0.5$, $0.5 \leq x \leq 0.9$ and $0.9 \leq x \leq 1.2$ [m]) is cooling similar to an indirect evaporative cycle. As the mixture enters the wet working porous media, it is already at a reduced temperature then the inlet conditions. Therefore, saturating the air will allow the temperature to be reduced below conditions achieved in the indirect evaporative cooling cycle. Although this test case is purely demonstrative, it shows that the

Maisotsenko cycle does have the potential to be a much more efficient evaporative cooling design and more work on this cycle should be investigated.

Again, as this was only a demonstrative simulation, improvements to the simulation can be made. It is recommended that in order to see the full potential of this particular configuration, optimization of the geometric parameters l_1, l_2, l_3, l_4, l_5, and l_6 be performed.

5.5 Summary

The three test cases investigated study the developmenet of the additional mass fraction and re-developed energy transport to the base model. These cases validate the model as they are able to simulate moisture transfer in the conjugate regions as well as resolve interfaces between differing regions. The complete work is summarized in chapter 6.

Chapter 6 - Summary, Contributions, and Future Recommendations

6.1 Summary

The principle aim of the presented work was to extend the capability of an in-house conjugate heat/flow model to include moisture exchange such that applications in food storage/ripening and heating, ventilation, and air conditioning (HVAC) could be considered. This task was accomplished by implementing a mass fraction transport equation into the existing model to account for a dry air-water vapour mixture, and re-formulating the energy transport equations to account for this multi component mixture. As stated, the model developed is utilized to solve conjugate fluid, porous, and solid domains. Formulation in the porous regions followed the works of Whitaker, where volume averaging the governing equations throughout the porous part of the conjugate domain simplified the media such that this part of the domain could be modelled. The derivation followed a non-equilibrium approach for species and heat transfer as this allowed more versatility in the model for future work. This non-equilibrium versatility is beneficial over traditional equilibrium approaches, as often in agricultural applications, internal moisture and temperature conditions dictate the transfer between constituents. Although this is a more versatile approach, extra transfer terms do exist between the constituents and the derivation must ensure proper representation of flux between constituents. Additionally, because this is a conjugate numerical code; treatment through fluid-porous, and porous-solid interfaces was also addressed. Applications in the HVAC industry were chosen for validation, as the

model was utilized to predict operating temperatures in evaporative cooling cycles, and study the energy and mass fraction transport processes throughout the modelled domains.

6.1 Contributions

The primary contributions of this work may be summarized as follows:

- The author presents a 3-D structured conjugate finite volume code that is used to model mass, momentum, and energy transport. This model is extended to include the capability to support vapour transport in the fluid and porous domains, and mass transfer in the porous domain. As the fluid being modelled is now represented as a mixture, re-formulation of the energy transport equations of the base code was also required.
- As interfaces between regions are modelled in the numerical code, special attention was given to the development of physically reasonable conditions at these interfaces. This included an approximation of the interfacial heat and mass fraction flux associated with extensions to the model. This also included an approximation for partial pressure at the interface between the pure fluid and porous regions. These conditions are implemented to ensure physically reasonable results are obtained, which is demonstrated by the validation cases presented.
- In order to validate the model, as the cases being studied were more complex then the code was designed for, the base code was re-structured such that it

could be executed on SHARCNET using faster processing power, and alleviating memory limitations.

6.3 Recommendations for Future Work

Further work is clearly required in making the model more applicable to the complex domains encountered in engineering processes. This model is limited to applications where the domain may be simplified to be nearly orthogonal. Although this is a good foundation for model development and for the evaporative cooling processes considered in this work, further extending the development to unstructured domains would be quite beneficial. Also, this model was developed to consider multi-component fluids, as in the applications being considered, excessive amounts of liquid is not desired and the assumption of having only a saturated surface is justifiable. Further extension of the model to include multi-phase fluid fields would be beneficial and it is seen that this model provides a good platform for the gas mixture part of any multiphase extension. As only HVAC applications are considered due to the lack of data for agricultural type applications, it is recommended that experiments be performed to quantify the necessary parameters needed to simulate domains in the food industry. Finally, it is suggested that a parametric study of the final test case be performed to optimize the geometry of the Maisotsenko evaporative cooler.

References

[1] Datta, A.K., 2006, " Porous media approaches to studying simultaneous heat and mass transfer in food processes. I: Problem formulations," J. Food Engineering **80**, pp 80-95

[2] Whitaker, S., 1997, *Volume Averaging of Transport Equations*, chap. 1, Fluid Transport in Porous Media, Springer-Verlag, Southampton, UK, pp. 1–59.

[3] Slattery, J. C., 1967, "Flow of viscoelastic fluids through porous media," A.I.Ch.E. Journal, **13**(6), pp. 1066–1071.

[4] Kaviany, M., 1995, *Principles of Heat Transfer in Porous Media*, Springer-Verlag, New York, NY, 2nd ed.

[5] V. A. F. Costa, L. A. Oliveira, B. R. Baliga, and A. C. M. Sousa, 2004 "Simulation of Coupled Flows in Adjacent Viscous and Porous Domains Using a Control-Volume Finite-Element Method", Numer. Heat Transfer A, **45**, pp. 675–697

[6] Betchen, L. J., Straatman, A. G., and Thompson, B. E., 2006, "A non-equilibrium finite-volume model for conjugate fluid/solid/porous domains," Numerical Heat Transfer, Part A, **49**(6), pp. 543–565.

[7] Whitaker, S., 1977, "Simultaneous Heat, Mass, and Momentum Transfer in Porous Media: A Theory of Drying," Advance in Heat Transfer, **13**, pp. 119–204

[8] Mujumdar, A.S., 2007, *Handbook of Industrial Drying*, CRC/Taylor & Francis, Boca Raton, FL, 3rd ed.

[9] Valencia-Lopez, J.J. , Espinosa-Paredes, G., Ochoa-Tapia, 2003, "Mass Transfer Jump Condition at the Boundary between a Porous Medium and a Homogeneous Fluid," J. Porous Media **6**(1), pp 33-49

[10] Xu., Y., Burfoot, D., 1998, "Simulating the bulk storage of foodstuffs," Journal of Food Engineering **39**, . pp23-29

[11] Ward, J. C., 1964, "Turbulent flow in porous media," J. Hydraulics Div. Proc. American Soc. Civil Engineers, **90**(5), pp. 1–12.

[12] K. Vafai and C. L. Tien, "Boundary and Inertia Effects on Flow and Heat Transfer in Porous Media," Int. J. Heat Mass Transfer, vol. 24, pp. 195–203, 1981

[13] Quintard, M., Kaviany, M., and Whitaker, S., 1997, "Two-medium treatment of heat

transfer in porous media: Numerical results for effective properties," Adv. Water Resources, **20**(2), pp. 77–94.

[14]Sahraoui, M. and Kaviany, M., 1994, "Slip and no-slip temperature boundary conditions at the interface of porous, plain media: Convection," Int. J. Heat Mass Transfer, **37**(6), pp. 1029–1044.

[15] Marchant, J.A. , 1976 ,"Predictions of fan pressure requirements in the drying of large hay bales," J. Agricultural Engineering Research, **21**(4) . pp 333-345

[16] Smith, E.A, Jayas, D. S, Muir, W.E, Alagusundaram, K., Kalbande, V. H, 1992, "Simulation of grain drying bins with partially perforated floors. Part I: Iso Traverse lines," American Society of Agricultural Engineers, **35** (3). pp. 909-915

[17] Smith, E.A, Jayas, D. S, Muir, W.E, Alagusundaram, K., Kalbande, V. H, 1992, "Simulation of grain drying bins with partially perforated floors. Part II: Calculation of moisture content," American Society of Agricultural Engineers, **35** (3). pp. 917-922.

[18] Tassou, S. A, Xiang, W., 1998, "Modelling the environment within a wet air-cooled vegetable store," Journal of Food Engineering, **38**. pp. 169-187.

[19] Becker, B.R., Misra, A., Fricke, B.A., 1995, "Bulk Refrigeration of Fruits and Vegetables Part 1: Theoretical Considerations of Heat and Mass Transfer," University of Missouri-Kansas City. pp 1-26.

[21] Hoang, M.L., Verboven, P., Baelmans, M., Nicolai, B.M., 2003, "A continuum Model for Airflow, Heat, and Mass Transfer in Bulk of Chicory Roots," American Society of Agricultural Engineers, **46** (60), pp. 1603-1611

[22] Jan Bom, G., Foster, R.,Dijkstra, E., Tummers, M., 1999, *Evaporative Air-Conditioning*, The International Bank for Reconstruction, Washington D.C.

[23] Erens P.J., 1993, "Modelling of Indirect Evaporative Air Coolers", International Journal of Heat and Mass Transfer, **36** (1), pp. 17-26

[24] Wang, T. A., Reid, R. L., 1996, " Surface wettability effect on an indirect evaporative cooling system," ASHRAE Transactions, **102** (1), pp. 427 – 433

[25] Cengel, Y. A, Boles, M.A, 2008, *Thermodynamics An Engineering Edition sixth edition*, McGraw Hill Company, New York, NY., pp 738-747

[26] Bird, B. R., Stewart, W. E., Lightfoot, E. N., 2007, *Transport Phenomena: Second Edition*, John Wiley & Sons, Inc., Madison Wisconsin

[27] Whitaker , S., 1998, "Coupled Transport in Multiphase Systems: A Theory of Drying," Advances in Heat Transfer, **31**, pp. 1 - 103

[28] Quintard, M., Whitaker, S., 1994, "Transport in ordered and Disordered Porous Media I: The Cellular Average and the use of Weighting Functions," Transport in Porous Media, **14**, pp. 163 - 177

[29] Patankar, S. V., 1980, *Numerical Heat Transfer and Fluid Flow*, Hemisphere, New
York, NY.

[30] Spekreijse, S., "Multigrid Solution of Monotone Second Second-Order Discretization of Hyperbolic Conservation Laws," Mathematics of Computation, **44** (179), pp. 135-155

[31] Van Leer, B., 1974,"Towards the Ultimate Conservative Difference Scheme II: Monotonicity and Conservation Combines in a Second Order Scheme," J. Comput. Phys., !$, pp. 361-370

[32] Blazek, J., 2001, *Computational Fluid Dynamics: Principles and Applications*, Elsevier, New York, NY, pp 75-180

[33] Venkatakrishnan, V., 1995, "Convergence to steady-state solutions of the Euler equations on unstructured grids with limiters," J. Computational Physics, **118**(1), pp. 120–130.

[34] Yee, H. C., Warming, R. F., 1985 "Implicit Total Variation Diminishing (TVD) Schemes for Steady stat calculations", J. Computation Physics, **57,** pp 327 - 360

[35] Fogler, S. H., 2006, *Elements of Chemical Reaction Engineering Fourth Edition*, Prentice Hall PTR, Upper Saddle River, NJ, pp 758-865

[36] Glassman, I., 1987, *Combustion Second edition*, Academic Press Inc, London England, pp 386-396

[37] Balay, S., Gropp, W. D., McInnes, L. C., and Smith, B. F., 2008, "PETSc users manual," Tech. Rep. ANL-95/11 - Revision 3.0, Argonne National Laboratory.

[38] Balay, S., Gropp,W. D.,McInnes, L. C., and Smith, B. F., 2009, "PETSc home page," http://www.mcs.anl.gov/petsc, accessed April 26, 2009.

[39] 2011, "SHARCNET homepage," http://www.sharcnet.ca, accessed Jan 26, 2011.

[40] Martins-Costa, M. L., Saldanha de Gama, R. M., "A Local Model for the Heat Transfer Process in Two Distinct Flow Regions," Int. J. Heat Fluid Flow, vol. 15, pp. 477–485, 1994.

[41] Costa, V. A. F, Oliveira, L. A., Baliga, B. R., Sousa, A. C. M., 2004, "Simulation of Coupled Flows in Adjacent Viscous and Porous Domains Using a Control-Volume Finite Element Method," Numer. Heat Transfer A, **45**, pp. 675-697

[42] Valdes-parada, F. J., Alvarez-Ramirez, J., Goyeau, B., Ochoa-Tapia, J. A. , 2009, "Jump Condition for Diffusive and Convective Mass Transfer Between a Porous Medium and a Fluid Involving Adsorption and Chemical Reaction," Transp. Porous. Med**, 78,** pp. 459-476

[43] Degroot, C. T., Gateman, D., Straatman, A.G., 2010, "The Effect of Thermal Contact Resistance at Porous-Solid Interfaces in Finned Metal Foam Heat Sinks," J. Electronic Packaging ASME, **32, 0401007** pp. 1-7

[44] Incropera, F., Dewitt, D., Bergman, T., and Lavine, A., 2007, *Fundamentals of Heat and Mass Transfer*, 6th ed., Wiley, Hoboken, NJ.

[45] Calmidi , V. V., Mahajan, R. L. , 2000, "Forced Convection in High Porosity Metal Foams", J. Heat Transfer, **122**, pp. 557–565

[46] Ingham, D. B., Pop, I., 2002, *Transport Phenomena in Porous Media II*, Pergamon, Elsevier, pp 429-439

[47] Melling, A., Noppenberger, S., Still, M., Venzke, H., 1997, "Interpolation Correlations for Fluid Properties of Humid Air in the Temperature range 100 – 200 Celsius," J. Phys. Chem, **26** (4), pp. 1111-1123

[48] Tsilingiris, P. T., 2007, "Thermophysical and transport properties of humid air at temperature range between 0 and 100 Celsius", Energy Conversion Management, **49**, pp. 1098-1110

[49] Zhan, C., Zhao, X., Duan, Z., Riffat, S.B. 2010, "Numerical Study on Indirect evaporative cooling performance comparison between counterflow and crossflow heat exchangers," J. Low-carbon technologies, **6,** pp 100-107

[50] Riangvilaikul, B., Kumar, S., 2010, "An experimental study of a novel dew point evaporative cooling system," Energy Build, **42**, pp. 637–644

[51] 2011, "Idalex homepage", http://www.idalex.com, accessed Nov 5, 2010